



جامعة
الأميرة سمية
للتكنولوجيا
Princess Sumaya University for Technology

Design and simulations of Multi-port DC-DC converter

By

Ahmad Barakat, Hussain Sabri & Jad Akl

Supervised by

Dr. Ibrahim Abuishmais

Submitted in partial fulfillment of the requirements for the degree of

BACHELOR OF SCIENCE

in

ELECTRICAL POWER AND ENERGY ENGINEERING

at

PRINCESS SUMAYA UNIVERSITY FOR TECHNOLOGY

Amman, Jordan

Fall Semester, 2025

This is to certify that I have examined
this copy of an engineering documentation by

Ahmad Barakat, Hussain Sabri & Jad Akl

And have found that it is complete and satisfactory in all respects,
And that any revisions required by the final Examining Committee have been made

Dr. Ibrahim Abuishmais

Acknowledgments

This project would not have been accomplished without the guidance, dedication, and assistance of our supervisor and instructor, Dr. Ibrahim Abuishmais. For this reason, we would like to thank him sincerely. Furthermore, we are grateful to Princess Sumaya University for Technology for their assistance, for giving us access to all the websites and libraries we needed, and for creating a friendly atmosphere. Being a part of this exceptional university has been an immense privilege. Being a part of this innovative and forward-thinking organization makes us incredibly proud.

To our professors, we would like to thank you because they helped us collect information and reach out to this place.

Last but not least, we also want to express our deepest gratitude to our family and friends for their support, love, and encouragement. We are truly grateful for their presence in our lives.

Thank You

Ahmad Barakat, Hussain Sabri & Jad Akl

Abstract

This paper will tackle the design and simulation of a multi-multi DC-DC converter by implementing PSIM and MATLAB softwares. The converter will have two input sources and two separate loads. A solar panel and a 48 V lithium iron phosphate (LiFePO₄) battery will provide the converter with sufficient power to supply an electric vehicle and a small household. The proposed multiport converter (mpc) is vital for the power system since the converter, its input sources and output loads will shape an independent DC microgrid. DC microgrids will be the face of the electrical grid; they offer decentralization, stability, and reliability to the power system. They are also environmentally friendly since they offer easier integration to solar panels and battery storage systems.

The paper aims to successfully design a multiport DC-DC converter that can efficiently supply the loads and offer a more energy-efficient power system. The converter, on the input side, is based on two boost converters and a full bridge galvanically isolated by an ideal single-phase 3-winding transformer design, feeding the two output buck circuits connecting the transformer to the loads. This is highly efficient since both inputs have an independent boost circuit, each with a separate duty cycle, and both outputs have an independent buck circuit. Using a transformer to interface the input and output sides provides more control over the output voltages and currents by adjusting the turns ratio, along with providing protection since it electrically isolates the input sources from the loads. The proposed system is suitable for residential applications, and expanding the input power sources ratings can make the system suitable for commercial applications.

Table of Contents

Abstract.....	4
Table of Contents.....	5
List of Figures.....	7
List of Tables.....	9
List of Equations.....	10
List of Symbols and Abbreviations.....	11
1. Introduction.....	13
1.1. Background.....	13
1.2. Objectives.....	14
1.3. Design Requirements.....	14
1.4. Realistic Constraints.....	14
1.5. Engineering Standards.....	15
1.6. Documentation Organization.....	15
1.7. Group Responsibility.....	16
2. Literature Review.....	17
2.1 Background.....	17
2.2 Microgrids.....	18
2.3 Household Appliances and Loads.....	19
2.4 PV Source and MPPT.....	19
2.5 Literature Review.....	20
3 Design.....	27
3.1 Design Requirements.....	27
3.2 Analysis of Design Requirements.....	27
3.3 Analysis of Design Constraints.....	28
3.3.1 Engineering Standards.....	28
3.4 Different Designs Approaches/choices.....	28
3.4.1 Design Option 1 DAB.....	28
3.4.2 Design Option 2: Buck Converter For Input Source.....	29
3.5 Developed Design.....	29
3.5.1 Input Boost Converters.....	30
3.5.1.1 PV Source Steady state.....	30
3.5.1.2 Battery Source Open Loop Analysis.....	32
3.5.2 Output Buck Converters.....	34
3.5.2.1 Buck Converter of High Voltage Output Terminal.....	34
3.5.2.2 Buck Converter of Low Voltage Output Terminal.....	38
3.6 Closed Loop Analysis.....	40
3.6.1 Input Boost Converters.....	42

3.6.1.1 Maximum Power Point Tracker (MPPT) Analysis.....	42
3.6.1.2 Perturb and Observe Algorithm.....	45
3.6.1.3 PV Source Closed Loop Analysis.....	46
3.6.1.4 Battery Source Closed Loop Analysis.....	50
3.6.2 Output Buck Converters Closed Loop.....	52
3.6.2.1 Buck Converter Closed Loop Design.....	52
3.6.3 Type-II Controller Explanation & Design.....	59
3.6.4 Controller Design Tests.....	62
3.7 Full Bridge Design.....	66
3.7.1 Rectifier Design.....	67
3.7.2 Transformer Design.....	67
4 Results.....	69
4.1 Simulation Results Setup.....	69
4.2 Input Open Loop Results.....	75
4.3 Input Closed Loop Results.....	79
4.3.1 MPPT Results.....	79
4.3.2 PV Source Results.....	81
4.3.3 Battery Source Results.....	82
4.4 Output Open Loop Results.....	83
4.4.1 High Voltage Buck Converter.....	83
4.4.2 Low Voltage Buck Converter.....	85
4.5 Output Closed Loop Results.....	88
4.5.1 High Voltage Buck Converter.....	88
4.5.2 Low Voltage Buck Converter.....	90
4.6 Full Circuit Results.....	93
4.6.1 Testing Multiport Converter (MPC).....	93
4.6.2 Transformer Voltages.....	96
4.6.3 Output Voltages and Currents.....	98
4.6.4 Full Circuit Efficiency Test.....	101
4.6.5 Voltage Regulation.....	102
4.6.6 Fault Test.....	102
4.6.7 Validation of The Requirements.....	103
5 Conclusion and Future Work.....	105
5.1 Conclusion and Future Work.....	105
References.....	107
Appendices.....	109
Appendix A: PV Datasheet.....	109
Appendix B: CODE.....	110

List of Figures

FIGURE 2.1: MPPT BUCK-BOOST CONVERTER [3].....	20
FIGURE 2.2: DC-MICROGRID SYSTEM CIRCUIT [4].....	21
FIGURE 2.3: PROPOSED ISOLATED DAB CONVERTER WITH NPC [6].....	23
FIGURE 2.4: MFT & RESONANT TANK CONVERTER [7].....	24
FIGURE 2.5: PROPOSED CONVERTER FROM BISWAS, DHOPLE, AND MOHAN [8].....	25
FIGURE 2.6: POWER MODES OF CUK CONVERTER [8].....	26
FIGURE 3.1: DUAL ACTIVE BRIDGE.....	29
FIGURE 3.2: DC-DC Boost Converter Circuit.....	30
FIGURE 3.3: Output BUCK Converter Circuit.....	35
FIGURE 3.4: Control Block Diagram for Both BUCK and Boost Converters.....	41
FIGURE 3.5: PWM Triangular Pulses, Reference Signal and Modulated Rectangular Output [14].....	42
FIGURE 3.6: MPPT Boost Circuit.....	43
FIGURE 3.7: PV Array System.....	44
FIGURE 3.8: PERTURB AND OBSERVE ALGORITHM.....	45
FIGURE 3.9: P&O MPPT CONTROLLER.....	46
FIGURE 3.10: BODE PLOT OF PV Boost Converter Transfer Function at 150 V Before Modification.....	47
FIGURE 3.11: BODE PLOT OF PV Boost Converter Transfer Function at 150 V After Modification.....	48
FIGURE 3.12: TYPE-III COMPENSATOR.....	49
FIGURE 3.13: BODE PLOT OF BATTERY Boost Converter Transfer Function at 48 V Before Modification.....	51
FIGURE 3.14: BODE PLOT OF BATTERY Boost Converter Transfer Function at 48 V After Modification.....	52
FIGURE 3.15: BODE PLOT FOR HIGH VOLTAGE BUCK CONVERTER BEFORE MODIFICATION.....	54
FIGURE 3.16: BODE PLOT FOR HIGH VOLTAGE BUCK CONVERTER AFTER MODIFICATION.....	55
FIGURE 3.17: BODE PLOT FOR LOW VOLTAGE BUCK CONVERTER BEFORE MODIFICATION.....	56
FIGURE 3.18: CLOSED LOOP BODE PLOT FOR LOW VOLTAGE BUCK CONVERTER AFTER MODIFICATION.....	57
FIGURE 3.19: TYPE-II CONTROLLER CIRCUIT.....	59
FIGURE 3.20: PV Closed Loop Output Voltage with Changing Voltage Reference.....	62
FIGURE 3.21: BATTERY Closed Loop Output Voltage with Changing Voltage Reference.....	63
FIGURE 3.22: PV Closed Loop Output Voltage with Changing Input Voltage.....	63
FIGURE 3.23: BATTERY Closed Loop Output Voltage with Changing Input Voltage.....	64
FIGURE 3.24: PV Closed Loop Output Voltage with Changing Load.....	64
FIGURE 3.25: BATTERY Closed Loop Output Voltage with Changing Load.....	65
FIGURE 3.26: FULL BRIDGE TOPOLOGY WITH TWO OUTPUTS.....	66
FIGURE 4.2: SOURCE SIDE OF MULTI-PORT DC-DC CONVERTER.....	70
FIGURE 4.3: BRIDGE OF MULTI-PORT DC-DC CONVERTER.....	71
FIGURE 4.4: LOAD SIDE OF MULTI-PORT DC-DC CONVERTER.....	71
FIGURE 4.5: MULTI-PORT DC-DC CONVERTER FULL CIRCUIT.....	72
FIGURE 4.6: CONTROLLERS OF MULTI-PORT DC-DC CONVERTER.....	72
FIGURE 4.7: MULTI-PORT DC-DC CONVERTER FULL CIRCUIT WITH CONTROLLERS.....	74
FIGURE 4.8: PV OPEN LOOP BOOST CONVERTER OUTPUT VOLTAGE.....	75
FIGURE 4.9: PV OPEN LOOP BOOST CONVERTER OUTPUT VOLTAGE RIPPLE.....	75

FIGURE 4.10: PV OPEN LOOP BOOST CONVERTER OUTPUT CURRENT RIPPLE.....	76
FIGURE 4.11: PV OPEN LOOP BOOST CONVERTER INDUCTOR CURRENT RIPPLE.....	76
FIGURE 4.12: BATTERY OPEN LOOP BOOST CONVERTER OUTPUT VOLTAGE.....	77
FIGURE 4.13: BATTERY OPEN LOOP BOOST CONVERTER OUTPUT VOLTAGE RIPPLE.....	77
FIGURE 4.14: BATTERY OPEN LOOP BOOST CONVERTER OUTPUT CURRENT RIPPLE.....	78
FIGURE 4.15: BATTERY OPEN LOOP BOOST CONVERTER INDUCTOR CURRENT RIPPLE.....	78
FIGURE 4.17: POWER DELIVERED BY MPPT AND MAX POWER OF PV ARRAYS.....	80
FIGURE 4.18: PV CLOSED LOOP OUTPUT VOLTAGE.....	81
FIGURE 4.19: PV CLOSED LOOP OUTPUT VOLTAGE RIPPLE.....	81
FIGURE 4.20: BATTERY CLOSED LOOP OUTPUT VOLTAGE.....	82
FIGURE 4.23: HIGH VOLTAGE OPEN LOOP BUCK CONVERTER OUTPUT CURRENT.....	84
FIGURE 4.24: HIGH VOLTAGE OPEN LOOP BUCK CONVERTER OUTPUT VOLTAGE.....	84
FIGURE 4.25: HIGH VOLTAGE OPEN LOOP BUCK CONVERTER OUTPUT VOLTAGE RIPPLE.....	85
FIGURE 4.26: LOW VOLTAGE OPEN LOOP BUCK CONVERTER INDUCTOR RIPPLE CURRENT.....	86
FIGURE 4.27: LOW VOLTAGE OPEN LOOP BUCK CONVERTER OUTPUT CURRENT.....	86
FIGURE 4.28: LOW VOLTAGE OPEN LOOP BUCK CONVERTER OUTPUT VOLTAGE.....	87
FIGURE 4.29: LOW VOLTAGE OPEN LOOP BUCK CONVERTER OUTPUT VOLTAGE RIPPLE.....	87
FIGURE 4.30: HIGH VOLTAGE CLOSED LOOP BUCK CONVERTER INDUCTOR RIPPLE CURRENT.....	88
FIGURE 4.31: HIGH VOLTAGE CLOSED LOOP BUCK CONVERTER OUTPUT CURRENT.....	89
FIGURE 4.32: HIGH VOLTAGE CLOSED LOOP BUCK CONVERTER OUTPUT VOLTAGE.....	89
FIGURE 4.33: HIGH VOLTAGE CLOSED LOOP BUCK CONVERTER OUTPUT VOLTAGE RIPPLE.....	90
FIGURE 4.34: LOW VOLTAGE CLOSED LOOP BUCK CONVERTER INDUCTOR RIPPLE CURRENT.....	91
FIGURE 4.35: LOW VOLTAGE CLOSED LOOP BUCK CONVERTER OUTPUT CURRENT.....	91
FIGURE 4.36: LOW VOLTAGE BUCK CONVERTER OUTPUT VOLTAGE AFTER MODIFICATION.....	92
FIGURE 4.37: LOW VOLTAGE BUCK CONVERTER OUTPUT VOLTAGE RIPPLE AFTER MODIFICATION.....	92
FIGURE 4.38: EV VOLTAGE IN CASE 1.....	94
FIGURE 4.39: HOUSEHOLD VOLTAGE IN CASE 2.....	94
FIGURE 4.40: EV VOLTAGE IN CASE 3.....	95
FIGURE 4.41: HOUSEHOLD VOLTAGE IN CASE 3.....	95
FIGURE 4.42: PRIMARY VOLTAGE.....	96
FIGURE 4.43: SECONDARY VOLTAGE.....	97
FIGURE 4.44: TERTIARY VOLTAGE.....	97
FIGURE 4.45: HIGH VOLTAGE BUCK CONVERTER VOLTAGE OUTPUT.....	98
FIGURE 4.46: HIGH VOLTAGE BUCK CONVERTER CURRENT OUTPUT.....	99
FIGURE 4.47: LOW VOLTAGE BUCK CONVERTER OUTPUT VOLTAGE.....	99
FIGURE 4.48: LOW VOLTAGE BUCK CONVERTER OUTPUT CURRENT.....	100
FIGURE 4.49: OUTPUT VOLTAGE AND RIPPLE AT HIGH VOLTAGE OUTPUT DURING SHORT CIRCUIT FAULT AT LOW VOLTAGE OUTPUT.....	103

List of Tables

TABLE 1.1: WORK DISTRIBUTION.....	16
TABLE 2.1: SUMMARY OF THE DISCUSSED CONVERTER TOPOLOGIES.....	26
TABLE 3.1: OPEN LOOP PARAMETER OF PV SOURCE.....	32
TABLE 3.2: OPEN LOOP PARAMETER OF BATTERY SOURCE.....	33
TABLE 3.3: BUCK CONVERTER PARAMETERS AT MAXIMUM INPUT VOLTAGE AND MINIMUM OUTPUT VOLTAGE.....	37
TABLE 3.4: BUCK CONVERTER PARAMETERS AT MINIMUM INPUT VOLTAGE AND MAXIMUM OUTPUT VOLTAGE.....	37
TABLE 3.5: INDUCTOR AND CAPACITOR PARAMETERS FOR THE HIGH VOLTAGE BUCK CONVERTER.....	38
TABLE 3.6: BUCK CONVERTER PARAMETERS AT MAXIMUM INPUT VOLTAGE AND MINIMUM OUTPUT VOLTAGE.....	39
TABLE 3.7: BUCK CONVERTER PARAMETERS AT MINIMUM INPUT VOLTAGE AND MAXIMUM OUTPUT VOLTAGE.....	40
TABLE 3.8: INDUCTOR AND CAPACITOR PARAMETERS FOR THE LOW VOLTAGE BUCK CONVERTER.....	40
TABLE 3.9: PV PANEL SPECIFICATIONS.....	43
TABLE 3.10: CLOSED LOOP DESIGN PARAMETERS FOR HIGH VOLTAGE BUCK CONVERTER.....	56
TABLE 3.11: CLOSED LOOP DESIGN PARAMETERS FOR LOW VOLTAGE BUCK CONVERTER.....	58
TABLE 3.12: TYPE-II CONTROLLER PARAMETERS FOR BOTH BUCK CONVERTERS.....	61
TABLE 4.1: INPUT AND OUTPUT POWER RATINGS AND CONVERTER EFFICIENCY.....	101
TABLE 4.2: THE PARAMETERS OF MOSFETS AND DIODES.....	101
TABLE 4.3: VALIDATION SUMMARY.....	103

List of Equations

EQUATION 2.1.....	21
EQUATION 3.1.....	32
EQUATION 3.2.....	33
EQUATION 3.3.....	33
EQUATION 3.4.....	33
EQUATION 3.5.....	33
EQUATION 3.6.....	34
EQUATION 3.7.....	37
EQUATION 3.8.....	37
EQUATION 3.9.....	37
EQUATION 3.10.....	38
EQUATION 3.11.....	38
EQUATION 3.12.....	38
EQUATION 3.13.....	38
EQUATION 3.14.....	40
EQUATION 3.15.....	41
EQUATION 3.16.....	48
EQUATION 3.17.....	48
EQUATION 3.18.....	51
EQUATION 3.19.....	51
EQUATION 3.20.....	52
EQUATION 3.21.....	52
EQUATION 3.22.....	52
EQUATION 3.23.....	52
EQUATION 3.24.....	52
EQUATION 3.25.....	54
EQUATION 3.26.....	54
EQUATION 3.27.....	55
EQUATION 3.28.....	62
EQUATION 3.29.....	62
EQUATION 3.30.....	62
EQUATION 3.31.....	62
EQUATION 3.32.....	63
EQUATION 3.33.....	63
EQUATION 3.34.....	63
EQUATION 3.35.....	63
EQUATION 3.36.....	69
EQUATION 3.37.....	69
EQUATION 3.38.....	70
EQUATION 3.39.....	70

List of Symbols and Abbreviations

MPC	Multiport Converter
RES	Renewable Energy Sources
PV	Photovoltaic
MPPT	Maximum Power Point Tracking
NPC	Neutral Point Clamped
DAB	Dual Active Bridge
CCM	Continuous Current Mode
DCM	Discontinuous Current Mode
DER	Distributed Energy Resources
P & O	Perturb and Observe
MFT	Medium Frequency Transformer
EMI	Electromagnetic Interference
ISOP	Input Series Output Parallel
PWM	Pulse Width Modulation
MOSFET	Metal-Oxide-Semiconductor Field-Effect Transistor
LCR	Inductance - Capacitance - Resistance
STC	Standard Temperature Conditions
LHP	Left Half Plane
RHP	Right Half Plane
PI	Proportional Integral
Q-factor	Quality Factor
PM	Phase Margin

LV	Low Voltage
HV	High Voltage
PSFB	Phase Shifted Full Bridge
EV	Electric Vehicle
ZVS	Zero Voltage Switching
ZCS	Zero Current Switching

1. Introduction

1.1. Background

The future of power grids is at significant risk if serious measures and actions are not taken; with the world's electricity consumption constantly increasing due to an increase in population and increasing dependence on electronic loads, the power grid will continually endure increasing pressure. DC-DC converters have been introduced as a key to sustain the power system.

DC-DC converters are vital and in constant demand due to their high efficiency and simple topology, with the continuous growth of renewable energy sources, and their changing power supply throughout the day, month, and year because of their dependence on weather and geological conditions, a converter that provides efficient control, and regulation is needed to safely integrate renewable energy sources and other sources into the power system. A multiport converter provides the required interface to apply multiple energy sources, including renewable sources and battery storage systems, to the power system and decentralize the power system; hence, a DC microgrid is developed with the interface between the sources and loads in the mpc.

In the modern age, most electronic household appliances use DC power instead of AC; many appliances rectify the input AC voltage to a DC voltage to supply the load by using a single-phase full bridge rectifier; moreover, some loads then invert the DC voltage to a modified AC voltage with lower amplitude and frequency to save more energy. This means that a DC voltage stage is present in almost all modern electronic loads. The future of electrical power systems will include the use of multiport DC-DC converters to connect household appliances to sustainable power sources. The multiport DC-DC converter allows a hybrid of input sources: a PV array and a 48 V battery. The outputs of the multiport converter will feed two loads at different voltage levels, 380 V and 12 V. The architecture of the multiport DC-DC converter allows it to have different voltage levels at both the input and the output. This key feature will make the future of the power system heavily dependent on multiport DC-DC converters similar to the proposed mpc. The resulting DC microgrid is composed of the two input sources mentioned previously interfaced with the mpc feeding two separate loads, one being an electric car and the other being a small household.

1.2. Objectives

This work aims to successfully design and implement a multiport DC-DC converter that meets all design requirements. To design a new multiport converter with two inputs, PV and battery, and two outputs, an electric vehicle and a small household, with the aid of PSIM and MATLAB, the outcomes of the converter will be simulated, and the controllers will be tuned and tailored accordingly. A detailed structure will be provided for the proposed design, as well as complete PSIM and MATLAB simulation files, codes, and results.

1.3. Design Requirements

The design shall achieve the following requirements:

- The input sources shall be a 150-250 V PV array and a 48 V battery unit.
- The output voltage levels shall be 380 V and 12V.
- Power rating PV array 1000 Wp.
- Battery capacity is 180 Ah.
- The power rating shall be 2 kW.
- Conversion efficiency should be higher than 90% at nominal load
- Output voltage regulation 90%-110%
- The input voltage of the battery is 48-52V.
- The MPPT function shall be implemented at the PV input terminal.
- PSIM or MATLAB tool shall be used to simulate the circuit.

1.4. Realistic Constraints

- **Economic Constraints:** The scaled-down prototype of the proposed project, when implemented, is expected to remain within the budget constraint of no more than JOD 500.
- **Manufacturability and Sustainability Constraints:** Prototyping, if done, should done at a scaled-down version, at a reduced voltage and power level to reduce the high cost of the project and to ensure safety from hazards.
- **Environmental Constraints:** No environmental constraints are required.

1.5. Engineering Standards

The system must comply with the engineering standards set by the Institute of Electrical and Electronics Engineers (IEEE).

The IEEE Standard 1547 consists of a series of standards developed in 2003, and this standard specifies the requirements for the interconnection of distributed energy resources (DER) with electric power systems, including requirements for inverters and converters used in renewable energy systems.

The IEEE Standard 1547a Amendment 1 to 1547 is one of the standards that considered smart grid advances such as setting the performance criteria that ensure safe and reliable integration of the Multi-port DC-DC, such as a focus on voltage regulation, power quality, and ride-through capabilities for voltage abnormalities.

1.6. Documentation Organization

Chapter 2 - Literature Review

In this section, multiple designs and topologies are considered to collect data and gain a better understanding of the required system. Each part tackles a specific problem, starting from the big idea of the DC microgrid to the most minor details. Other ideas include the importance of MPPT function isolation of a system using transformers and the use of inverters and rectifiers.

Chapter 3 & 4 - Design & Results

This section goes into detail about the calculations and designs of the mpc. Describe the implementation of an MPPT function and the detailed analysis of both open and closed-loop analysis for each converter used, both boost and buck. In addition to the input side inverter, the isolation transformer and the rectification stage are also included. This section also shows the results of each stage and the entire system, along with different real-life scenarios, efficiency and voltage regulation of the mpc.

Chapter 5 - Conclusion & Future Work

The final section summarizes the work done at each stage and briefly comments on the entire system, in addition to other ideas that could be implemented to improve the system's performance, transient response, controllability, stability, and protection.

1.7. Group Responsibility

Table 1.1: Work Distribution

Task	Ahmad Barakat	Hussain Sabri	Jad Akl
Literature Review	✓	✓	✓
Analysis of Design Requirements	✓	✓	✓
Analysis of Design Constraints	✓	✓	✓
Design (Simulation)	Input Side	✓	✓
	Bridge	✓	✓
	Output Side		✓
	Different Design Approaches	✓	✓
	Design Selection	✓	✓
Results & Discussion	✓	✓	✓
Conclusion & Future Work	✓		✓
Documentation	Main/Initial Writing	✓	✓
	Final Edit/Proofreading	✓	✓

2. Literature Review

2.1 Background

Alternating current (AC) has been the conventional way of generating power throughout history; its ability to easily change and control voltage levels for multiple applications and power up rotating machines made it the more attractive choice, with the increasing demand, the rise of global warming dangers, the deterioration of the current power systems due to aging, and with the new more sustainable changing technologies, the need for direct current has become more essential than ever, to implement DC microgrids to sustain the power system.

Many power sources now provide direct current (DC) power; for example, one of the most popular renewable energy sources (RES), the solar photovoltaic (PV) cells, generate DC voltage, and other non-renewable sources such as batteries, fuel cells, and supercapacitors. DC microgrids are gaining popularity because of their benefits, similar to the more traditional way of generating power using AC systems. DC microgrids have a frequency of zero Hz, which solves the synchronization challenge, removes harmonics, and has fewer power losses during transmission, making DC microgrids more popular than AC microgrids. To increase the reliability of any system, especially when implementing renewable energy sources, other sources must also be integrated into the grid to ensure continuous power generation, leading to one of the complications associated with DC microgrids. The incorporation of different sources, such as PV, fuel cells, batteries, etc., in a common DC bus leads to complications in controlling the bus voltage and in the ability to share the power. Some control techniques to secure and safely operate the microgrids are centralized control, decentralized control, and distributed multilevel control.

The everlasting increase in demand for energy is outpacing the capabilities of non-renewable energy sources due to their limited supply; moreover, today's technology can not reverse the negative environmental impacts of most non-renewable sources, so the need for more RES is crucial for the survival of our power system and for the preservation of the environment.

2.2 Microgrids

Renewable energy sources are usually connected near the loads through the distribution network in any conventional power system, lacking the need for a transmission system; thus, RES are also known as distributed generation systems. This will cause a bidirectional power flow inside the system, negatively impacting the distribution network. Increasing the level of distribution will increase the problems associated with bidirectional power flow, and these issues can affect the power quality, thus increasing the magnitude of fault currents, requiring more dense relays, in addition to more frequent maintenance of the equipment, to resolve these problems, DC microgrids are integrated into the distribution system. Microgrids have proven significant benefits to the distribution system and the end-user; they lower the average cost and reduce disturbance, optimizing the system by ensuring the implementation of renewable energy systems.

Usually, a microgrid can control the load and have an energy storage system, a device that can convert energy from one form to another and convert it back to electrical power when needed; this implementation is critical to ensure the continuous operation of a system mainly when renewable energy sources are utilized, resulting in smoother power fluctuations, increase power quality, frequency control, and the ability to enable the distribution generator to behave like dispatchable units, microgrids can operate in the grid in connected mode and islanded mode. When the microgrid can absorb or supply power to and from the grid depending on the power consumption or production, that mode is called connected mode, while in islanded mode, the source's primary function is to supply all local loads.

Renewable energy sources rely heavily on climate and weather conditions and the geographical location where they are implemented; hence, their power constantly fluctuates. Microgrids offer the solution for the fluctuating supply of renewable sources by offering better control of renewable energy sources by the use of converters and storage units to store excess energy, while providing a more reliable and emission-free network. Microgrids will bring many benefits to the power system, such as decentralization and digitalization.

2.3 Household Appliances and Loads

The production of household appliances is increasing rapidly, which forces the implementation of external or internal converters. Usually, an AC-DC converter links the DC appliances to the AC energy source, but DC-DC converters are implemented in DC microgrids. DC-DC converters are essential to utilize the power consumption of the appliances, especially when connected to a PV system; additionally, loads have different ranges of voltage because of the lack of standardization of household appliances, where the variation of voltage range from 12V to 800V, it is impossible to make a converter to fit all power ratings. Instead, voltage standardization is implemented in the DC distribution network to reduce losses and system complexity. Finding a suitable voltage level that fits almost every appliance is a near-impossible task, especially when considering energy efficiency, the safety of the customer, and cost reduction.

2.4 PV Source and MPPT

Photovoltaic (PV) technology is made of solar cells; these cells can be grouped in parallel and series to make up a module; these modules are then connected in series, making up a string, and the combination of strings in parallel forms an array of PV. The output voltage is not constant due to its dependence on weather conditions; output voltage changes depending on the time, location, and weather conditions, causing the microgrid to be a non-linear system, to have better controllability, and to accommodate the constant load, in addition, to increase the PV system efficiency, maximum power point tracking (MPPT) need to be implemented. MPPT is the point where the current and voltage characteristics peak, resulting in the maximum power. MPPTs are usually made from a DC-DC buck-boost converter used to increase or decrease the output voltage. Figure 2.1 [3] illustrates a typical buck-boost converter; when the switch is closed, the source voltage is applied across the inductor that drives a current, and the diode blocks the current, forcing it to build up magnetic energy in the inductor when the switch is open, the current will flow through the capacitor keeping the voltage high enough to charge the load. In contrast, the inductor loses its energy slowly. The switch must be fast enough to ensure the current in the inductor and voltage across the capacitor is almost constant.

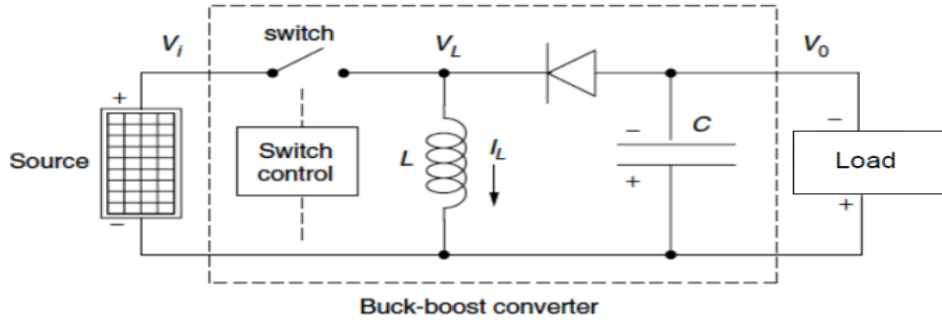


Figure 2.1: MPPT Buck-Boost Converter [3]

The duty cycle of the switch plays a vital role in determining the buck or boost ratio. Equation 2.1 shows the simple relation between the out voltage (V_o) to the input voltage (V_i) specified by the duty cycle (D); if the duty cycle is 0.5, the input and output voltage are the same, and if D is less than 0.5, the converter acts as a buck converter, and if D is more than 0.5 the converter is a boost.

$$\frac{V_o}{V_i} = \frac{D}{1-D} \quad (2.1)$$

A controller is needed to adjust the converter's duty cycle to keep the PV array output voltage on its maximum power point. MPPT controller measures the voltage and current from an array and generates the suitable duty cycle to control the switching speed. There are two standard methods for controlling; the first is Perturb and Observe (P & O); this method is based on observing the derivative of peak power, trying to keep it close to zero; this method is more stable. The other method is called Incremental conductance; it tends to be less stable as it fluctuates more and is more sensitive to surroundings.

2.5 Literature Review

Sun et al. have considered a DC microgrid consisting of a PV panel, an energy storage battery, a DC bus, multiple DC-DC converters, and two different loads; the converter is used as an MPPT placed between the buses and PV. The battery storage system is connected to the bus through a bidirectional DC-DC buck-boost converter for voltage regulation purposes on the bus. One of the loads is connected through a DC-DC converter to be considered a constant power load, and the other load is connected directly to the voltage bus. The circuit in Figure 2.2 [4] has been

used; the PV module is represented by a current source indicating the irradiation and temperature connected to a shunt diode and resistance to represent the output of the PV. Energy storage is represented by an electromotive force and a series of resistances; the battery is connected to the converter to regulate and control charging and discharging. If the PV source generates more power than is consumed, the battery absorbs the additional power. If the PV source is insufficient in providing the needed power to the load, the battery releases power. Three control variables are to be considered in the microgrid: the converters' duty cycles. The control objectives are to find the maximum output power of the PV and to regulate the DC bus and the voltages of the load. Simulations have been developed using MATLAB, which resulted in voltage regulation for the source side of the PV and energy storage device, in addition to constant power on the loads using three inputs of controllability. [4]

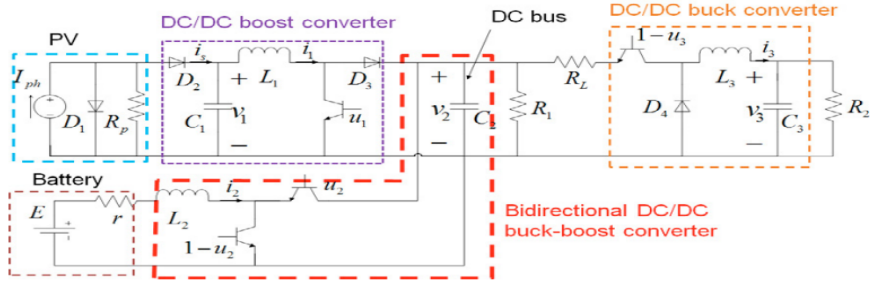


Figure 2.2: DC-microgrid System Circuit [4]

Sabry et al. have proposed a topology to determine the compatibility of household appliances that considers the efficiency of all stages; a traditional ON-grid PV house shows a cumulative efficiency of 81%, resulting from implementing four main converters. These aspects were the main goals to overcome the following: the losses of power conversion devices, the different voltage levels, and the limitations of local loads. One concept to overcome these issues is to implement a voltage-matching device between the source and the load; this can be done by setting the battery's fully-charged voltage equal to the PV output voltage at the maximum power point and equal to the DC value of the utility grid. For appliances that require a voltage of 48V, the power losses and voltage drop were very high; it's not applicable for these types of appliances, but when using appliances that require voltages of 120, 230, or 326 V, it was shown that it is possible to supply these appliances with a DC source directly for PV or a battery, power losses were lower by avoiding converting from DC to AC and then back to DC [5].

Many research papers have implemented different topologies and circuit architectures to implement the multiport DC-DC converter into the microgrid. Some papers implemented a boost-based converter, while some other topologies included a buck-boost-based converter. Many of these used converters have a common characteristic: no matter the voltage ratings, all the converters are galvanically isolated. A galvanic isolation converter means having two coupled inductors (a transformer) implemented in the converter. A transformer in the middle of the converter provides many advantages and more freedom in designing the converter parameters. A transformer provides isolation, which means protection of the converter and the load if any fault occurs on the input side since the transformer provides electrical isolation. If a fault occurs and the voltage increases drastically on the input side, the transformer core will become saturated to protect the circuit elements and load on the output side. The second advantage of having the transformer offers is the wider ability to have a wider range to scale voltage by using the turns ratio on the transformer; this provides us with more flexibility and higher control over the voltage levels in the different stages of the converter. By using the transformer turns ratio to scale the voltage, stresses are reduced on the switching devices; this way, a more appropriate and efficient duty ratio for the converter can be chosen, typically between 40% and 70% rate. Finally, the transformer can easily have multiple outputs by connecting several windings on the core or using a center-tapped transformer if needed.

On the other hand, integrating a transformer has some disadvantages. Adding a transformer increases the converter's weight and volume, reducing efficiency because the transformer has conduction losses due to the transformer's working principle. Electrical energy incoming at the primary side, is transformed into magnetic energy at the core and back to electrical energy on the secondary side.

Kolahian et al. have proposed a bipolar DC-DC converter that combines both a neutral point clamp (NPC) and a multi-port dual active bridge (DAB). The design can be integrated with renewable energy sources such as photovoltaic(PV), and this converter is characterized by the ability to handle high power, has fewer switches than the standard converters, and is isolated. The converter can track the maximum power point of a PV and find the optimum region for the over-charge and discharge of a battery. Bipolar means it supplies a positive and negative DC voltage with the same magnitude, separated by a neutral line, which is used for bipolar DC microgrids

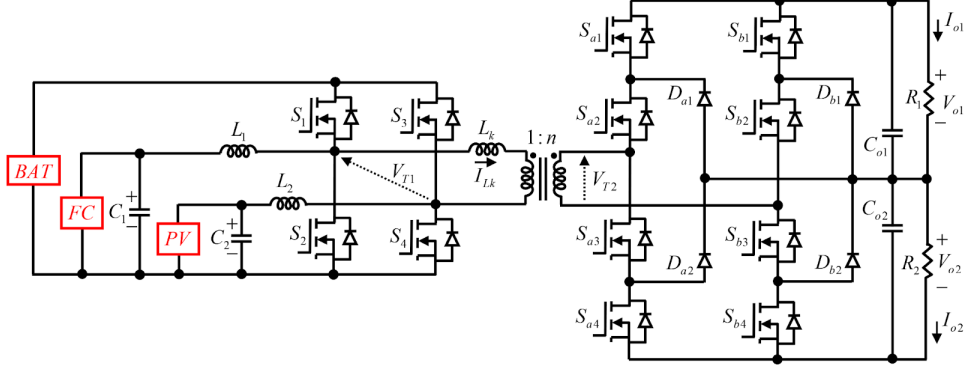


Figure 2.3: Proposed isolated DAB Converter with NPC [6]

As shown in Figure 2.3 [6] above, the converter uses three power supplies, which are PV cells, a fuel cell, and a battery bank, all feeding two outputs. As shown above, the fuel cell (FC) and photovoltaic cells (PV) circuits represent a boost configuration; meanwhile, the battery tank (BAT) circuit represents a buck configuration. This is shown since the battery circuit has no inductor; meanwhile, the (FC) and (PV) circuits contain an inductor constantly charging and discharging in CCM mode. The key feature of this converter is that it offers bidirectional power flow, where FC and PV can charge the battery (BAT) simply by controlling the switches. This architecture guarantees high efficiency and, hence, better battery life. The dual active bridge (DAB) used in the converter achieves the bidirectional power flow. The DAB consists of two full bridges connected to the transformer's primary and secondary sides. The other key feature of this converter design is that it is independent of the power grid frequency, which is either 50Hz or 60Hz. The converter is not tied to the grid frequency, and its switching rate is determined by its internal frequency, which is later designed in the control and feedback circuit. This key feature is achieved by using a neutral point converter (NPC) along with the dual active bridge (DAB). The neutral point converter offers multiple stages of voltage levels instead of just having two voltage levels; the term neutral refers to the midpoint in the voltage levels of the neutral point converter. This neutral point provides secure and balanced power conversion. The neutral point converter (NPC) and the neutral point can be seen in the secondary side of the multiport converter in Figure 2.3, consisting mainly of the diodes $D_{a1}, D_{a2}, D_{b1}, D_{b2}, C_{a1}, C_{a2}$, and the switches. [6]

The second tackled converter is by Tran and Dujic, who proposed an innovative multiport medium voltage isolated DC-DC converter with multiple windings and integrated energy storage, using an input series output parallel (ISOP) schematic. The designed converter in this paper allows for

multiple outputs but only proposes a single input voltage source. The proposed converter is based on a multi-winding medium frequency transformer (MFT) and uses the dual-active bridge (DAB) topology. One of the advantages of this converter is that it contains three windings, which allows for more freedom in design parameters. The three windings allow girds of different voltage levels to be interfaced, but their power flow is controlled and monitored through PWM or phase shift. Moreover, this is the disadvantage of this converter, which uses PWM or phase shift to control power flow because soft switching is diminished, which results in a smaller range. The solution to this disadvantage to decrease the switches' stresses is using multi-stacked stage structures and a resonant tank to enhance system reliability and efficiency. [7]

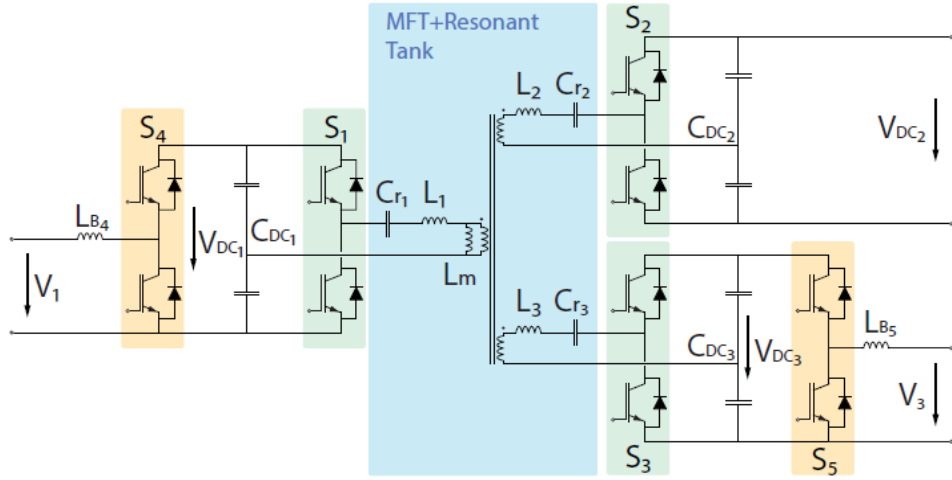


Figure 2.4: MFT & Resonant Tank Converter [7]

As shown in Figure 2.4 [7], the medium of the converter is a three-winding medium frequency transformer connected to the half bridges (S_1 , S_2 , and S_3). To benefit from soft switching, each of the three windings leakage inductances is combined with an external inductor to create a resonant tank. The resonant tank decreases switching losses and electromagnetic interference (EMI) and makes the switching operation of the transistor smoother; this is because, with the presence of the resonance tank, the switching occurs when the current or voltage is zero, so at zero crossing, hence increases the efficiency of the system. Moreover, the resonant tank filters out harmonics in the square wave signal to output a sine wave. The converter is based on a multi-winding transformer and uses the dual-active bridge topology. [7]

The proposed topology by Biswas, Dhople, and Mohan is based on a three-port bidirectional integrated magnetic Ćuk converters with zero ripple analysis. The proposed converter will have a zero terminal current ripple, which simplifies the control of the converter since it reduces the order of the converter, which means the converter will have fewer state variables. Ideally, the converter will only operate at continuous conduction control (CCM) and will not experience discontinuous conduction mode (DCM). Still, more research should be conducted on core and copper losses to build a reliable prototype.

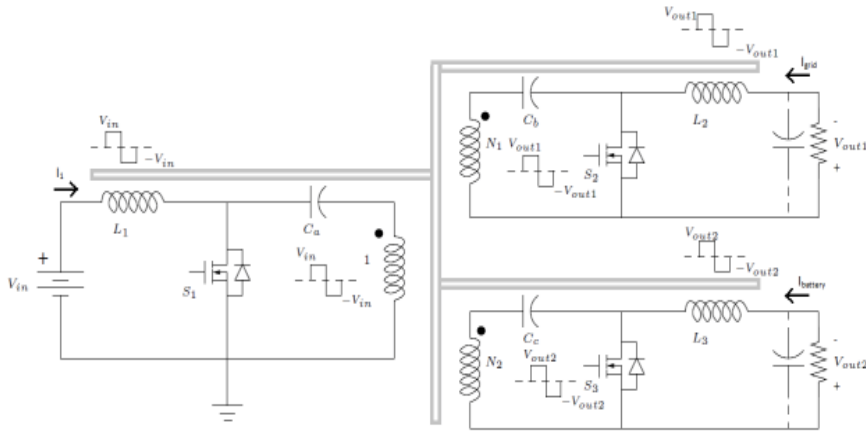


Figure 2.5: Proposed converter from Biswas, Dhople, and Mohan [8]

As shown in Figure 2.5 [8], the proposed converter has one input source, a fuel cell or PV cell; meanwhile, the converter has two directional outputs, representing a grid-tied inverter and a storage port. One approach to achieve zero ripple terminal currents includes circuit transformation and a coupled-inductor filter approach; for this approach to work, it needs highly accurate knowledge of the capacitance values. The advantage of this converter is that there is a bidirectional power flow. The strong point of this converter is that it easily integrates bidirectional power flow; this is because it employs a battery that allows for maximum power point tracking (MPPT) while conducting load regulation; this is possible because the battery manages mismatched power this is done when the battery stores excess power during lighter loads and off-peak demand, and supplying power during peak demand and heavier loads.

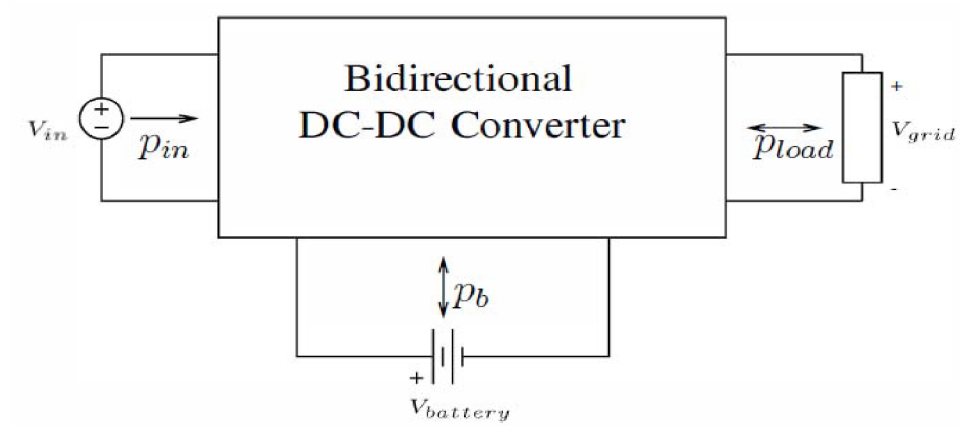


Figure 2.6: Power Modes of Cuk Converter [8]

The converter operates in three modes, as shown in Figure 2.6 [8]; in mode 1, the PV source or fuel cell (V_{in}) supplies power to the grid and charges the battery. In mode 2, if V_{in} is not operating, the battery is still being charged from the grid; finally, in mode 3, if V_{in} is still offline, the battery can supply power to the grid. The disadvantage of the proposed converter is that the zero current ripple technique using a coupled inductor filter cannot provide significant attenuation across all frequencies, and it is highly dependent on the capacitance value to operate effectively.

Table 2.1: Summary of The Discussed Converter Topologies

Converter	No.of Inputs	No.of Outputs	No.of Switches	No.of Diodes	No.of Inductors	Transformer type	Max. capacity (W)	Control Complexity	Efficiency
1	3	2	12	4	3	2-winding	3400	Medium	Medium
2	1	2	10	0	5	3-winding (2-primary windings)	500K	High	High
3	1	2	3	0	3	3-winding (2-secondary windings)	250	Low	Low

3 Design

3.1 Design Requirements

- The design shall achieve the following requirements:
- The input sources shall be a 150-250 V PV-array and a 48 V battery unit.
- The output voltage levels shall be 380 V and 12V.
- Power rating PV array 1000 Wp.
- Battery capacity is 180 Ah.
- The power rating shall be 2 kW.
- Conversion efficiency should be higher than 90% at nominal load.
- Output voltage regulation 90%-110%.
- The input voltage of the battery is 48-52V
- MPPT function shall be implemented at the PV input terminal.
- PSIM or MATLAB tool shall be used to simulate the circuit.

3.2 Analysis of Design Requirements

- **The input sources shall be a 150-250 V PV-array and a 48 V battery unit:** The converter shall be supplied by two input sources, where the first input source is a PV array that has a rated voltage between 150-250V, and the second input source shall be a battery storage system with a 48V rated voltage.
- **The output voltage levels shall be 380 V and 12V:** The output voltages of the converter shall be 380V and 12V. Where 380V feeds the electric vehicle, and the 12V output feeds the small household. The converter shall maintain these two rated output voltage levels no matter load variations and input source fluctuations. Definitely the output loads are all fed DC voltage from the converter.
- **Power rating PV array 1000 Wp:** a 1000Wp refers to the maximum power the PV array can supply under STC conditions. This means in ideal sunny conditions, the PV will supply 1000W to the converter, while the battery unit will complement the PV array to feed the output loads with there power requirements.
- **Battery capacity is 180 Ah:** This is measure for the chosen battery unit capacity, this parameter cannot be validated in simulation, and can only be validated by creating a prototype for the design.

- **The power rating shall be 2 kW:** The rated output power of the converter is 2kW, meaning that both output loads can consume a rated power of 2kW, so the converter will be designed on the basis of supplying a total rated power of 2kW, which is shared between the electric vehicle and the small household.
- **Conversion efficiency should be higher than 90% at nominal load:** At nominal load rated at 2kW the converter should operate at least at 90% efficiency, meaning the ratio of output power to the input power shall at least be 90% at rated load.
- **Output voltage regulation 90%-110%:** The proposed design should have a voltage regulation between 90%-110%. Meaning at no load conditions, the output voltage should not deviate from the rated voltage more than 10%. This should be true for both output loads at no load conditions, meaning when the electric vehicle is disconnected, the converter output voltage should be between 90%-110% of the rated load voltage of the electric vehicle, which is 380V. The same applies for the small household terminal.
- **The input voltage of the battery is 48-52V:** The battery unit rated voltage should be between 48-52V, this also cannot be validated on simulation and only by implementing a prototype this parameter can be validated.
- **MPPT function shall be implemented at the PV input terminal:** MPPT is the maximum power point tracking function that enhances the output power of the PV, there are two main MPPT functions which are perturb and observe and incremental conductance, one of these functions will be chosen to design a charge controller for the PV array.
- **PSIM or MATLAB tool shall be used to simulate the circuit:** The converter along with its full analysis shall be conducted and simulated by using PSIM or MATLAB or both. Both PSIM and MATLAB provide the required design tools and needed analysis schematics to creatively design, test and implement a DC-DC converter.

3.3 Analysis of Design Constraints

- **Economic Constraints:** If a prototype is implemented, the cost should not exceed the limit budget of JOD 500 which includes all necessary components, materials, and any associated expensive to ensure the working of the scaled-down version of the prototype.
- **Manufacturability and Sustainability Constraints:** Prototyping, if done, should done at a scaled-down version, operating at a reduced voltage and power level which is necessary to minimize the overall cost with ensuring affordability and efficiency. In addition, operating at

a lower voltage and power level ensure the safety and makes the prototype more practical during development and testing,

- **Environmental Constraints:** No environmental constraints are required.

3.3.1 Engineering Standards

The system must comply with the engineering standards set by the Institute of Electrical and Electronics Engineers (IEEE). This organization sets and updates the standards regarding electrical trends and equipment.

The IEEE Standard 1547 consists of a series of standards developed in 2003 and updated until the present. This standard specifies the requirements for interconnection and interoperability of distributed energy resources (DER) with electric power systems, including requirements for inverters and converters used in renewable energy systems.

The IEEE Standard 1547a Amendment 1 to 1547 is one of the standards that considered smart grid advances, such as setting the performance criteria that ensure safe and reliable integration of the Multi-port DC-DC, such as a focus on voltage regulation, power quality, and ride-through capabilities for voltage abnormalities.

The standard also requires standards regarding the multi-port DC-DC converter that service is continued if part of the system is isolated, this means if a fault happens at a terminal, the system will not affect any other terminals.

3.4 Different Designs Approaches/choices

3.4.1 Design Option 1 DAB

Figure 3.1 shows a schematic of the dual active bridge converter (DAB). A DAB is an isolated switching converter that allows bidirectional power flow between two DC voltage sources that may have different voltage levels; as seen in Figure 3.1, the DAB configuration is made of four transistors connected to the primary side of the transformer and four other transistors connected to the secondary side. The dual active bridge provides soft switching, which improves efficiency by reducing switching losses and minimizing electromagnetic interference, which can affect the performance of the transformer and nearby electronic devices. Soft switching is when the transistor turns on and off when the sinusoidal voltage or current is zero; these methods are zero voltage switching (ZVS) and zero current switching (ZVC). Since the required design has two input sources and two or more output sources, this design needs to have multiple output channels, which can be handled by managing the power distribution to each of them. Depending on the control method used, the DAB's output sides will supply the power loads from the PV system, battery storage, or a combination of both.

While the DAB is a tailored option to use for an MPC, implementation of soft switching offers complexity to the system's architecture and needs further research.

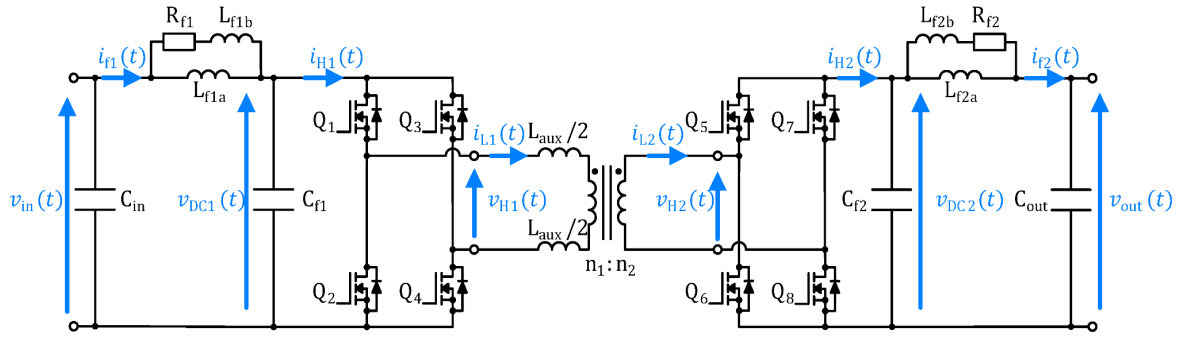


Figure 3.1: Dual Active Bridge

3.4.2 Design Option 2: Buck Converter For Input Source

One of the design options that had been considered was implementing buck converters for the PV and battery sources instead of the boost converters, but that idea was discarded because when following through with the same idea of merging the two inputs into one input for the transformer, the PV source would be stepped down five times smaller with a duty cycle of 0.192 which would cause larger switching losses due because the MOSFET would spend more time switching on and off. Also, stepping down the voltage at the same power level will result in larger current and high power losses. Because one of the loads requires a voltage of 380 V, the transformer would have to step up a large value when using a buck converter, which results in more trunks that will cause more power losses.

3.5 Developed Design

3.5.1 Input Boost Converters

In the open-loop analysis, a comprehensive evaluation of each section within the system. This aims to identify and acquire key parameters essential for understanding the system. The information collected is a crucial key for subsequent analysis.

3.5.1.1 PV Source Steady state

In the system's first part, the PV source is one of the inputs. This input ranges from 150 V to 250 V, depending on the insolation. The output of this stage is desired to be stepped up to 280 V for fewer losses, which can be done using a DC-DC Boost Converter, Figure 3.2. Because of the variation in the input side of the boost converter, the analysis must be repeated twice to consider

the worst-case scenario. For medium-size systems such as this, a switching frequency of 50 kHz is a good choice for the boost converter to minimize the switching losses and for appropriate sizing of the capacitor and inductor.

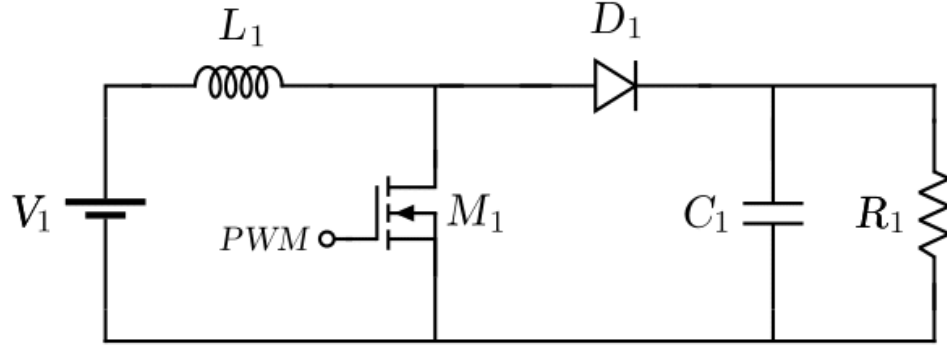


Figure 3.2: DC-DC Boost Converter Circuit

The PV is required to generate 1 kW, and starting the analysis with the input being 150 V, the known parameters are:

- $V_{in} = 150 \text{ V}$
- $V_{out} = 280 \text{ V}$
- $f_s = 50 \text{ kHz}$
- $P_{in} = 1 \text{ kW}$

First, from Equation (3.1), where V_{in} is the input voltage, V_{out} is the output voltage, and D is the duty cycle of the converter, it is determined that $D = 0.4643$

$$D = 1 - \frac{V_{in}}{V_{out}} \quad (3.1)$$

Next, to find the resistance of the converter using Equation (3.2), where R is the resistance, V_{out} is the output voltage, and P_{out} is the output power, assuming a lossless system for more straightforward analysis, where the input power is equal to the output power $P_{in} \approx P_{out} = 1000 \text{ W}$, then $R = 78.4 \Omega$.

$$R = \frac{V_{out}^2}{P_{out}} \quad (3.2)$$

To find the minimum required inductance to keep the current out of discontinuous current mode (DCM), Equation (3.3) will be used, where D is the duty cycle, R is the resistance, f_s is the switching frequency, and L_{min} is the minimum inductance. D and R found in previous steps, resulting in $L_{min} =$

104.4619 μH ; any value greater will ensure the boost converter is working in continuous current mode (CCM).

$$L_{min} = \frac{D(1-D)^2 R}{2f_s} \quad (3.3)$$

To find the minimum capacitance to get a smoother output and less voltage ripple, Equation (3.4) is used, where C_{min} is the minimum capacitance, D is the duty cycle, R is the output resistance, f_s is the switching frequency, and $\Delta V_o/V_o$ is the ripple percentage which will be set at 5%, resulting $C_{min} = 2.3689 \mu\text{F}$

$$C_{min} = \frac{D}{R(\Delta V_o/V_o)f_s} \quad (3.4)$$

One of the most critical parameters of a boost converter is the equivalent series resistor (ESR), which minimizes the output voltage ripple and plays an essential role in the control. Here, the maximum ESR will be found using Equation (3.6), but first, the maximum inductor current, which also goes through the capacitor, needs to be found using Equation (3.5), where:

- $I_{L,max}$ is the maximum inductor current.
- V_{in} is the converter's input voltage.
- D is the duty cycle.
- L is the converter's inductance.
- f_s is the switching frequency.
- R is the output resistance.

$I_{L,max} = 13.3340 \text{ A}$, after obtaining the maximum inductor current, ESR can be found using Equation (6), where $\Delta V_{o,ESR}$ is the output voltage ripple, r_C is the ESR and $I_{L,max}$ is the maximum current through the inductor, $r_C = 1.0499 \Omega$, this maximum permissible resistance, anything less would give smaller ripple.

$$I_{L,max} = \frac{V_{in}}{(1-D)^2 R} + \frac{V_{in}D}{2Lf_s} \quad (3.5)$$

$$\Delta V_{o,ESR} = I_{L,max} r_C \quad (3.6)$$

Repeating the same steps for the 250 V of the PV input source, the following results are shown in Table 3.1

Table 3.1: Open Loop Parameter of PV Source

Parameter	$V_{in} = 150 \text{ V}$	$V_{in} = 250 \text{ V}$
Vout (V)	280	280
Freq (kHz)	50	50
Ripple $\Delta V/V_o(\%)$	5	5
Power (kW)	1	1
DutyCycle	0.4643	0.1071
Resistance (Ω)	78.4	78.4
Lmin (μH)	104.4619	66.9439
Cmin (μF)	2.3689	0.5464
Imax (A)	13.3340	7.9992
ESR (Ω)	1.0499	1.7502

To design a boost converter that works for the range of 150-250 V, the inductance and capacitance must be chosen to be the highest between the two extremes, while the ESR must be selected the lowest, resulting in:

- $L_{min} = 104.4619 \mu\text{H}$
- $C_{min} = 2.3689 \mu\text{F}$
- $\text{ESR} = 1.04999 \Omega$

To ensure that the boost is working correctly, far from DCM, and has a small ripple, a factor of 1.5 will be multiplied by the inductance and capacitance while the ESR is divided by 1.5.

- $L_{PV} = 156.6929 \mu\text{H}$
- $C_{PV} = 3.5534 \mu\text{F}$
- $\text{ESR}_{PV} = 696.6 \text{ m}\Omega$

3.5.1.2 Battery Source Open Loop Analysis

The second input of the system is the battery source, which also ranges from 48 V to 52 V. Another DC-DC boost converter will be used to boost the voltage to the same output of the PV source to combine both sources as one source; in doing so, the switching frequency must be the same to ensure smoother output. The analysis is similar to the PV input, which was performed twice to consider the two extremes. The power generated by the battery is the same as the PV.

With the following parameters known:

- $V_{in} = 48\text{-}52 \text{ V}$
- $V_{out} = 280 \text{ V}$
- $f_s = 50 \text{ kHz}$

- $P_{in} = 1 \text{ kW}$

Starting with the 48 V input, the duty cycle can be found using Equation (3.1), $D = 0.8286$, then finding the resistance using Equation (3.2), $R = 78.4 \Omega$. For the inductor current to stay in CCM, the minimum inductance must be found using Equation (3.3), $L_{min} = 19.0846 \mu\text{H}$; choosing the ripple percentage of 5% to match the ripple of the PV source, the minimum capacitance is $C_{min} = 4.2276 \mu\text{F}$, found using Equation (3.4), and finally, finding the maximum current going through the inductor to find the ESR, using Equation (3.5) and Equation (3.6), $I_{L, max} = 41.6805 \text{ A}$, $ESR = 335.8885 \text{ m}\Omega$. The same analysis was repeated for the 52 V input; the results are shown in Table 3.2.

Table 3.2: Open Loop Parameter of Battery Source

Parameter	$V_{in} = 48 \text{ V}$	$V_{in} = 52 \text{ V}$
Vout (V)	280	280
Freq (kHz)	50	50
Ripple $\Delta V/V_o(\%)$	5	5
Power (kW)	1	1
DutyCycle	0.8286	0.8143
Resistance (Ω)	78.4	78.4
Lmin (μH)	19.0846	22.0153
Cmin (μF)	4.2276	4.1546
Imax (A)	41.6805	35.5084
ESR (mΩ)	335.8885	394.2729

Similar to the PV analysis, the inductance and capacitance must be chosen to be the highest between the two extremes, while the ESR must be selected as the lowest, resulting in:

- $L_{min} = 22.0153 \mu\text{H}$
- $C_{min} = 4.2276 \mu\text{F}$
- $ESR = 335.8885 \text{ m}\Omega$

Once again, to ensure that the boost is working correctly and far from DCM and to ensure a small ripple, a factor of 1.5 will be multiplied by the inductance and capacitance while the ESR is divided by 1.5.

- $L_B = 33.0230 \mu\text{H}$
- $C_B = 6.3414 \mu\text{F}$
- $ESR_B = 223.9257 \text{ m}\Omega$

3.5.2 Output Buck Converters

3.5.2.1 Buck Converter of High Voltage Output Terminal

At the output side of the multiport converter, there are two buck converters present: the high voltage side, rated at 380 V, and the low voltage side, rated at 12 V. The 380 V output port was responsible for charging an electric vehicle, while the 12 V output port was responsible for powering up a small household. A buck converter was added for each output side to control the output voltage while the loads changed by changing the duty cycle of the converter.

For the high voltage side, the input voltage from the transformer is 650 V at a frequency of 50 kHz, while the output is 380 V with a 1% ripple voltage $\left(\frac{\Delta V_o}{V_o}\right)$. The switching frequency of the high-voltage buck converter was 30 kHz. At first, this frequency was chosen based on the high voltage side power output range, which was 500-2000 W. This frequency suited the range of output powers while maintaining low switching losses. This range of output power was used since it modeled the different charging modes of the electric vehicle, where, from 500-1000 W, it charged at low currents and, from 1500-2000 W, the electric vehicle charged faster since it consumed higher power, during nighttime where the household approximately consumes little to no power, the EV can quickly charge from 1500-2000 W. The chosen frequency gave minimal losses at minimum and maximum power ratings while maintaining a suitable capacitor and inductor sizing. Moreover, the switching frequency should not be similar to another frequency present in the converter to prevent unwanted interference and oscillations such as electromagnetic interference.

The analysis of the buck converter was tackled twice for each of the high and low voltage outputs; the analysis was done for two extreme cases; the first case was minimum input voltage ($V_{s,min}$) with maximum output voltage ($V_{o,max}$), and the second extreme was the maximum input voltage ($V_{s,max}$) with minimum output voltage ($V_{o,min}$). A voltage fluctuation of 110%-90% was considered while the minimum and maximum voltages were calculated, respectively.

The two extreme cases were used to choose the LC filter on the buck converters to ensure maximum reliability and efficiency under all possible circumstances, especially under varying load conditions.

A detailed analysis was carried out on the extreme case with maximum input voltage ($V_{s,max}$) and minimum output voltage ($V_{o,min}$), where at the minimum output voltage, the power consumed was minimal at 500 W.

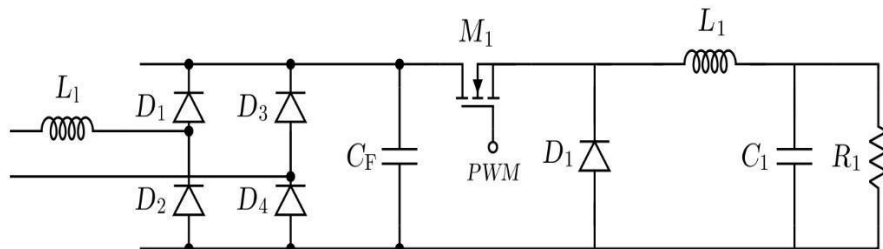


Figure 3.3: Output Buck Converter Circuit

As shown in Fig. 3.3 in the circuit above, an inductor was connected in series with the square wave voltage source; this inductor represented the leakage inductance L_l found in the transformer; in ideal calculations, this inductor is usually neglected, but in real life, it cannot be neglected. This inductance is due to the magnetic flux that was not coupled between the primary and secondary winding (high voltage side) and between primary and tertiary winding (low voltage side). The real value cannot be mathematically derived, but in real life, it can be physically measured by the short circuit test or an LCR meter while ideal conditions are taken.

At first $V_{s,max} = 715 V$, $V_{o,min} = 342 V$ by the use of Equation (3.7), the duty cycle was $D = 0.478$

$$D = \frac{V_s}{V_o} \quad (3.7)$$

The output resistance was found easily in this case since the output voltage and power were known by the use of Equation. (3.8) the output resistance $R = 233.93 \Omega$

$$R = \frac{V_o^2}{P} \quad (3.8)$$

Now, to find the minimum inductance to keep the inductor out of discontinuous current mode, DCM Equation (3.8) was used. Duty cycle (D) and resistance (R) were found, and (f) is the switching frequency of the converter, which was 30kHz. $L_{min} = 2.03 mH$. A 1.2 factor was multiplied by the minimum inductance value to ensure the inductor will stay in continuous conduction mode (CCM), and to have a smaller ripple current $L = 2.44 mH$.

$$L_{min} = \frac{(1-D)R}{2f} \quad (3.9)$$

The use of a capacitor decreases the voltage ripple and smoothes the output voltage that feeds the output load. First, the desired output ripple is $\frac{\Delta V_o}{V_o} = 1\%$. By using Equation (3.10), the minimum capacitor value is $C_{min} = 2.97 \mu F$. A 1.5 factor is multiplied by the minimum capacitor value to ensure smoother output voltage and smaller ripple. $C = 4.16 \mu F$

$$C_{min} = \frac{1-D}{8L\left(\frac{\Delta V_o}{V_o}\right)f^2} \quad (3.10)$$

One of the most pivotal steps was to find the equivalent series resistor (ESR) of the capacitor to minimize the ripple in the output current. First, the maximum current going through the inductor $I_{L,max}$ was found, where the maximum inductor current was the DC current passing through the

output load plus the ripple current divided by two. By using Equation (3.11) $I_{L,max} = 2.68 A$.

$\Delta V_{o,ESR}$ is assumed to be the same as the ripple voltage $\left(\frac{\Delta V_o}{V_o}\right)$, which was 1% of the output voltage, so $\Delta V_{o,ESR} = 3.42 V$, finally $ESR = 1.28 \Omega$, this value was multiplied by a factor of 0.5 to ensure better output current, so $ESR = 0.64 \Omega$

$$I_{L,max} = V_o \left(\frac{1}{R} + \frac{1-D}{2Lf} \right) \quad (3.11)$$

$$\Delta V_{o,ESR} = I_{L,max} \times ESR \quad (3.12)$$

Finally, the filter capacitor, which was the capacitor between the full wave rectifier and the buck converter, was used to smooth out the rectified voltage to deliver a better DC voltage to the converter. It was calculated by using Equation (3.13) where (f_r) was the ripple frequency, which was defined as being twice the switching frequency, $I_{Load} = 5.26 A$, which was calculated by dividing the maximum power by the rated output voltage. Finally, $V_R = 3.8 V$, which was the ripple output voltage. After these values were plugged into Equation (3.13), $C_{filter} = 23.1 \mu F$.

$$C_{filter} = \frac{I_{Load}}{f_r \times V_R} \quad (3.13)$$

The filter capacitor was very important for the converter, and its effect cannot be disregarded, in both high and low voltage sides, because it helps to deliver to the buck converter an almost pure DC voltage with minimal ripple due to filtering most ripple and fluctuations that accompanied the voltage signal supplied from the transformer.

The same analysis was carried out on the second case, which was the minimum input voltage ($V_{s,min}$) with maximum output voltage ($V_{o,max}$). The calculations for both cases were displayed in the tables below.

Table 3.3: Buck Converter Parameters at Maximum Input Voltage and Minimum Output Voltage

V_s (V)	715
V_{out} (V)	342
Freq (kHz)	30
Ripple $\Delta V/V_o(\%)$	1
Power(W)	500
Duty Cycle (D)	0.48
Resistance (Ω)	233.93
L_{min}(mH)	2.03
L*1.2(mH)	2.44
C_{min}(μF)	2.97
C*1.2(μF)	4.16
ESR(Ω)	1.28
ESR*0.5(Ω)	0.638

Table 3.4: Buck Converter Parameters at Minimum Input Voltage and Maximum Output Voltage

V_s (V)	585
V_{out} (V)	418
Freq (kHz)	30
Ripple $\Delta V/V_o(\%)$	1
Power(kW)	2
Duty Cycle (D)	0.71
Resistance (Ω)	87.36
L_{min}(mH)	0.416
L*FACTOR(mH)	0.499
C_{min}(μF)	7.95
C*FACTOR(μF)	11.1
ESR(Ω)	0.477
ESR*FACTOR(Ω)	0.238

For the high voltage buck converter design, (L_{min}) was multiplied by a factor of 1.2 to get the desired inductance, while (C_{min}) was multiplied by a factor of 1.4 to get the desired capacitance, ensuring that the converter operates in CMM while further decreasing current and voltage ripples.

As shown in the tables above, the inductor and capacitor values changed in each case, so the maximum inductor and maximum capacitor value were chosen to model the buck converter at the high voltage output side; the higher value was chosen to withstand both extreme cases while still keeping the converter in CCM and delivering the rated voltage. The filter capacitor is the same in

both cases and was unaffected by the different voltage input and output values since its calculation was based on the rated values of the converter.

The leakage inductance was the final piece of the puzzle for the open loop design to work; without the leakage inductance, the current on the filter capacitor reached unimaginable values like 50 kA; this was because the current incoming from the transformer was building up in the capacitor and does not have enough time to discharge.

The addition of the leakage inductance in both high and low-voltage buck converters was the solution to the high current building up in the filter capacitor. This is because the inductor opposed current changes by inducing an opposing electromotive force (V_L); hence, it did not allow the current to build up in the capacitor and reach high amplitudes.

$$V_L = L \frac{di}{dt} \quad (3.14)$$

Table 3.5: Inductor and Capacitor Parameters for The High Voltage Buck Converter

Inductor (mH)	2.44
Capacitor (μF)	11.1
Filter Capacitor (μF)	23.1
Leakage Inductance (μH)	10

The leakage inductance was designed based on the maximum ripple current that the filter capacitor can endure; the same procedure was used for both low and high-voltage sides.

3.5.2.2 Buck Converter of Low Voltage Output Terminal

For the low voltage side, the output was designed to supply 12 V to a small household, and this means that the power varies with a great range, depending on several factors. The output power range that the converter was based on is from 100-500 W. As seen, the upper bound is five times the lower bound for the output power. This range was capped at 500 W since this port supplies a small household where 1-2 people live, and no high-power electrical appliances will be used. The AC voltage incoming from the tertiary transformer winding was 30 V. This value was chosen so the buck converter can easily step it down to 12 V at high efficiency, which occurs at a moderate duty cycle, typically between 0.4-0.7.

The switching frequency for the low-voltage buck converter was 90 kHz. This frequency was the most suitable for our application and power ratings, with respect to the inductor and capacitor sizing, especially the capacitor, because at the low voltage side, the rated load current is 41.67 A, and according to Equation (3.15), the frequency should be relatively high to decrease the capacitance.

$$i = C \frac{dV}{dt} \quad (3.15)$$

Moreover, the switching frequency was different from the switching frequency of the high voltage buck converter, which was 30 kHz, to avoid disturbances and harmonic distortions.

The same analysis applied on the high voltage side for the two cases of minimum input voltage ($V_{s,min}$) with maximum output voltage ($V_{o,max}$) and maximum input voltage ($V_{s,max}$) with minimum output voltage ($V_{o,min}$) was under study. A 110%-90% voltage fluctuation was taken into consideration while calculating the minimum and maximum voltages, respectively. As done previously, the buck converter parameter was calculated for each extreme case, and then the largest value for both inductor and capacitor was chosen to successfully design the converter and keep it operating at CCM while it delivered rated output voltage smoothly.

Table 3.6: Buck Converter Parameters at Maximum Input Voltage and Minimum Output Voltage

V_s (V)	33.00
V_{out} (V)	10.80
Freq (kHz)	90
Ripple $\Delta V/V_o(\%)$	1
Power(W)	100
Duty Cycle (D)	0.33
Resistance (Ω)	1.17
L_{min}(μH)	4.36
L*FACTOR(μH)	6.54
C_{min}(mF)	0.159
C*FACTOR(μF)	0.191
ESR($m\Omega$)	7
ESR*FACTOR($m\Omega$)	3.50

Table 3.7: Buck Converter Parameters at Minimum Input Voltage and Maximum Output Voltage

V_s (V)	27.00
V_{out} (V)	13.20
Freq (kHz)	90
Ripple $\Delta V/V_o(\%)$	1
Power(W)	500
Duty Cycle (D)	0.49
Resistance (Ω)	0.35
L_{min}(μH)	0.99
L*FACTOR(μH)	1.48
C_{min}(mF)	0.531
C*FACTOR(μF)	0.638
ESR($m\Omega$)	2.09
ESR*FACTOR($m\Omega$)	1.05

For the low voltage buck converter design, (L_{min}) was multiplied by a factor of 1.5 to get the desired inductance, while (C_{min}) was multiplied by a factor of 1.2 to get the desired capacitance, ensuring that the converter operates in CMM, with an additional decrease in current and voltage ripples.

Table 3.8: Inductor and Capacitor Parameters for The Low Voltage Buck Converter

Inductor (μH)	6.54
Capacitor (mF)	0.638
Filter Capacitor (mF)	0.233
Leakage Inductance (μH)	2

3.6 Closed Loop Analysis

After the open loop design was conducted, constant voltage monitoring and a feedback system were needed to ensure high accuracy, minimum error, and better durability for both input and output converters.

The type of control used across all the designed converters is voltage-mode control; it was more convenient and suitable than current control because the loads must have constant voltage no matter the current fluctuations. Also, when constant voltage is maintained, the converter can supply a wider range of loads, which is desired since the loads drastically vary.

Also, voltage supply control offers simpler control mechanism than current control because precise current control requires shunt resistors with integrated current sensing to ensure accurate results. In

comparison, the feedback system for voltage supply control offered a simpler solution and accurate results by constantly comparing the output voltage to a fixed reference, resulting in an error signal, which is then converted to adjust the duty cycle of the converter accordingly. This ensured accurate and efficient results while having a simpler feedback loop than current-mode control.

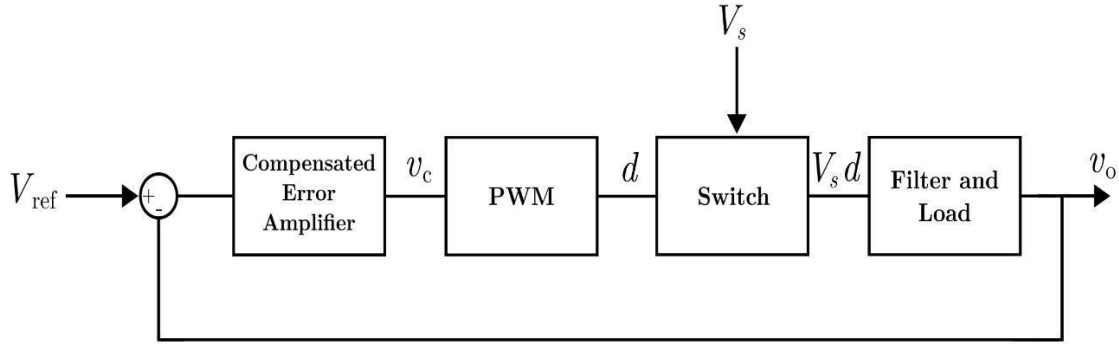


Figure 3.4: Control Block Diagram for Both Buck and Boost Converters

Analog control was used to control both buck and boost converters, respectively. The feedback loop was comprised of the following procedure to ensure maximum accuracy:

- i) Output voltage (v_o) is sensed, then enters the negative terminal of the analog controller and is compared with a fixed reference voltage (v_{ref}); the output of the error amplifier is a voltage signal denoted as (v_c), this value represents the difference between the desired output (v_{ref}) and the actual output (v_o), which is the steady-state error.
- ii) (v_c) Enters the PWM block. The PWM block produces triangular pulses, the v_c signal is compared with these triangular pulses, resulting in an output of rectangular pulse signals, as seen in Figure 3.5. The width of these pulses is proportional to v_c . As v_c increases, the width of the generated rectangular pulses increases; hence, the duty cycle of the converter is greater, and vice versa.

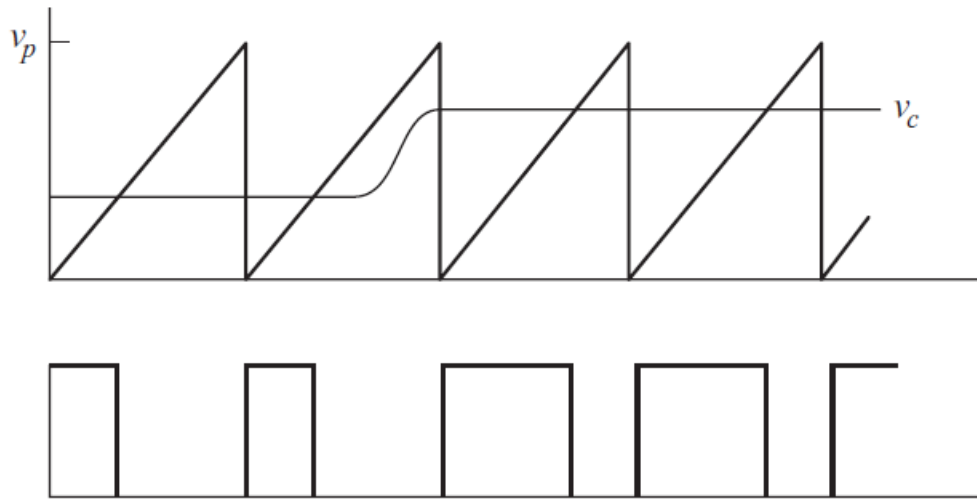


Figure 3.5: PWM Triangular Pulses, Reference Signal and Modulated Rectangular Output [14]

- iii) The output of the PWM block is the adjusted duty cycle (d), which is represented by the modulated rectangular pulses.
- iv) This attenuated duty cycle (d) is fed back to the gate of the IGBT switch, while the source of the switch is supplied by the input voltage (v_s).
- v) Finally, the voltage supplying the load is $v_s d$ for the buck converter and $\frac{v_s}{1-d}$ for the boost converter.

This voltage supply control was simply achieved by keeping the output voltage monitored and adjusting the duty cycle accordingly. This was executed in both the boost and buck converters found in the system.

3.6.1 Input Boost Converters

Once the initial parameters for the open loop analysis have been established, further analysis will be conducted to ensure the system's output voltage and current is constant and stable throughout the whole operation; the analysis will be conducted across each system component.

3.6.1.1 Maximum Power Point Tracker (MPPT) Analysis

A Maximum Power Point Tracker (MPPT) must be implemented to ensure the solar module delivers its maximum potential power. The MPPT adjusts the operating point of the solar module to align with its maximum power by optimizing the voltage and current. The MPPT ensures that the system is operating at its highest efficiency. To implement the MPPT, a boost converter with a switching frequency of 50 kHz to match the control stage is chosen.

The input ranges from 150 V to 250 V, and the power must be maximized at 1 kW. The system is not a conventional boost because the intent is to maximize the power; the duty cycle can not have a constant value, forcing finding a non-conventional method for calculating the parameters of the boost converter. Figure 3.6 shows an additional capacitor for the boost converter, which is added to ensure the outgoing voltage does not fluctuate due to changes in sunlight.

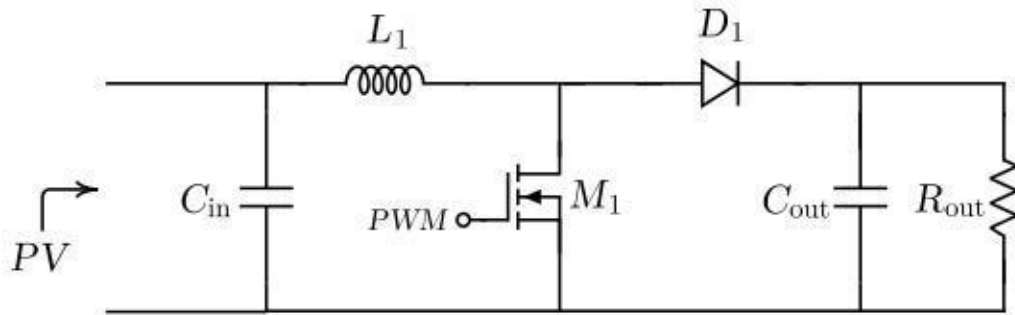


Figure 3.6: MPPT Boost Circuit

To start the analysis, a PV module that meets the requirements is chosen to analyze, as shown in Table 3.9.

Table 3.9: PV Panel Specifications

Parameter	Value
Model	PMH530W
Number of Cells	144
Nominal Power (P_{\max}) (W)	530
Max Power Voltage (V_{mp}) (V)	41.27
Max Power Current (I_{mp}) (A)	12.85
Open-Circuit Voltage (V_{oc}) (V)	49.15
Short-Circuit Current (I_{sc}) (A)	13.74

The PV module is connected, as shown in Figure 3.7, to two strings with one module each to give a total power of 1060 W. A bypass diode is connected in parallel to the panels to allow the current to conduct in case of shading, and the capacitor to limit any fluctuations.

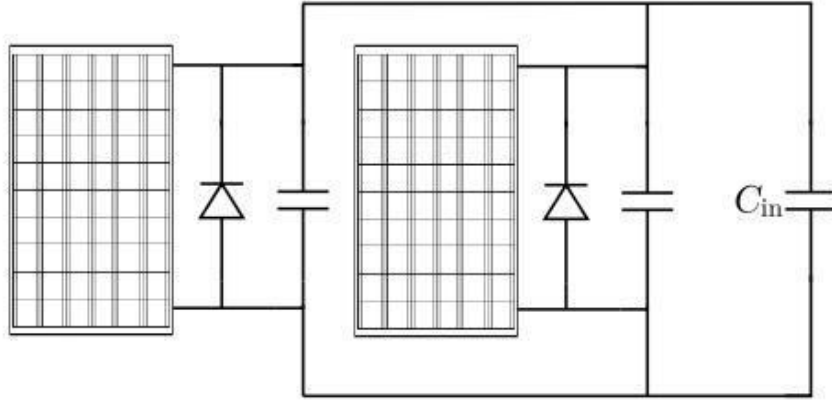


Figure 3.7: PV Array System

The PV module specification is at Standard Test Conditions (STC), i.e., at irradiance 1000 W/m^2 , air mass 1.5, and cell temperature of 25°C . To calculate the parameters, the specifications must be found at an irradiance of 50 W/m^2 ; the analysis must simultaneously be conducted for both 1000 W/m^2 and 50 W/m^2 , choosing the output and input voltage ripple 5% and 40% for the output current.

1000 W/m^2	50 W/m^2
$P_{\max} = 1060 \text{ W}$ $V_{mp} = 41.27 \text{ V}$ $I_{mp} = 2 \text{ strings} * 12.85 = 25.7 \text{ A}$ $R_{mp} = \frac{V_{mp}}{I_{mp}} = 1.6058 \Omega$ $R_{out} = 2.5 * R_{mp} \text{ at } 50 \text{ W/m}^2 = 65.0765 \Omega$ $D_{mp} = 1 - \sqrt{\frac{R_{mp}}{R_{out}}} = 0.8429$ $V_{out} = \frac{V_{mp}}{1-D} = 262.6989 \text{ V}$ $I_{out} = \frac{V_{out}}{R_{out}} = 4.0368 \text{ A}$ $\Delta V_{in} = 5\% * V_{mp} = 2.0635 \text{ V}$ $\Delta V_{out} = 5\% * V_{out} = 13.1349 \text{ V}$ $R_{in} = R_{out} * (1 - D_{mp})^2 = 18.8409 \Omega$ $C_{in} = \frac{4V_{mp}D_{mp}}{\Delta V_{in}R_{in}f_s} = 71.5804 \mu\text{F}$ $C_{out} = \frac{2V_o D_{mp}}{\Delta V_o R_{out} f_s} = 10.3620 \mu\text{F}$	$P_{\max} = 1060 \text{ W} * \left(\frac{50 \text{ W/m}^2}{1000 \text{ W/m}^2} \right) = 53 \text{ W}$ $V_{mp} = 41.27 * 0.9 = 37.143 \text{ V}$ $I_{mp} = \frac{P_{\max}}{V_{mp}} = 1.4269 \text{ A}$ $R_{mp} = \frac{V_{mp}}{I_{mp}} = 26.0306 \Omega$ $R_{out} = 2.5 * R_{mp} \text{ at } 50 \text{ W/m}^2 = 65.0765 \Omega$ $D_{mp} = 1 - \sqrt{\frac{R_{mp}}{R_{out}}} = 0.3675$ $V_{out} = \frac{V_{mp}}{1-D} = 58.7241 \text{ V}$ $I_{out} = \frac{V_{out}}{R_{out}} = 0.9024 \text{ A}$ $\Delta I_{out} = 40\% * I_{out} = 0.3610 \text{ A}$ $L = \frac{V_{mp}D_{mp}}{2\Delta I_{in}f_s} = 378.1178 \mu\text{H}$

The final parameters of the MPPT boost converter will be taken as the following:

- $C_{in} = 75 \mu F$
- $C_{out} = 15 \mu F$
- $L = 400 \mu H$
- $R_{out} = 65 \Omega$

3.6.1.2 Perturb and Observe Algorithm

A Perturb and Observe (P&O) Algorithm will be implemented to achieve the maximum power from the PV arrays. The algorithm is described in Figure 3.8, and the controller circuit is shown in Figure 3.9. The algorithm measures the present voltage and current value, calculates the power, and compares it with the preceding voltage and power values. Depending on the results, an incremental difference of the duty cycle $\Delta D = 0.1$ is either added or subtracted.

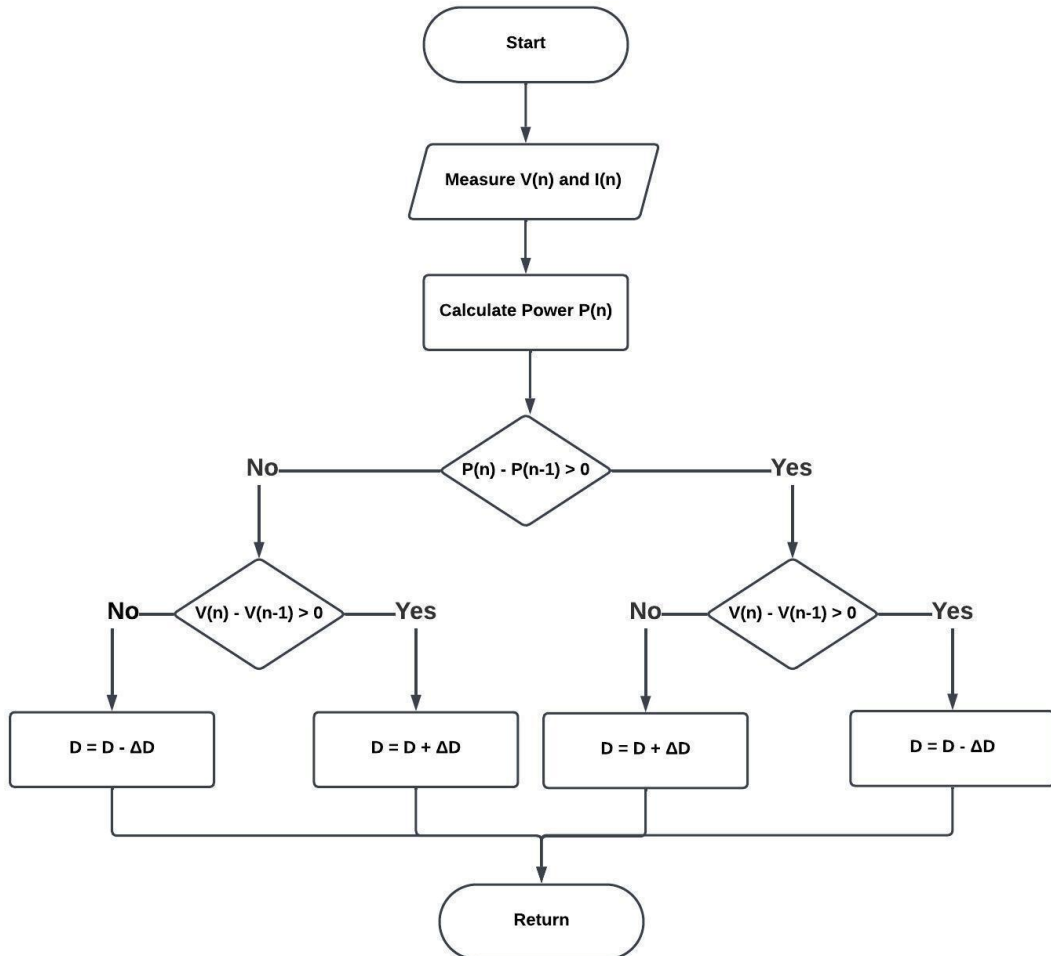


Figure 3.8: Perturb and Observe Algorithm

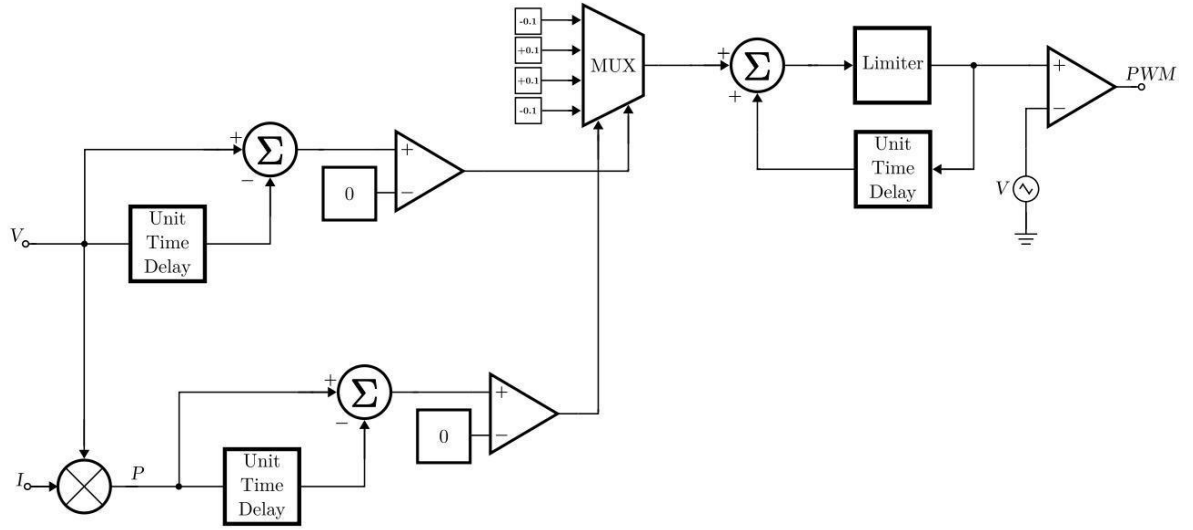


Figure 3.9: P&O MPPT Controller

3.6.1.3 PV Source Closed Loop Analysis

To effectively control the PV source linked to the boost converter, the transfer function of the boost converter must be implemented. This approach allows for a comprehensive understanding of how the input parameters influence the output behavior; the transfer function of a boost converter can be shown in Equation (3.16), where:

- V_{in} is the input voltage
- D is the duty cycle
- R is the output resistance
- C is the capacitance
- r is the ESR of the capacitor
- L_e is shown in Equation (3.8)
- L is the inductance

$$\frac{v_o}{d} = \frac{V_{in}}{(1-D)^2} \left(1 - \frac{sL_e}{R}\right) \frac{1+srC}{L_e C [s^2 + s(\frac{1}{RC} + \frac{r}{L_e}) + \frac{1}{L_e C}]} \quad (3.16)$$

$$L_e = \frac{L}{(1-D)^2} \quad (3.17)$$

With the previously obtained parameters of the PV boost converter, the transfer function is graphed using MATLAB, shown in Figure 3.10.

- $V_{in,PV} = 150 \text{ V}$
- $D_{PV} = 0.4643$
- $R_{PV} = 78.4 \Omega$
- $L_{PV} = 156.6929 \mu\text{H}$
- $C_{PV} = 3.5534 \mu\text{F}$
- $\text{ESR}_{PV} = 696.6 \text{ m}\Omega$

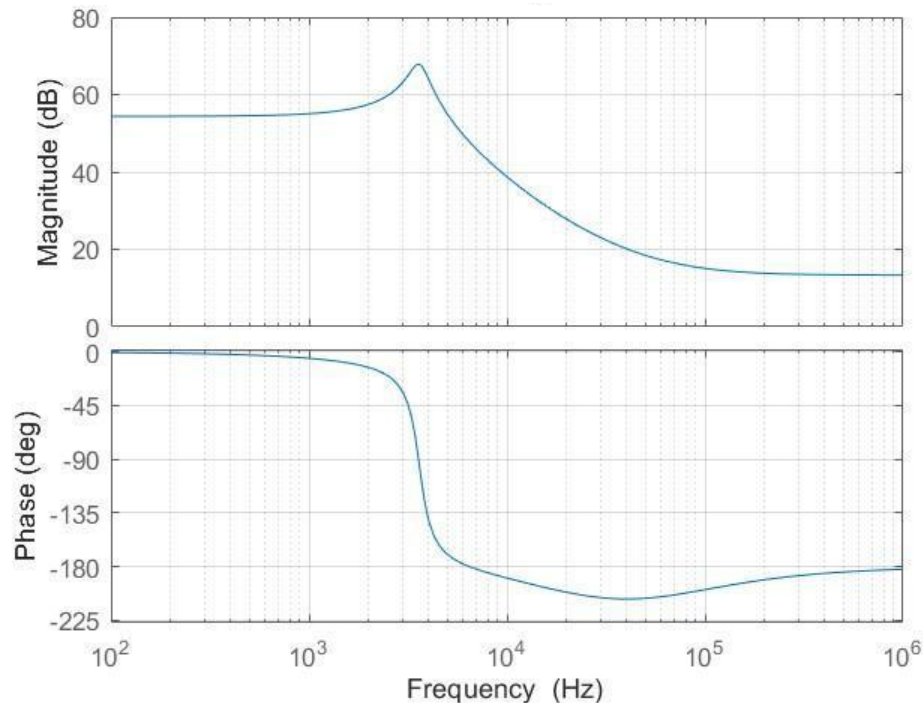


Figure 3.10: Bode Plot of PV Boost Converter Transfer Function at 150 V Before Modification

From Figure 3.10, the system is unstable after 6 kHz because the phase of the system exceeds the -180° limit. To control the system, the parameters of the boost converter are adjusted for better controllability; the three parameters that can be controlled are inductance, capacitance, and ESR. The ESR plays a crucial role in deciding the system's stability, and it affects the phase margin of the system, which is desired to be low; here, ESR was chosen to ensure stability and avoid low phase margin. The capacitance mainly affects the gain and phase margin. The inductance also plays an essential role in deciding the crossover frequency, where L affects the placement of the right half plane (RHP) zero, which drives the system into instability if the crossover frequency were taken after the RHP zero. After adjusting to meet the previous criteria and taking into consideration the boundary achieved in the open loop analysis, the newly obtained values through trial and error are:

- $L_{PV} = 160 \mu\text{H}$
- $C_{PV} = 50 \mu\text{F}$
- $\text{ESR}_{PV} = 149 \text{ m}\Omega$

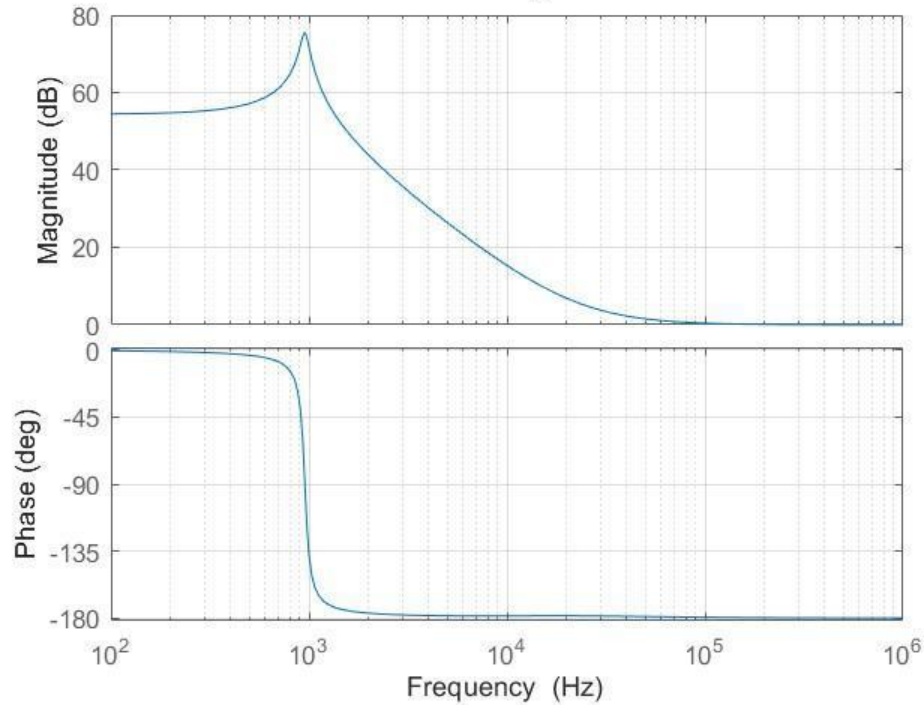


Figure 3.11: Bode Plot of PV Boost Converter Transfer Function at 150 V After Modification

From Figure 3.11, the system is now modified as it can be seen it crosses 0 dB and the phase is larger than -180° . A suitable compensator must be chosen to control the system. Type-III compensator is an excellent choice in this case since the phase margin of the system is quite large and requires a large phase boost, which the Type-III compensator can provide. Type-III compensator, which can be seen in Figure 3.12, creates two poles and two zeros depending on the values of the capacitances and resistors. Three main parameters must be obtained to find the parameters of the compensator: the crossover frequency, gain, and phase margin.

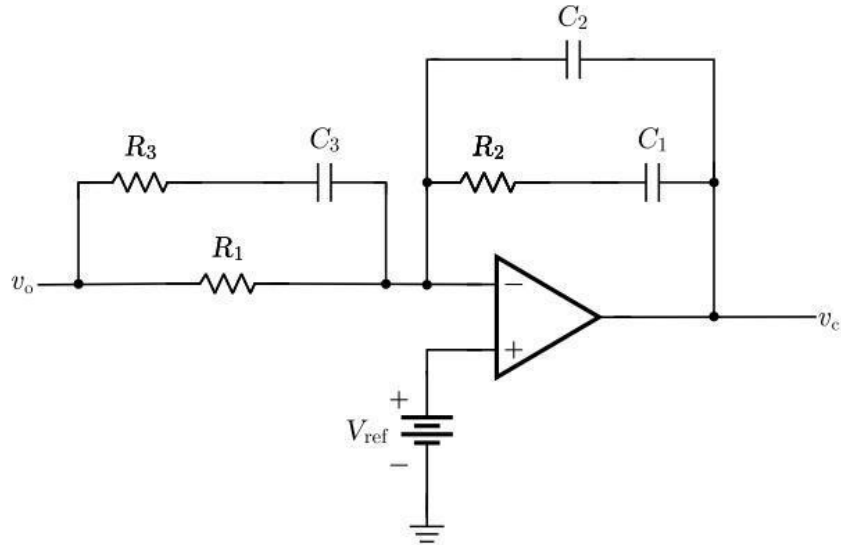


Figure 3.12: Type-III Compensator

The crossover frequency, f_{co} , is usually set ($\frac{1}{5} - \frac{1}{20}$) of the switching frequency and, as mentioned earlier, it also depends on the RHP zero; using MATLAB, the RHP zero is located at $f = 22.3804$ kHz, taking one-tenth of frequency $f_{co} = 5$ kHz which is well under the RHP zero frequency. After choosing the crossover frequency, the gain margin and phase margin can be obtained from Figure 3.11 at f_{co} ; the gain margin is $|G(jw)| = 26.3$ dB, and the phase margin of the converter is $\theta_{converter} = -178^\circ$. Before finding the parameters of the compensator, the compensated angle and the K-factor must be found using Equation (3.18) and Equation (3.19), where θ_{comp} is the compensated angle, $\theta_{converter}$ is the converter's angle, and $\theta_{phase\ margin}$ is how much will the system be shifted away from instability, i.e., -180° , the phase margin is typically chosen to be $\theta_{phase\ margin} = 45^\circ$ as it provides a good damping ratio, stability, and moderate response speed.

The compensated angle can be found through Equation (3.18) $\theta_{comp} = 223^\circ$ and the K-factor using Equation (3.19) $K = 23.1138$.

$$\theta_{comp} = \theta_{phase\ margin} - \theta_{converter} \quad (3.18)$$

$$K = \left[\tan\left(\frac{\theta_{comp} + 90}{4}\right) \right]^2 \quad (3.19)$$

The values of the capacitors and resistances can be found from the K-factor and the crossover frequency using the following equations and by assuming $R_1 = 1 \text{ k}\Omega$

$$R_2 = \frac{|G(j\omega_{co})|R_1}{\sqrt{K}} \quad (3.20)$$

$$C_1 = \frac{\sqrt{K}}{2\pi f_{co} R_2} \quad (3.21)$$

$$C_2 = \frac{1}{2\pi f_{co} R_2 \sqrt{K}} \quad (3.22)$$

$$C_3 = \frac{\sqrt{K}}{2\pi f_{co} R_1} \quad (3.23)$$

$$R_3 = \frac{1}{2\pi f_{co} C_3 \sqrt{K}} \quad (3.24)$$

- $R_{1,PV} = 1 \text{ k}\Omega$
- $R_{2,PV} = 4.2960 \text{ k}\Omega$
- $R_{3,PV} = 43.2641 \Omega$
- $C_{1,PV} = 35.6223 \text{ nF}$
- $C_{2,PV} = 1.5412 \text{ nF}$
- $C_{3,PV} = 153.0333 \text{ nF}$

It is worth noting that repeating the previous step at $V_{in} = 250 \text{ V}$ will result in a gain margin of 31.2 dB and a phase margin of -169° , which will not be sufficient in the case of a 150 V input. However, the compensator parameters of the 48 V input will be sufficient for both extremes.

3.6.1.4 Battery Source Closed Loop Analysis

Following the same procedure as the previous one and using the same transfer function in Equation (3.16) and with parameters found in open loops analysis of the battery source, the bode plot of the system can be seen in Figure 3.13.

- $V_{in,B} = 48 \text{ V}$

- $D_B = 0.8286$
- $R_B = 78.4 \Omega$
- $L_B = 33.0230 \mu\text{H}$
- $C_B = 6.3414 \mu\text{F}$
- $\text{ESR}_B = 223.9257 \text{ m}\Omega$

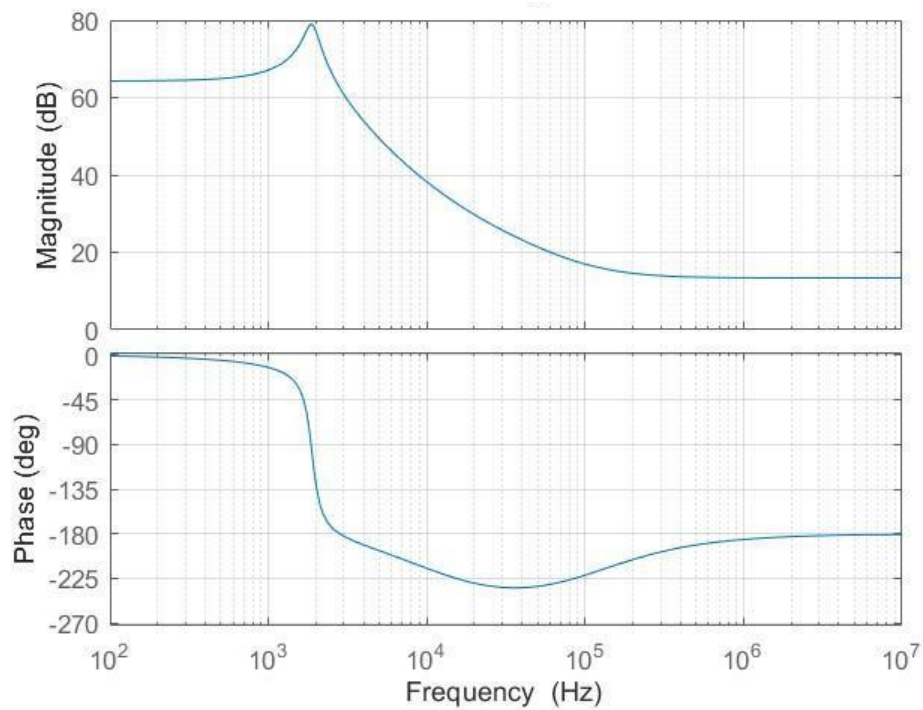


Figure 3.13: Bode Plot of Battery Boost Converter Transfer Function at 48 V Before Modification

Once again, the system is unstable after 3 kHz because the phase of the system exceeds -180° ; following the same rules and procedure in the PV closed-loop analysis, the newly found parameters are:

- $L_B = 33 \mu\text{H}$
- $C_B = 300 \mu\text{F}$
- $\text{ESR}_B = 47.8 \text{ m}\Omega$

The improved system can be shown in Figure 3.14. The system requires a large amount of compensation that the Type-III compensator can provide. The RHP zero is located at $f = 11.1082 \text{ kHz}$, and through trial and error, it was found the most suitable cross-over frequency is $f_{co} = 2.5 \text{ kHz}$, from Figure 3.14 at f_{co} ; the gain margin is $|G(jw)| = 26.4 \text{ dB}$, and the phase margin of the converter is $\theta_{converter} = -179^\circ$. Using the same phase margin of 45° , the compensated angle is $\theta_{comp} = 224^\circ$ and the K-factor using Equation (3.19) $K = 24.1588$. The resistances and capacitances can be found in Equation (3.20) - (3.24).

- $R_{1,B} = 1 \text{ k}\Omega$
- $R_{2,B} = 4.2507 \text{ k}\Omega$

- $R_{3,B} = 41.3928 \Omega$
- $C_{1,B} = 73.6135 \text{ nF}$
- $C_{2,B} = 23.0471 \text{ nF}$
- $C_{3,B} = 312.9088 \text{ nF}$

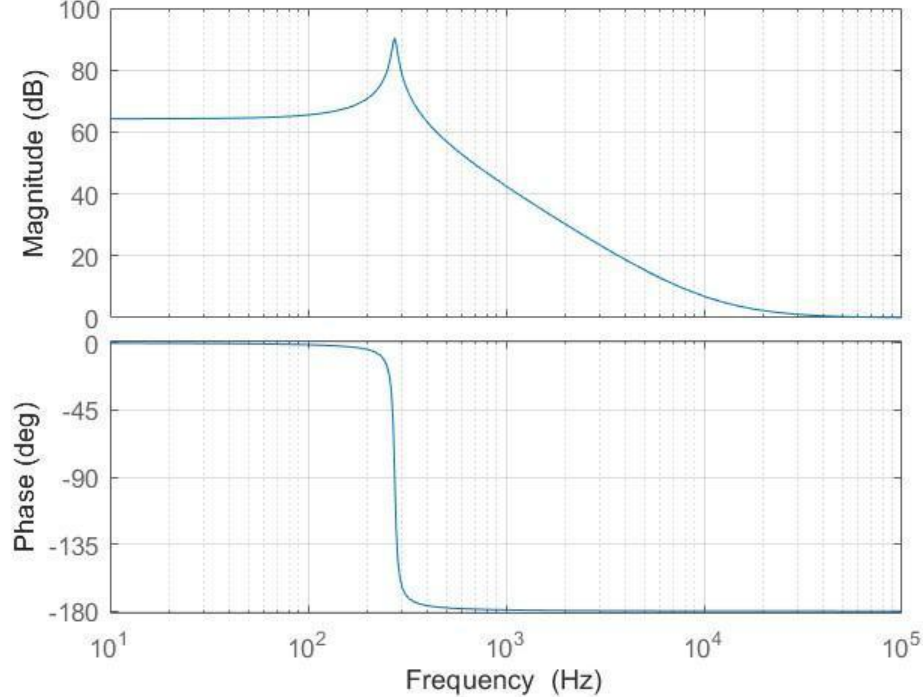


Figure 3.14: Bode Plot of Battery Boost Converter Transfer Function at 48 V After Modification

Similar to the PV analysis, the other range of input $V_{in} = 52 \text{ V}$ parameters will not be sufficient for 48 V input, but the parameters of the 48 V will be sufficient for both cases.

3.6.2 Output Buck Converters Closed Loop

3.6.2.1 Buck Converter Closed Loop Design

The following is the transfer function of the buck converter

$$G(s) = \frac{v_o(s)}{d(s)} = \frac{v_s}{LC} \left[\frac{1+sESRC}{s^2 + s\left(\frac{1}{RC} + \frac{ESR}{L}\right) + 1/LC} \right] \quad (3.25)$$

From the transfer function, it is obvious that the system has a single zero and two poles due to the numerator being of the first order and the denominator being of the second order; the zero and the two poles of the system are represented below, where the zero is denoted as s_{z1} , and the poles are denoted as $s_{p1,2}$, since the poles are a complex conjugate pair.

$$s_{z1} = -\frac{1}{ESRC} \quad (3.26)$$

$$s_{p_{1,2}} = \frac{-\left(\frac{1}{RC} + \frac{ESR}{L}\right)}{2} \pm j \sqrt{\frac{1}{LC} - \left(\frac{\frac{1}{RC} + \frac{ESR}{L}}{2}\right)^2} \quad (3.27)$$

By observing the poles of the buck converter it contains both a real and imaginary part, where the real part is responsible for damping, and the imaginary part is responsible for the oscillating frequency where the poles occur. When the imaginary part of the poles is observed, it is seen that the poles approximately occur at the same frequency as the resonant frequency of the converter since the resonant frequency occurs at $\omega_o = \frac{1}{\sqrt{LC}}$.

As explained in the open loop design, the filter capacitor in both circuits is used to smooth out the voltage incoming from the H-bridge, supplying the converters with a DC voltage with minimal fluctuations. As shown above, the transfer function of the buck converter represents a second-order system; this is obvious because a buck converter contains only two energy storage elements.

In the case of both buck circuits, the filter capacitor raises the order of the system to become a third-order system, but the system will be approximated to a second-order system for simplicity of the design and to adjust and alter the control system of the circuit easily. Moreover, second-order system magnitude and frequency responses can be easily interpreted and comprehended; hence, approximating higher-order systems to a second-order system is of common practice and was used in designing the controller for both buck controllers.

In order to successfully conduct the closed loop design, an analog controller was designed for each circuit respectively. This was done by graphing the bode plot for each converter by using each of the converter's transfer functions.

From both the magnitude and frequency response of the bode plot, the crossover frequency (f_{co}), the magnitude (g_m) and angle ($\theta_{converter}$) at that cross-over frequency will be found. These are the parameters needed to design a tailored analog controller for each converter.

A detailed analysis of both the high and low-voltage buck converters was conducted. The open and closed-loop analysis was carried out by assuming rated input and output voltage values and the assumption that each load consumed its maximum rated power; for the high voltage, the maximum output power was 2000 W, and for the low voltage output, it was 500 W.

Below is the resulting bode plot for the open loop design for the high-voltage converter.

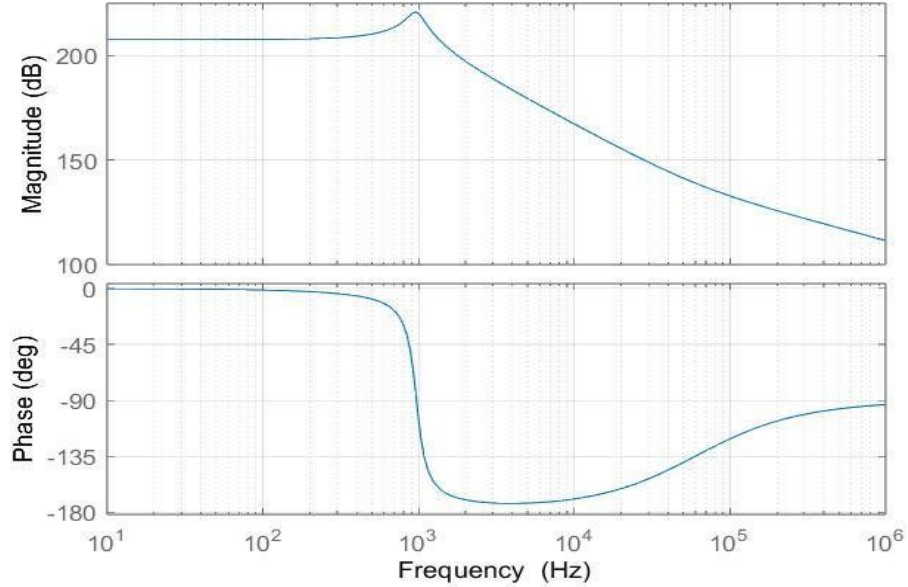


Figure 3.15: Bode Plot for High Voltage Buck Converter Before Modification

After the bode plot of the open loop design was observed from Figure 3.15, emphasizing the frequency response, a type-II error compensation controller was chosen to control the following buck converter. The type-II controller was chosen because the open loop frequency response of the converter never reaches or exceeds -180° , and the minimum phase reached was -173° , moreover, both magnitude and phase are positive at 0 Hz, hence the response is stable.

Moreover, this is an indication that the implementation of a type-II controller is sufficient, and there is no need for further error compensation; hence, there is no need for the implementation of a type-III controller.

From Figure 3.15, adjustments will be made to successfully design a controller for the following two main reasons. At first, the initial magnitude of the system or the DC gain is too high where it reaches 208 dB; this large gain value will result in unrealistic resistor values for the controller, meaning the controller may not reach stability and will not provide fast system responses.

As mentioned previously, the double pole effect of the system approximately occurs at the resonance frequency, which can be seen in the plot above. The resonance frequency is where the magnitude reaches its maximum, and the pole effect is seen in the phase response, where it starts to decrease from 500Hz till it recovers at 9 kHz. Moreover, this will result in an incorrect choice of the crossover frequency; the crossover frequency is the frequency where the controller operates. Typically, this frequency is $\frac{1}{5} - \frac{1}{20}$ of the switching frequency, the chosen crossover frequency (f_{co}), for the high voltage buck converter was 3 kHz. The gain at that frequency is denoted as g_m , while the phase angle at crossover is denoted as $\theta_{converter}$.

In order to have a successful control operation, the crossover frequency must occur after the double pole effect, which means when the frequency response of the system starts to recover and reach a stable value.

So, the poles of the system should be shifted to the left to occur at lower frequencies while also decreasing the gain. This was done by manipulating the values of the inductor, capacitor, and ESR since, as shown in the transfer functions, these parameters dictate the gain, zero, and pole placements of the bode plot.

After constant manipulation of the parameters mentioned, the following are the closed loop parameters of the circuit, along with the adjusted bode plot.

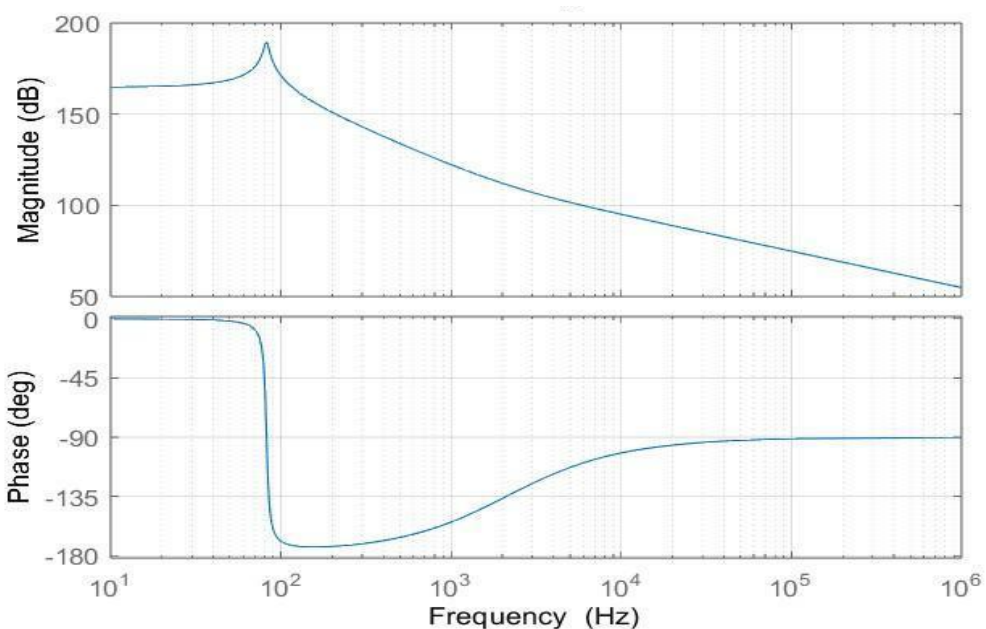


Figure 3.16: Bode Plot for High Voltage Buck Converter After Modification

By drastically increasing the capacitor value, the poles of the system were shifted to the left; hence, the resonant frequency also occurs at lower frequencies, and the DC gain of the system was also decreased. As shown in Table 3.10, the design parameters for the type-II controller can be chosen because now, at the crossover frequency (f_{co}), the phase is stable and recovered from the poles' negative phase effect, and the gain of the system at crossover frequency (g_m) is not too high to effect controller stability as shown in Figure 3.16.

Table 3.10: Closed Loop Design Parameters for High Voltage Buck Converter

V_s(V)	650
V_{out}(V)	380
Freq(kHz)	30
Power(kW)	2
Duty Cycle (D)	0.5846
Resistance (Ω)	72.2
L(mH)	2.5
C(mF)	1.5
ESR (mΩ)	50.
f_{co} (kHz)	3
g_m (dB)	107
$\theta_{converter}$ ($^\circ$)	125

As done, for the high voltage buck converter controller design, the open loop bode plot for the low voltage output was deducted based on the rated input and output voltages, assuming the load is dissipating maximum power, which is 500 W. This is done to assess if a type-II or type-III controller is needed.

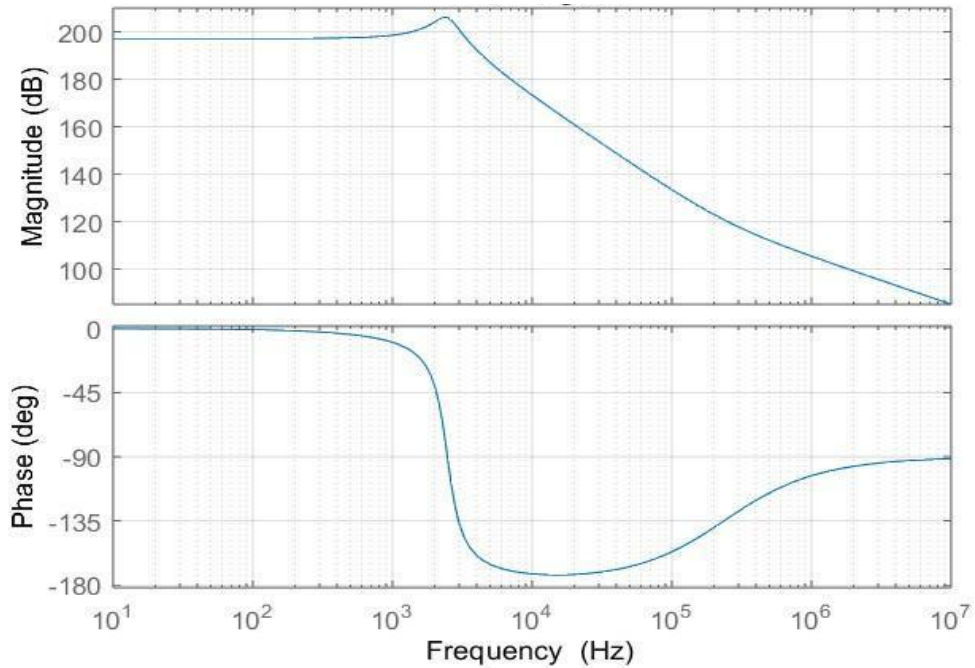


Figure 3.17: Bode Plot for Low Voltage Buck Converter Before Modification

As seen in Figure 3.17, the open loop system response is inherently stable; at first, this is due to both magnitude and phase being positive at 0 Hz; secondly, the lowest phase reached is -173° , meaning that the system is stable, a system is considered to be unstable when its phase reaches -180° or lower. A type-II controller with error compensation will be chosen to control the voltage feedback loop of the converter.

The main problem of the system response is the high DC gain, which is 197 dB, and in the phase response, where the poles occur at a high frequency, the effect of these poles can be seen from 1 kHz to 50 kHz. This means a suitable crossover frequency cannot be chosen since the crossover frequency must be chosen in the region where the system begins to reach a stable phase value. In this, the system begins to recover from the pole effects and reach stability at frequencies higher than 50 kHz, which is even too high with reference to the switching frequency.

In order to successfully design the type-II controller with error compensation, the poles must be shifted to the left to allow the system to recover from the poles' negative phase shift at lower frequencies in order to choose a stable crossover frequency to design the controller. Finally, the DC gain also must be decreased, this is dominantly done by increasing the capacitance and inductor values.

As previously done in the design of the high voltage type-II controller design with constant manipulation of the inductor, capacitance, and ESR parameters, the following are the closed loop parameters of the circuit along with the adjusted bode plot.

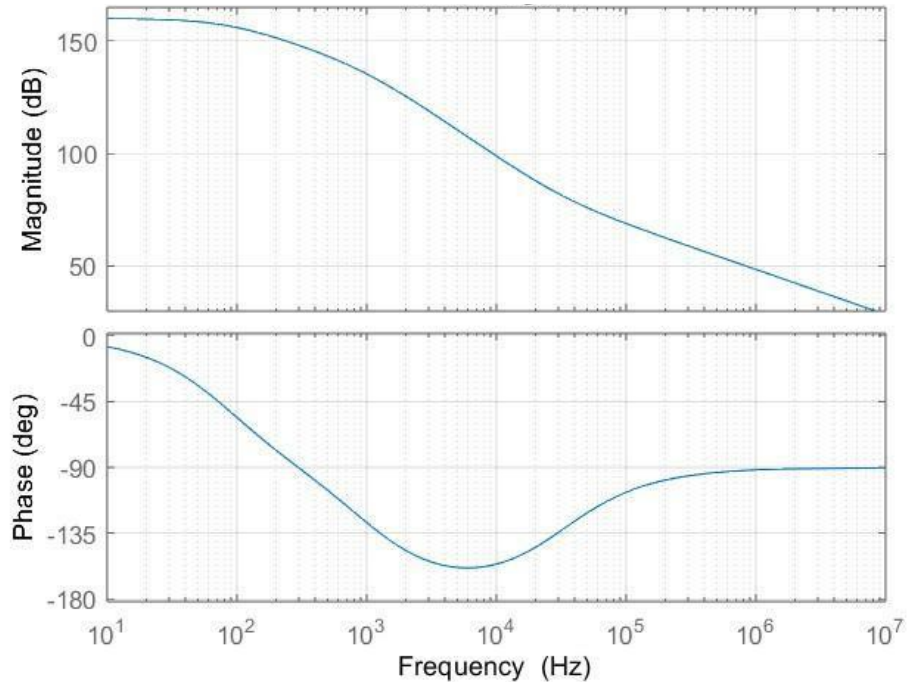


Figure 3.18: Closed Loop Bode Plot for Low Voltage Buck Converter After Modification

Table 3.11: Closed Loop Design Parameters for Low Voltage Buck Converter

V_s(V)	30
V_{out}(V)	12
Freq(kHz)	150
Power(W)	500
Duty Cycle (D)	0.4
Resistance (Ω)	0.288
L(mH)	0.6
C(mF)	0.5
ESR (mΩ)	10
f_{co} (kHz)	30
g_m (dB)	82.2
$\theta_{converter}$ (°)	-135

As shown in Table 3.11, the switching frequency of the converter was increased from 90 kHz to 150 kHz; the frequency was increased in order not to further increase the sizing of the inductor and capacitor and to choose a crossover frequency where the system's frequency response recovers from the pole effect, and begins to reach a stable value; hence the crossover frequency is chosen at 30 kHz, which is 5 times smaller than the adjusted switching frequency.

The bode plot above displayed a textbook system response of a buck converter; as shown by manipulating the buck converter parameters, the DC gain was successfully lowered from 197 dB to 160 dB, and the poles of the system were shifted to the left; hence the closed loop system started to recover from the poles negative phase and reach stability for frequencies higher than 10 kHz.

3.6.3 Type-II Controller Explanation & Design

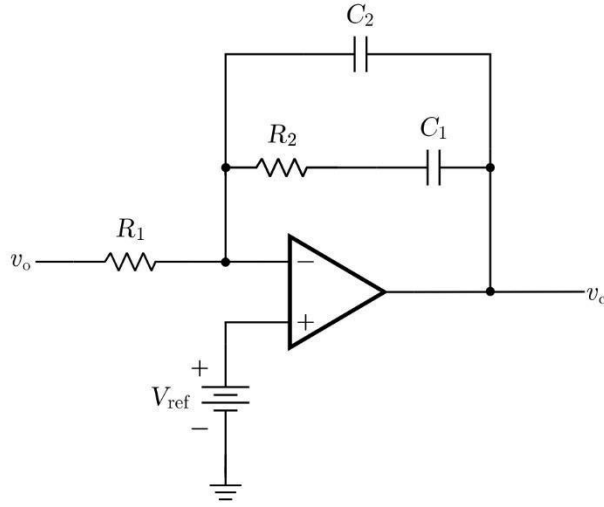


Figure 3.19: Type-II Controller Circuit

The type-II controller is mainly composed of a PI (proportional-integral) structure, where the proportional part of the controller corrects the steady-state error represented as v_c , but a proportional controller is insufficient since the steady-state error will be constant and cannot be decreased further to ensure precise results, so the integral part is responsible for decreasing the steady state error by integrating the error over time.

Moreover, the type-II controller offers a much-needed phase boost. The main reason that the type-II controller was chosen over the type-III controller was that both buck converters require moderate control bandwidth and do not need to control signals at high frequencies, which is the main advantage of the type-III controller over the type-II controller. The other advantage of the type-III controller is its quicker response to rapid changes that may occur in the system. In the case of the two buck converters, the type-II controller response speed is sufficient, and a faster response is not needed since the open loop system is inherently stable.

Also, the type-III controllers are used for systems with a high-quality factor. The quality-factor is described as the sharpness of the resonance peak that is found in the magnitude bode plot of both converters.

Both buck converters did not require additional control at high frequencies, nor was the quality-factor too high that it required a type-III controller; hence, the type-II controller was chosen since it provided the needed output voltage while being less complex and economically the better option than implementing the type-III controller.

To further understand the nature of the type-II error compensation controller, its transfer function must be derived.

The gain function $G(s)$, which is the relation between output and input voltage, is expressed as the negative feedback impedance (Z_f) over the input impedance, (Z_i) as seen in Equation.

$$G(s) = -\frac{Z_f}{Z_i} \quad (3.28)$$

$$G(s) = -\frac{s+1/R_2C_2}{R_1C_2s[s+(C_1+C_2)/R_2C_1C_2]} \quad (3.29)$$

Assuming $C_2 \ll C_1$ to get the following gain equation:

$$G(s) = -\frac{s+1/R_2C_1}{R_1C_2s(s+1/R_2C_1C_2)} \quad (3.30)$$

With reference to the results obtained from the closed loop system bode plot, a detailed analysis of the type-II controller design for the high-voltage buck converter will be tackled; the same procedure will be followed to design the controller of the low-voltage buck converter. In order to design the controller, the resistors and capacitors must be found.

The phase margin PM is assumed 45° for the high voltage buck converter.

The phase margin PM is assumed 40° for the low voltage buck converter.

The compensated angle was found to be $\theta_{compensated} = 170^\circ$ after substituting the converter angle and the phase margin into Equation 3.18:

Where PM is the phase margin, the phase margin is a fixed value usually from $(40^\circ - 65^\circ)$ its purpose is to guarantee the stability of the controller under disturbances and design errors; this is done by further shifting the controller system response to the right, where the phase of the system is almost constant.

The K-factor of the system is found by substituting the compensated angle into Equation (3.31), where the K-factor $K = 11.43$.

$$K = \tan\left(\frac{\theta_{compensated}}{2}\right) \quad (3.31)$$

G , which represents the ratio between the two resistors of the controller, was found by substituting $g_m = 107 \text{ dB}$ into Equation(3.32) to get $G = 2.23872 \times 10^5$

$$G = 10^{\frac{g_m}{20}} \quad (3.32)$$

Let $R_1 = 100\Omega$, and after G was found, R_2 can be found by using the Equation(3.33) to get

$$R_2 = 2.2387 \times 10^7 \Omega$$

$$R_2 = GR_1 \quad (3.33)$$

Both resistor values(R_1, R_2), K-factor(K), crossover frequency(f_{co}), and compensated angle ($\theta_{compensated}$) are plugged by in the following equations: Equation (3.34) and Equation (3.35), to find (C_1, C_2). $C_1 = 2.7086 \times 10^{-11} F$, $C_2 = 2.0732 \times 10^{-13} F$

$$C_1 = \frac{K}{2\pi \times f_{co} \times R_2} \quad (3.34)$$

$$C_2 = \frac{1}{K \times 2\pi \times f_{co} \times R_2} \quad (3.35)$$

The same procedure was followed to design the low-voltage controller. All derived parameters required to design the type-II controller for both high and low-voltage buck converters are displayed in the table below:

Table 3.12: Type-II Controller Parameters for Both Buck Converters

	High Voltage Controller Parameters	Low Voltage Controller Parameters
$\theta_{compensated} (\circ)$	170	175
G	2.23872×10^5	1.2882×10^4
$K - factor$	11.43	22.90377
$R_1 (\Omega)$	100	100
$R_2 (M\Omega)$	22.387	1.2882
$C_1 (pF)$	27.086	94.320
$C_2 (pF)$	0.20732	0.1798

3.6.4 Controller Design Tests

The following disturbances and variations were simulated on both closed-loop converter circuits to test the robustness and the sensitivity of the controller to disturbances:

- 1) A step signal with a 10% magnitude of square wave voltage was added.
- 2) A step signal with a 10% magnitude of the controller's reference voltage
- 3) Testing under minimum and maximum loads

For the four closed loop circuits (two input boost circuits and two output circuits), the tests successfully proved the robustness and flexibility of the controller since the output voltages and currents were unaffected, and the controller adapted to the disturbances and load changes it faced and still provided the rated voltage required in both high and low voltage buck converters.

For the PV and battery source controllers, the first test is shown in Figure 3.20 and Figure 3.21; both controllers were able to follow the reference voltage ranging from 0.9 V to 1.1 V. The second test is shown in Figure 3.22 and Figure 3.23; the input voltage varied by 10% and decreased up to 10% above the required range; both controllers handled the changes in the input voltage and generated the same desired output voltage. The final test is shown in Figure 3.24 and Figure 3.25; both controllers handled the load changes. Similar results were obtained while testing the type-II controllers for both output buck circuits, where the controller in both output circuits handled the disturbances and continued to supply the desired voltage.

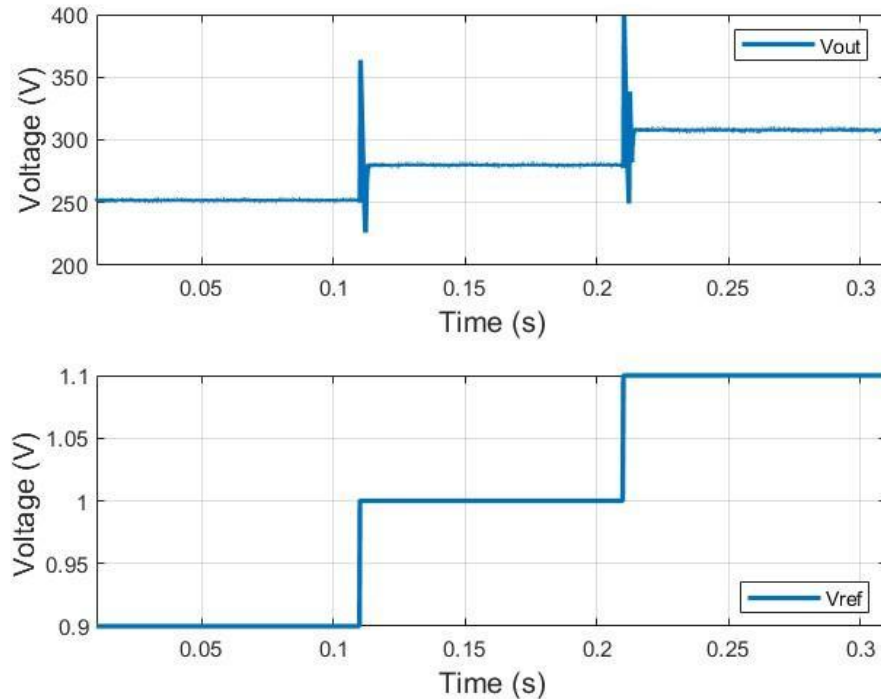


Figure 3.20: PV Closed Loop Output Voltage with Changing Voltage Reference

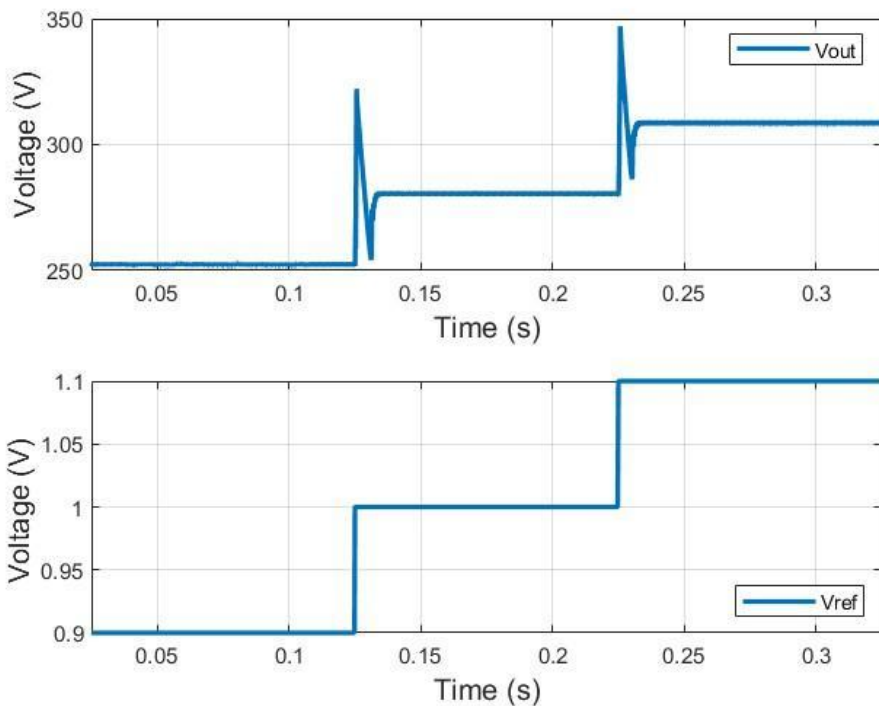


Figure 3.21: Battery Closed Loop Output Voltage with Changing Voltage Reference

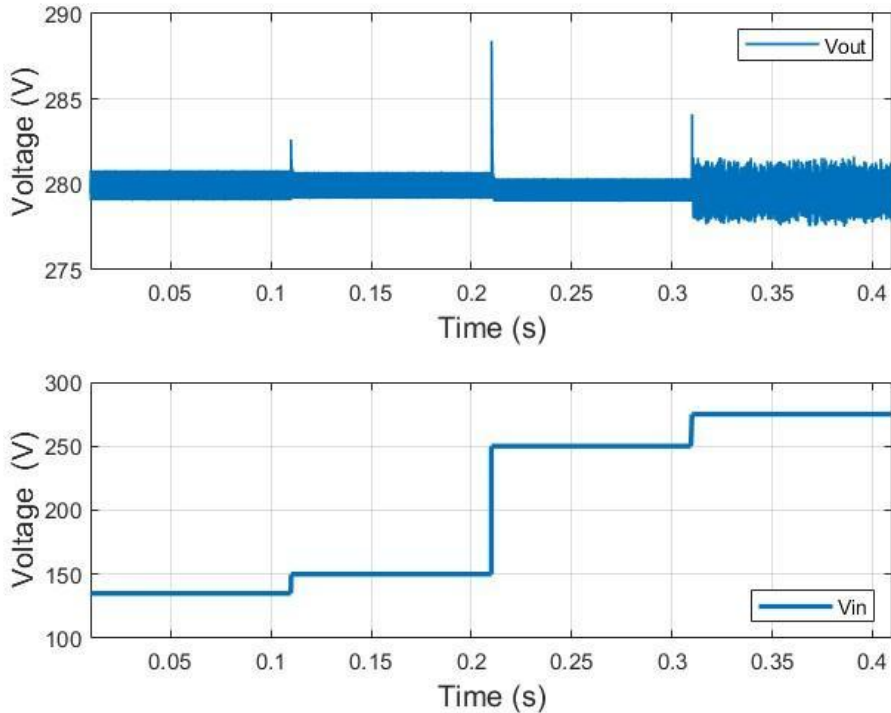


Figure 3.22: PV Closed Loop Output Voltage with Changing Input Voltage

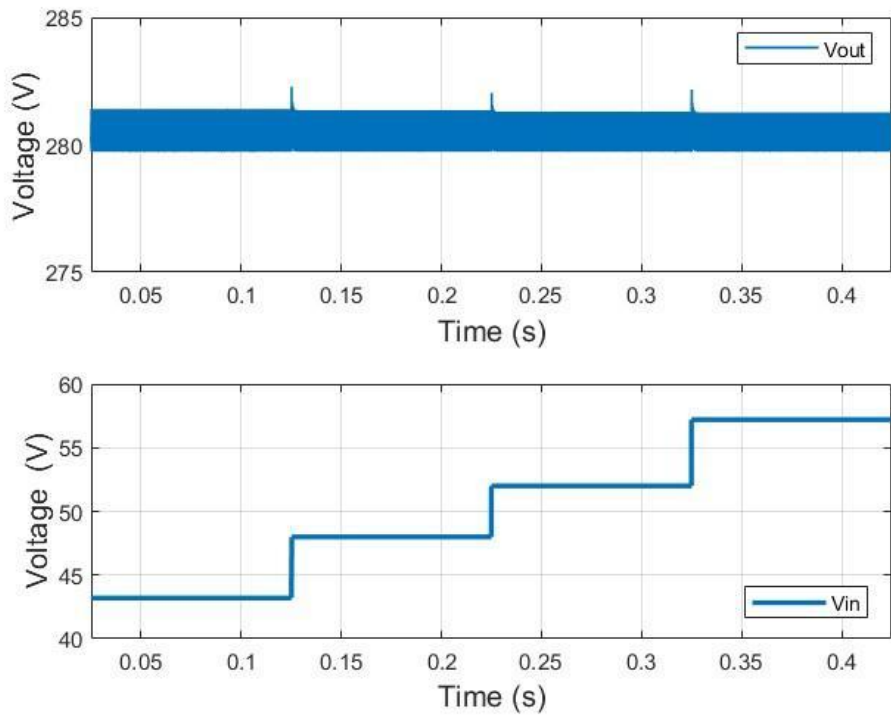


Figure 3.23: Battery Closed Loop Output Voltage with Changing Input Voltage

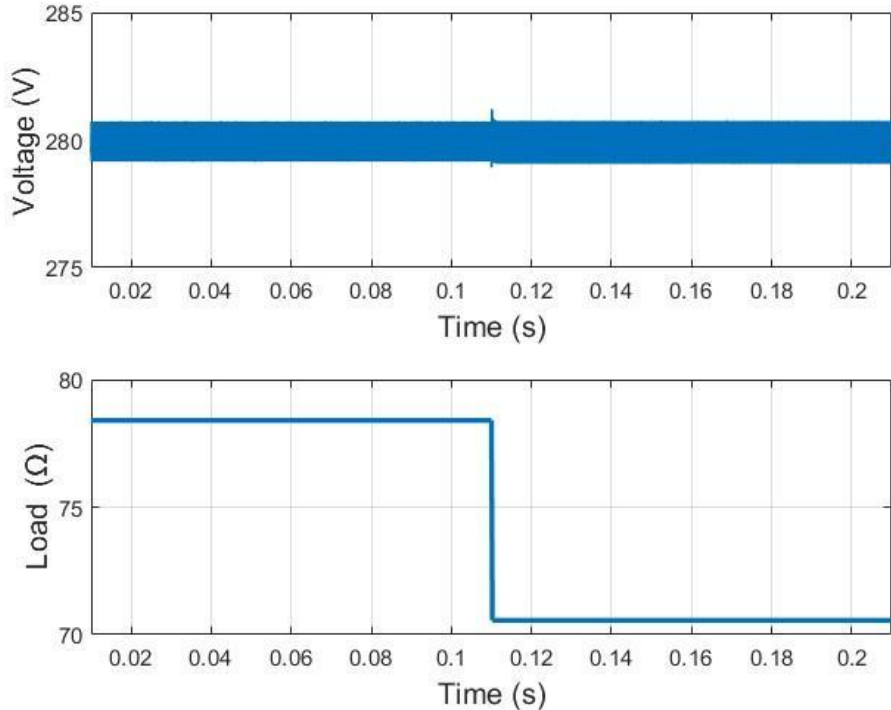


Figure 3.24: PV Closed Loop Output Voltage with Changing Load

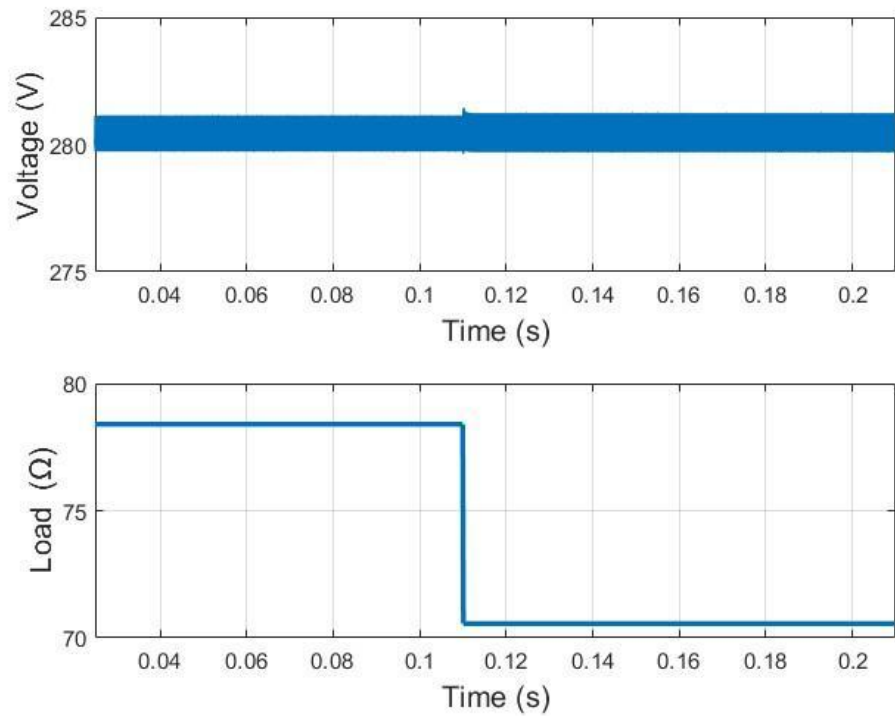


Figure 3.25: Battery Closed Loop Output Voltage with Changing Load

3.7 Full Bridge Design

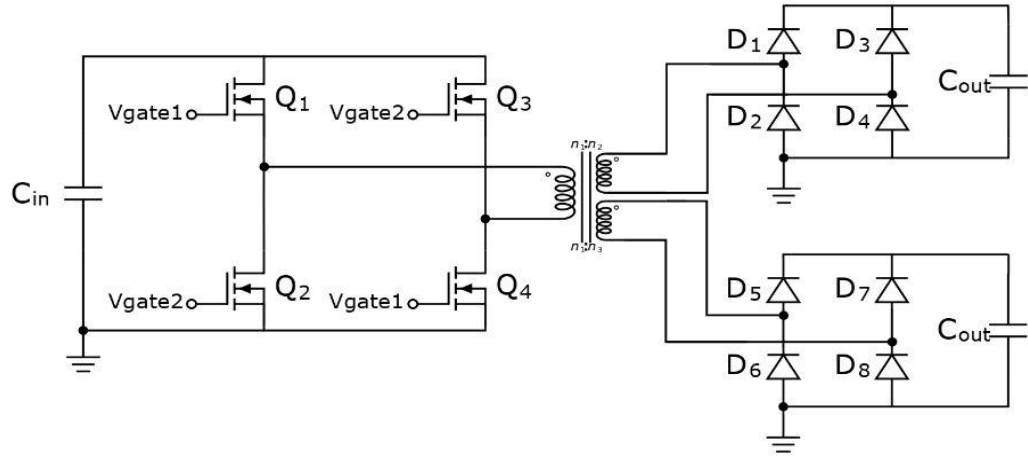


Figure 3.26: Full Bridge Topology With Two Outputs

The full-bridge converter topology is commonly used, as its transistors are only exposed to the input voltage supplied. It is used to change the input DC voltage into an AC square wave voltage to feed the primary winding of the three-winding transformer shown in Figure 3.26.

In each half-cycle of the switching period, the pairs of switching transistors Q1-Q4 and Q2-Q3 are activated separately.

When the Q1-Q4 pair is switched on in the first half cycle, the full bridge connects the dotted end of the primary winding to the input supply voltage incoming from the DC link capacitor, and the undotted end of the primary winding is connected to the ground; hence a positive voltage is supplied from the bridge to the transformer.

When the Q2-Q3 pair is switched on in the second half of the cycle, the full bridge connects the undotted end of the primary winding to the input supply voltage incoming from the DC link capacitor, and the dotted end of the primary winding is connected to the ground; hence a negative voltage is supplied from the bridge to the transformer. The generated signal is a square-wave signal with a chosen frequency of 40 kHz.

Where the duty cycle (D) of each transistor pair is between $0 < D < 0.5$, this is to ensure pure square wave voltage and for both pairs not to turn on at the same time, which leads to a short circuit connection.

The three-winding transformer is used for electrical isolation and further voltage magnitude control, which can be easily achieved via the turns ratio between the primary and secondary winding, as well as primary and tertiary winding. The square wave voltage from both secondary and tertiary windings enters an H-bridge, which is composed of 4 diodes, each pair connected in parallel, to rectify the square wave AC voltage into a DC voltage, then this voltage is filtered out by a filter capacitor to further smooth voltage and remove unwanted fluctuations from the transformer. In this design, the full-bridge converter supplies a single-phase, three-winding transformer, with one input port at the primary side and two output ports, a secondary and tertiary winding.

3.7.1 Rectifier Design

As shown in Figure 3.26, an H-bridge consisting of diode rectifiers is implemented to rectify the voltage coming from both the secondary and tertiary windings. Diode rectifiers offer the simplest rectification in medium and high-power applications, but the voltage drop over the diode and the reverse recovery time may affect the system's efficiency. On the other hand, synchronous rectifiers are an alternative instead of diodes. The voltage drop is decreased; hence, higher efficiency is achieved. On the other hand, synchronous rectifiers offer more complexity due to their control and drive circuits. For this reason, diode rectification has been implemented in this design.

3.7.2 Transformer Design

For the Transformer design, it is considered an ideal transformer in terms of losses. The primary Voltage side V_p is set to be 280 V ; the secondary voltage V_s is set to be 650 V , this is the voltage supplying the high voltage buck circuit; it was chosen to be 650V to allow the buck converter to operate at a duty cycle not exceeding 0.7 and not less than 0.4 to function with high efficiency. The tertiary voltage side V_t is set to be 30 V , due to the rated output voltage being 12V , to allow the low voltage buck converter also to operate efficiently, meaning operating at a duty cycle D between $0.4 < D < 0.7$.

The primary turns ratio (Np) is assumed to be 100 ; based on this assumption, the secondary winding $N_s = 233$ and tertiary winding $N_t = 11$, according to Equations 3.36-3.37

To find N_s ,

$$N_s = Np \times \frac{V_s}{V_p} \quad (3.36)$$

$$N_t = Np \times \frac{V_t}{V_p} \quad (3.37)$$

When both turns ratios are plugged in Equations 3.38 - 3.39 and $D=0.5$, the peak voltage for both secondary and tertiary windings are found to be $V_s = 650\text{V}$ $V_t = 30\text{V}$

Where D is the duty cycle of the switches, $0 < D < 0.5$.

$$V_s = 2V_{in} \left(\frac{N_s}{N_p} \right) \times D \quad (3.38)$$

$$V_t = 2V_{in} \left(\frac{N_t}{N_p} \right) \times D \quad (3.39)$$

4 Results

The open loop and closed loop designs for all boost and buck converters, along with the full bridge, were fully analyzed in the design section. The design is a one-of-a-kind multi-input multi-output DC-DC converter, comprising two boost converters, two buck converters, 2 H-bridges, and a full bridge, along with additional inductors and capacitors to ensure smooth voltage and current transitions.

The input side is made of two input sources: a 48-52 V battery at a rated capacity of 180Ah, along with a PV array rated at 1000 Wp. With the aid of two type-III controllers, one for each input boost circuit, the voltage supplied is kept constant under disturbances and output load changes. Then, both boost output voltages will enter the full bridge circuit to transform the voltage from a DC voltage pulsating voltage to an AC voltage so it can be transmitted to the output circuits by a 3-phase winding transformer. The 3-phase transformer offers electrical isolation and protection and allows for more control over design parameters by simply changing voltage ratings via transformer turns ratio. Finally, the transformer primary winding magnetically induces a voltage on both the secondary and tertiary windings to supply both buck converters to both loads, respectively.

The incoming voltages from both secondary and tertiary windings are AC voltage and will be rectified by an H-bridge and then further filtered out by a filter capacitor connected in parallel to supply both buck converters with a smooth DC voltage, with minimal disturbances.

Finally, with the aid of a type-II controller for each buck converter, the output voltages are kept constant at 380 V for the high voltage output supplying the electric vehicle and 12 V for the low voltage output supplying the small household.

4.1 Simulation Results Setup

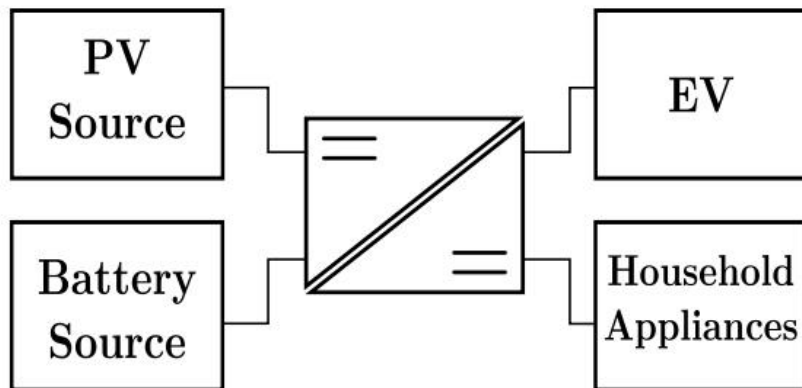


Figure 4.1: Multi-port DC-DC Converter Block Diagram

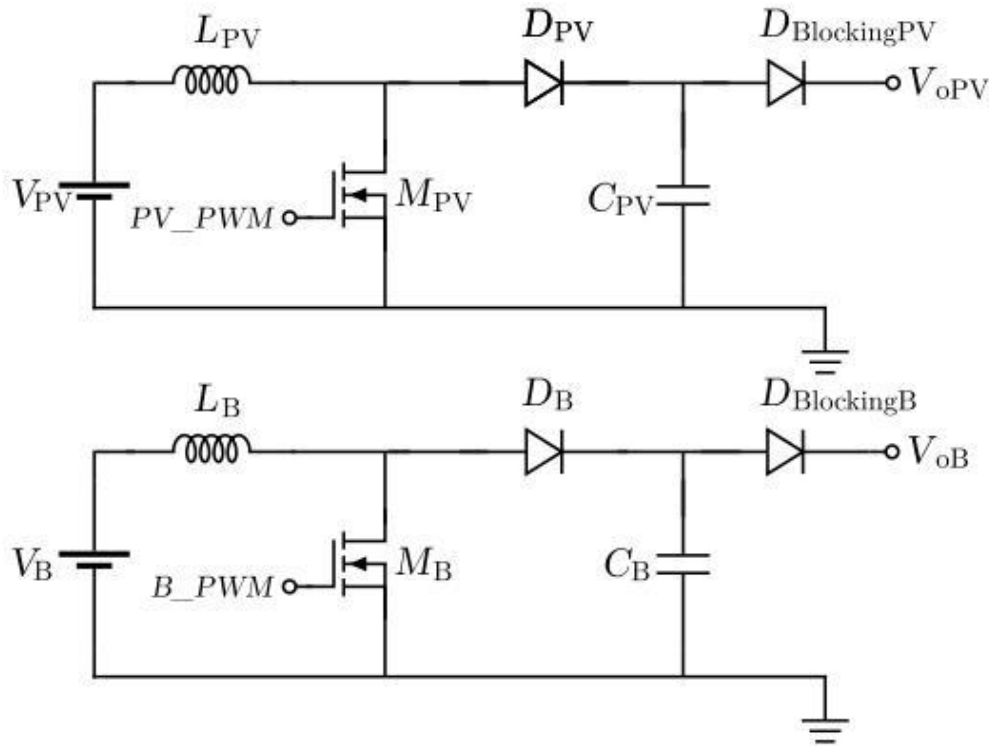


Figure 4.2: Source Side of Multi-Port DC-DC Converter

Figure 4.1 shows the simple representation of the system consisting of two input sources, PV and battery, an isolation stage, and the output stage, and electric vehicle and household appliances. in Figure 4.2, the input stage of the converter consists of two boost converters to step up the voltage and a blocking diode is added for both sources to prevent inverse power flow direction and to ensure proper operation for the boost converters.

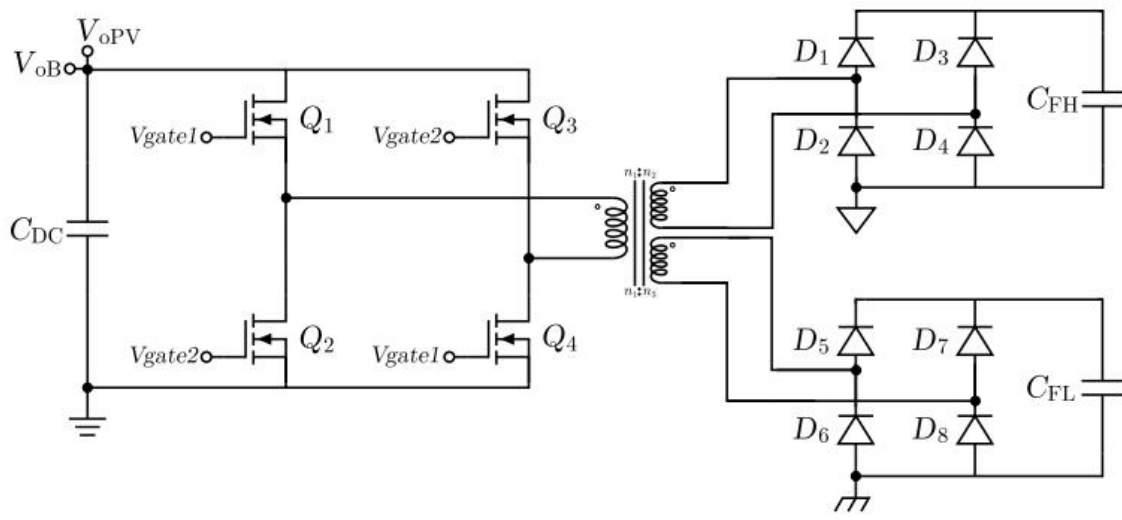


Figure 4.3: Bridge of Multi-Port DC-DC Converter

Figure 4.3 shows the DC-link capacitor, the full bridge, the transformer with the secondary connected to the high-voltage side of the load, and the tertiary connected to the low-voltage side of the load along with a full wave rectifier for each load connected to a filter capacitor to ensure a smoother result.

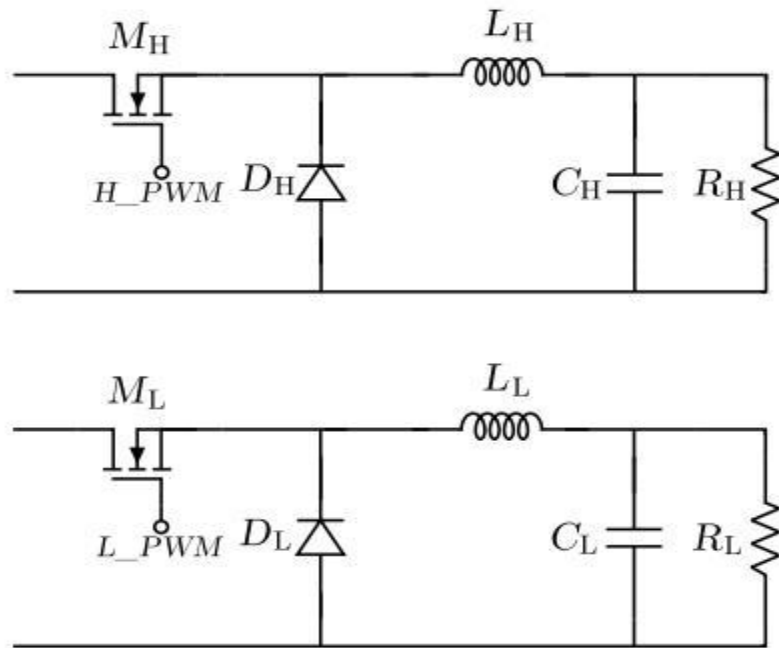


Figure 4.4: Load Side of Multi-Port DC-DC Converter

Figure 4.4 shows the buck converter for the high-voltage and low-voltage sides of the system's load.

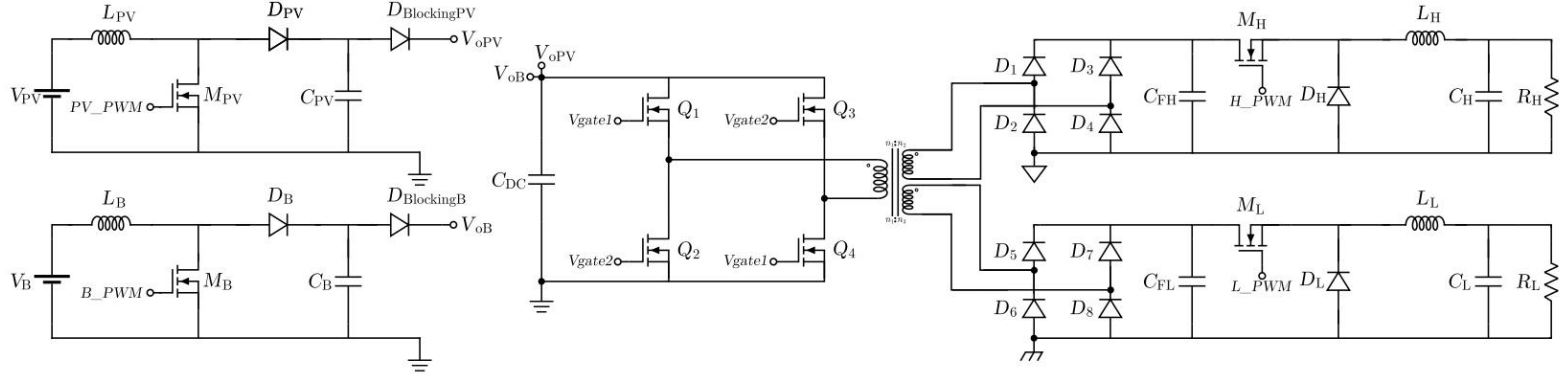


Figure 4.5: Multi-Port DC-DC converter Full Circuit

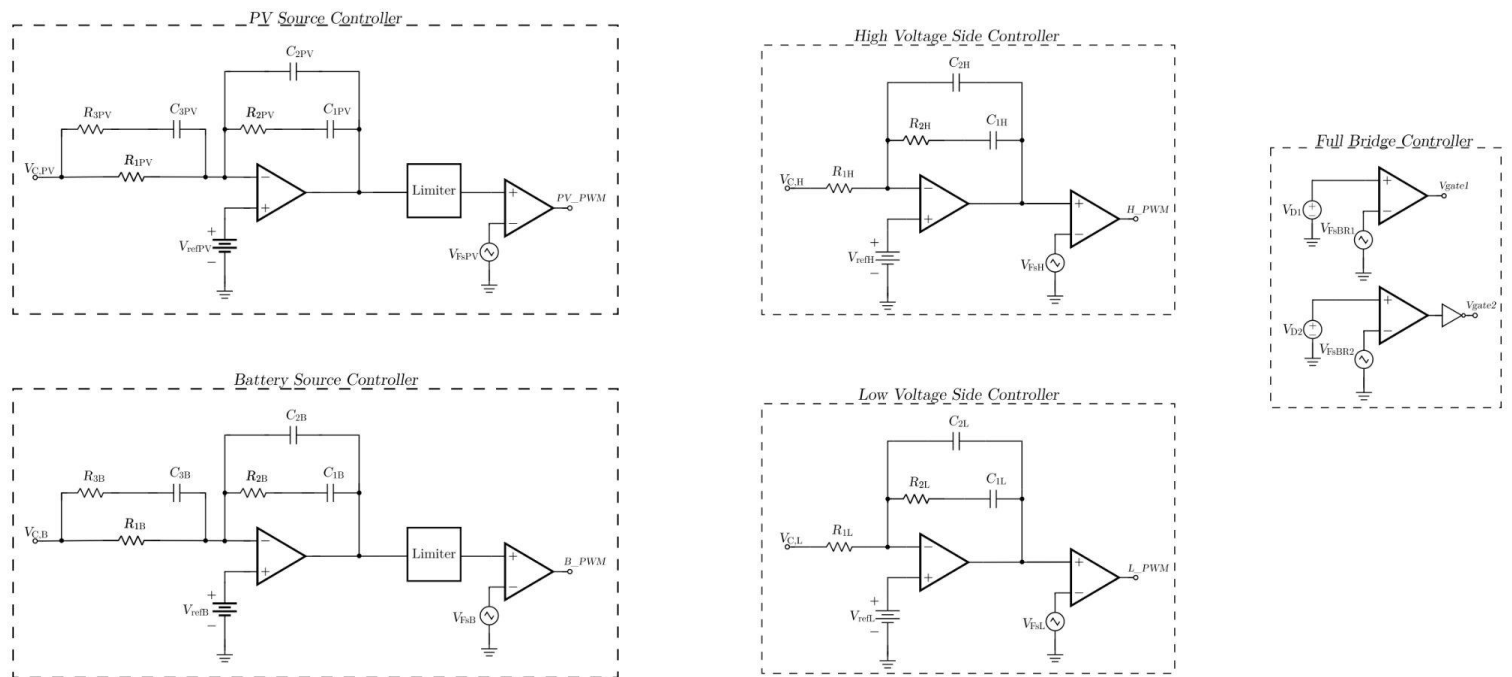


Figure 4.6: Controllers of Multi-Port DC-DC Converter

Figure 4.5 displays the final mpc design; as seen, the two input boost converters are connected in parallel, with their output voltage feeding the DC-link capacitor, which is then inverted and then rectified again by the full bridge and the H-bridges, respectively. Finally, rectified voltage supplies both buck output circuits, in order for the buck converters to supply each of the loads with its specified voltage level independently.

Figure 4.6 shows all the controllers that were implemented; as seen above, each converter had its own controller. Each stage has its unique frequency to prevent any cross interferences or disturbances such as electromagnetic interference (EMI). For each of the converters, the controller's output is the positive input to the comparator that generates the modified duty cycle for each converter respectively. For the full bridge, two comparators are present to generate two PWM signals to control each switching pair (Q1, Q4) and (Q2, Q3).

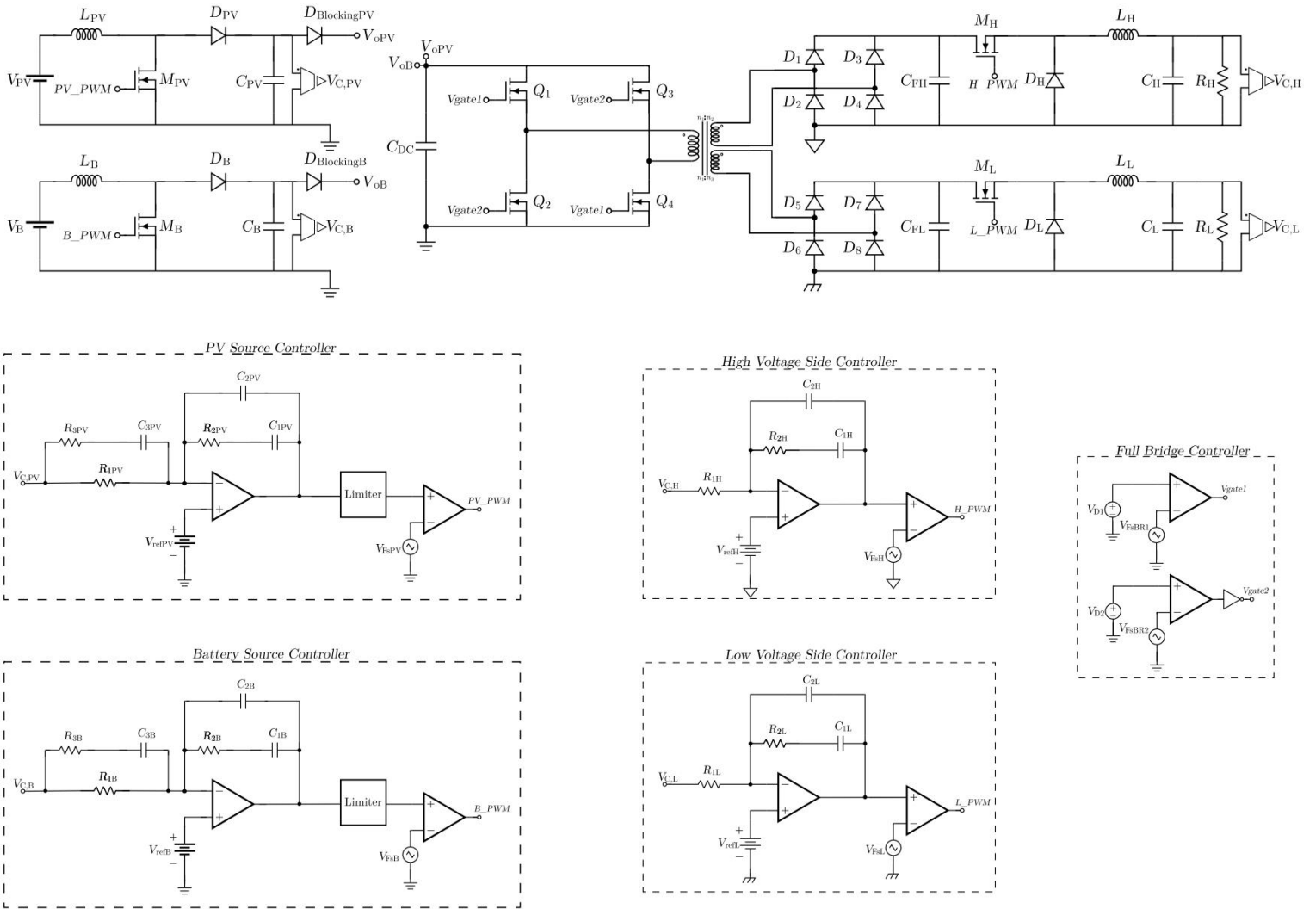


Figure 4.7: Multi-Port DC-DC Converter Full Circuit with Controllers

Figure 4.7 shows the full circuit of the Multi-Port DC-DC converter, each part of the system is connected to its designated controller.

4.2 Input Open Loop Results

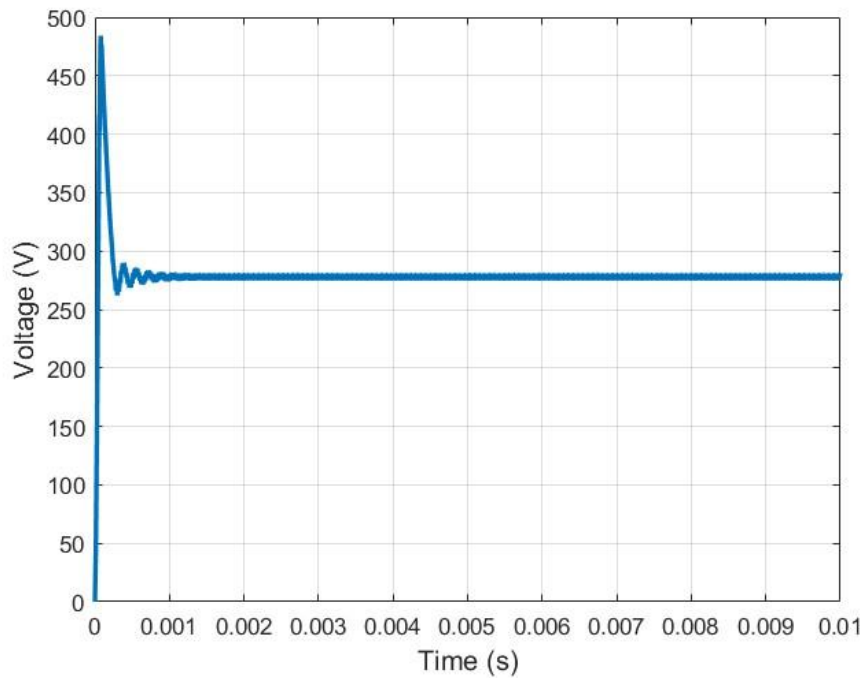


Figure 4.8: PV Open Loop Boost Converter Output Voltage

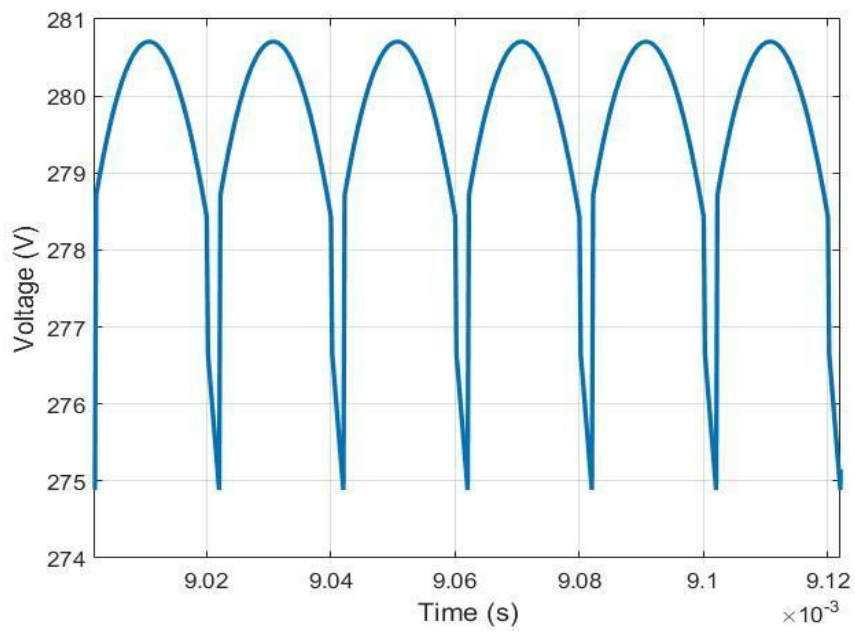


Figure 4.9: PV Open Loop Boost Converter Output Voltage Ripple

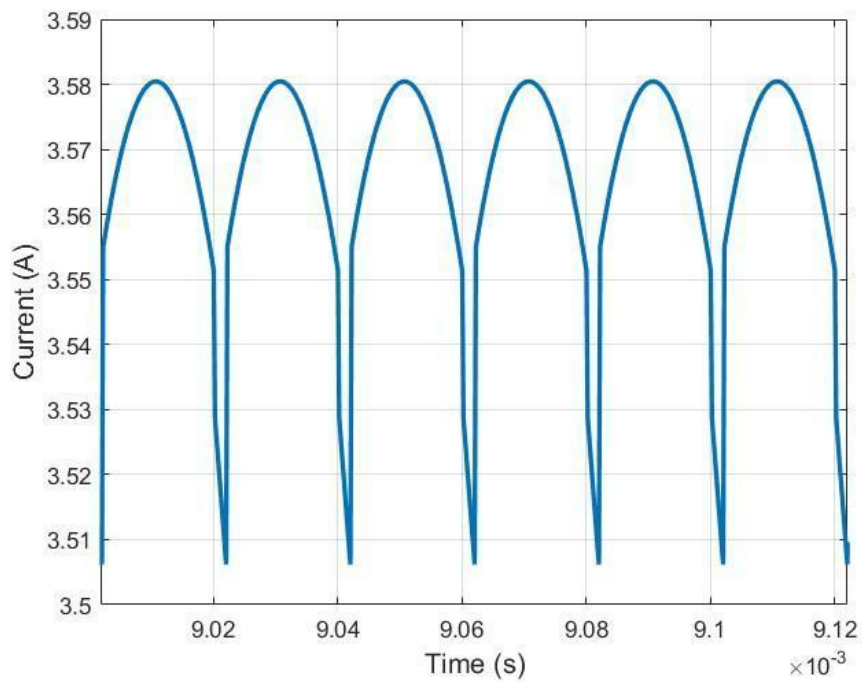


Figure 4.10: PV Open Loop Boost Converter Output Current Ripple

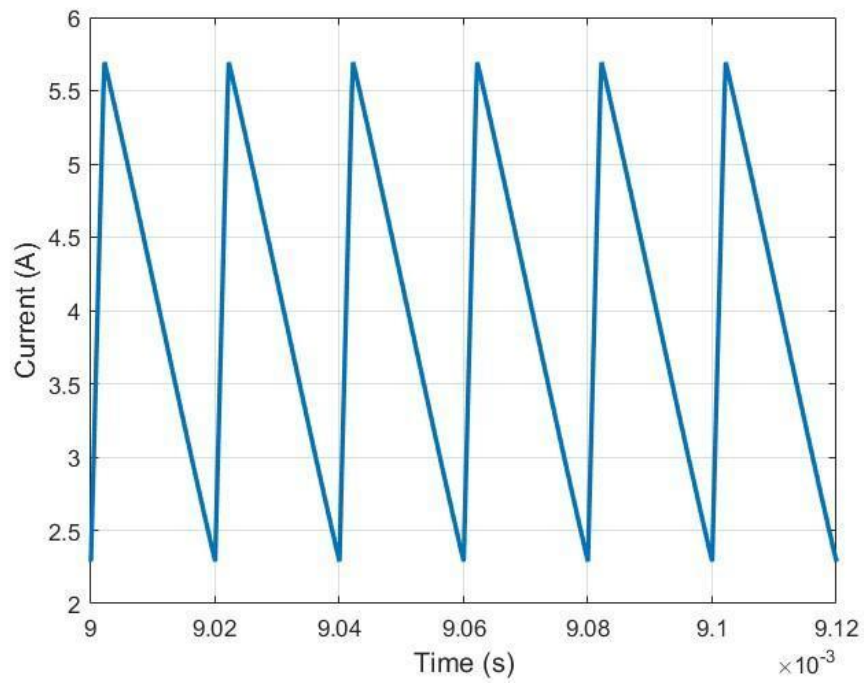


Figure 4.11: PV Open Loop Boost Converter Inductor Current Ripple

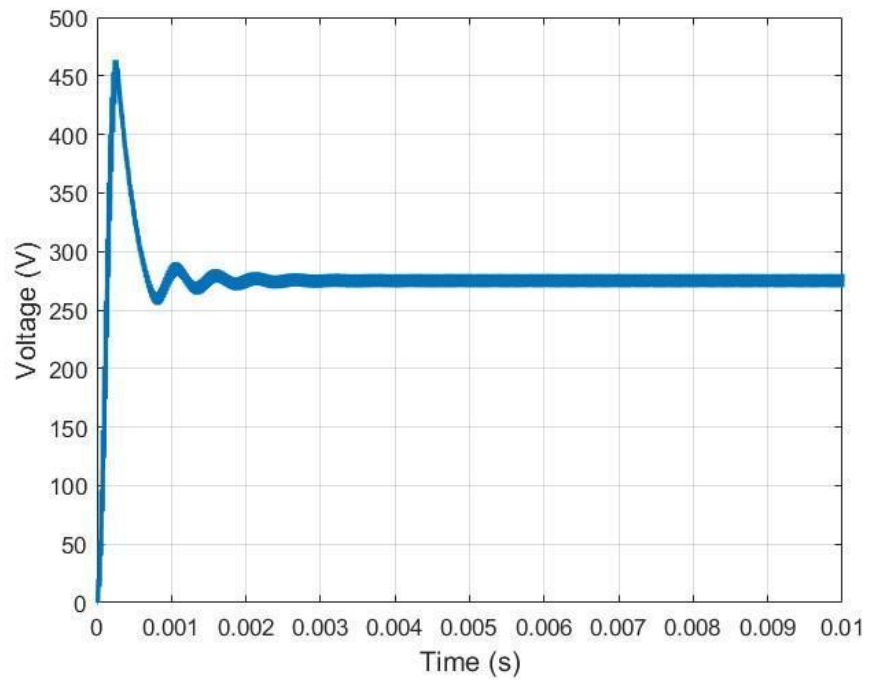


Figure 4.12: Battery Open Loop Boost Converter Output Voltage

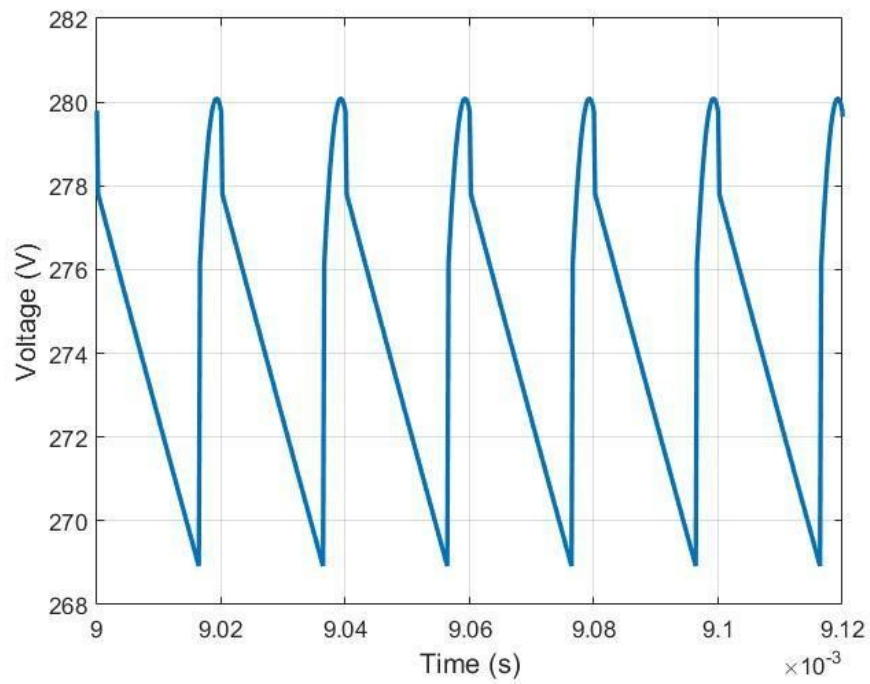


Figure 4.13: Battery Open Loop Boost Converter Output Voltage Ripple

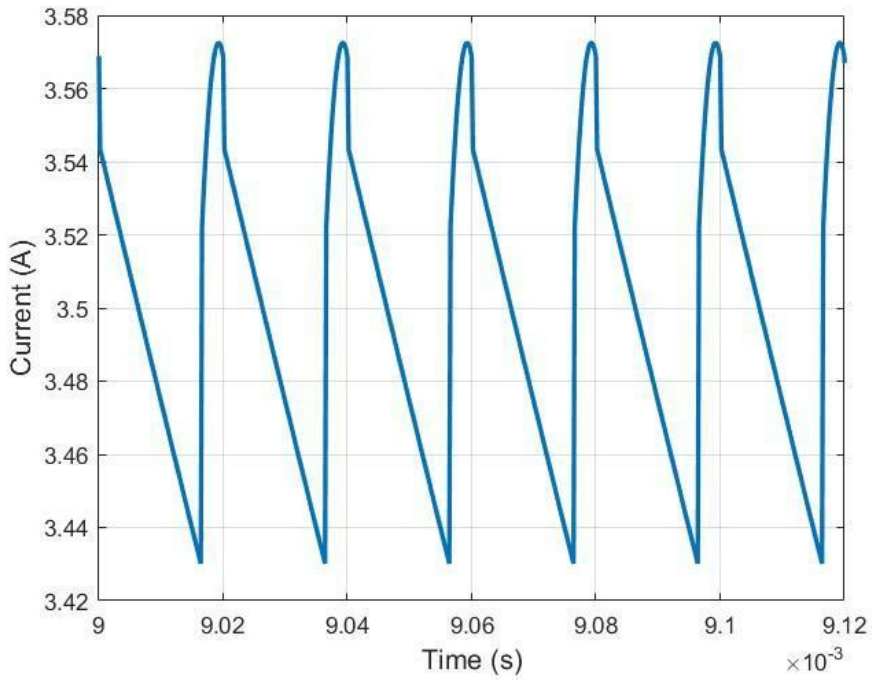


Figure 4.14: Battery Open Loop Boost Converter Output Current Ripple

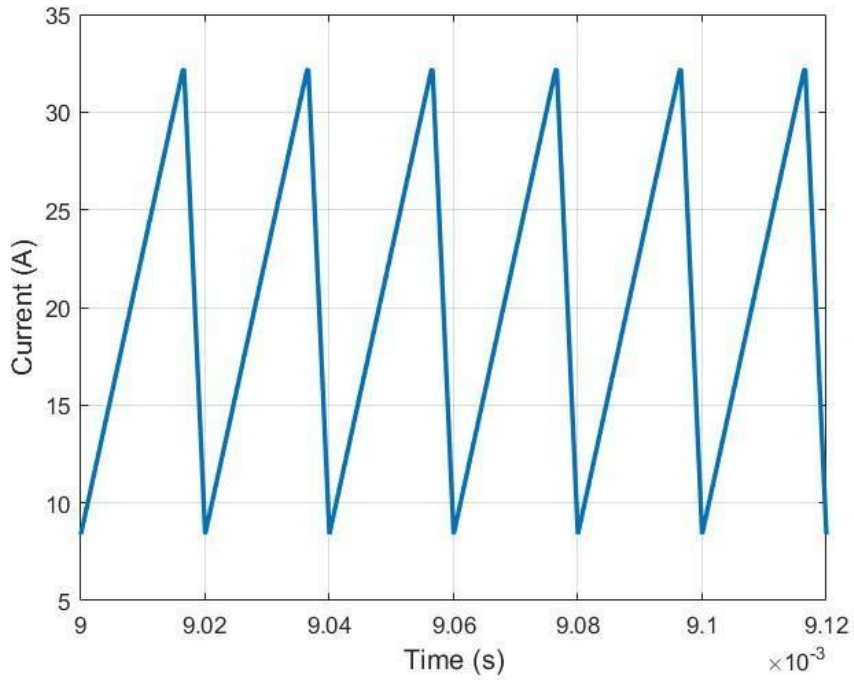


Figure 4.15: Battery Open Loop Boost Converter Inductor Current Ripple

In the figures above, for the PV source, the open loop results of the boost converter reach the required output voltage of 280 V, as seen in Figure 4.8. Figure 4.9 and Figure 4.10 show the output voltage and current of the converter with a ripple of about 2%, and the inductor current shown in Figure 4.11 can be seen in CCM. Similar observations can be seen for the battery source; the output

reaches the intended voltage of 280 V, which can be seen in Figure 4.12. The output voltage and current of the battery boost converter can be seen in Figure 4.13 and Figure 4.14, with a voltage ripple of 3.9%, and the inductor current is in CCM, as shown in Figure 4.15.

4.3 Input Closed Loop Results

4.3.1 MPPT Results

Figure 4.16 shows the MPPT voltage at 250 V at full insolation; it is worth mentioning the MPPT function does not control the voltage produced by the PV arrays; rather, it only maximizes the power production, as can be seen in Figure 4.17; the MPPT controller follows the maximum power that could be produced by the PV arrays.

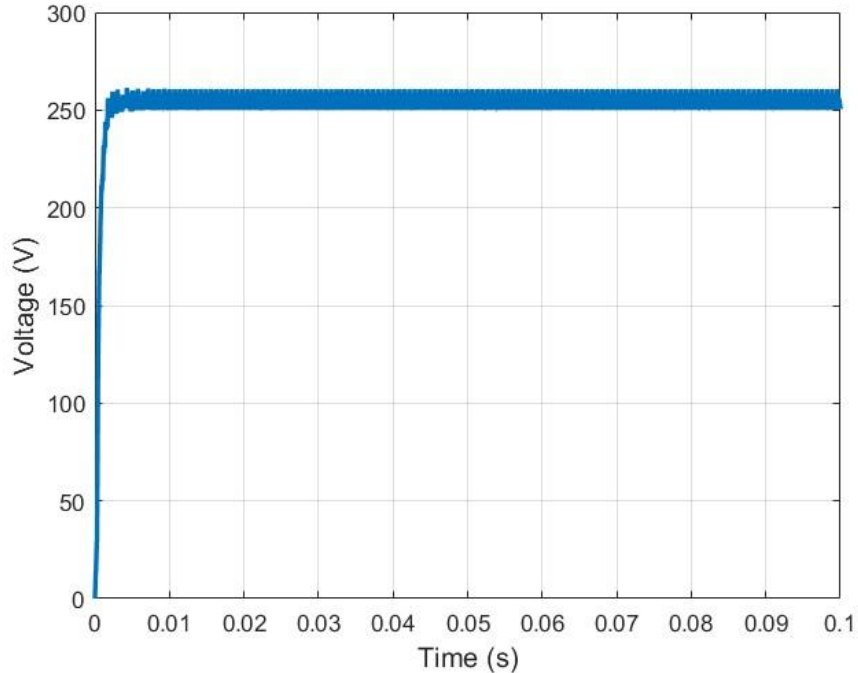


Figure 4.16: Output Voltage of MPPT

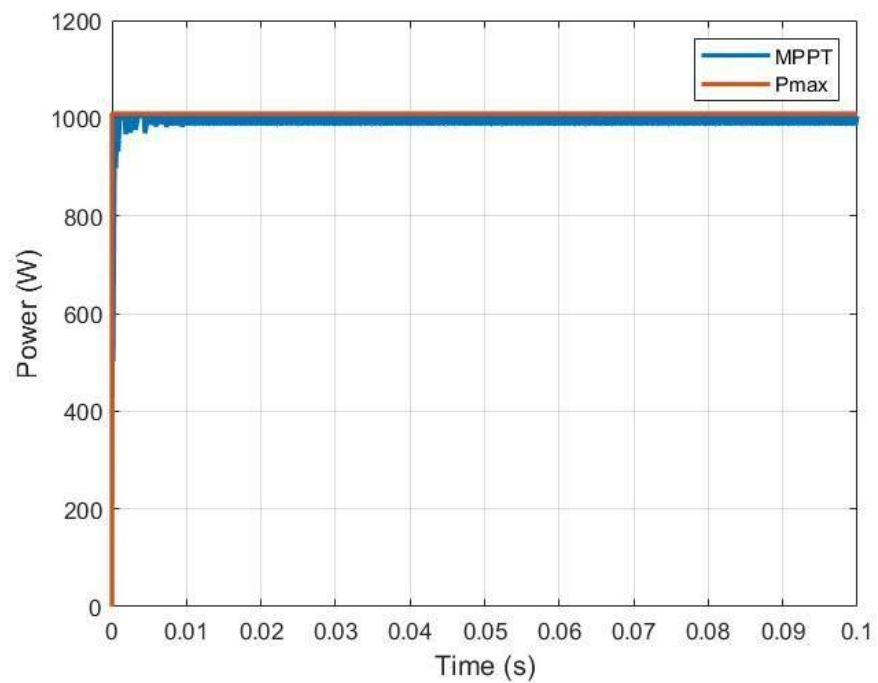


Figure 4.17: Power Delivered by MPPT and Max Power of PV Arrays

4.3.2

PV Source Results

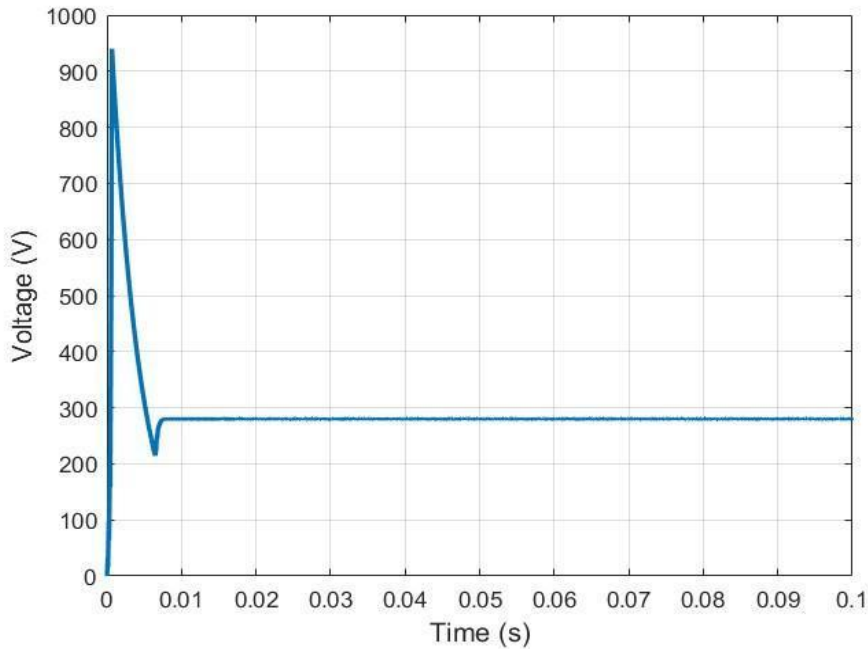


Figure 4.18: PV Closed Loop Output Voltage

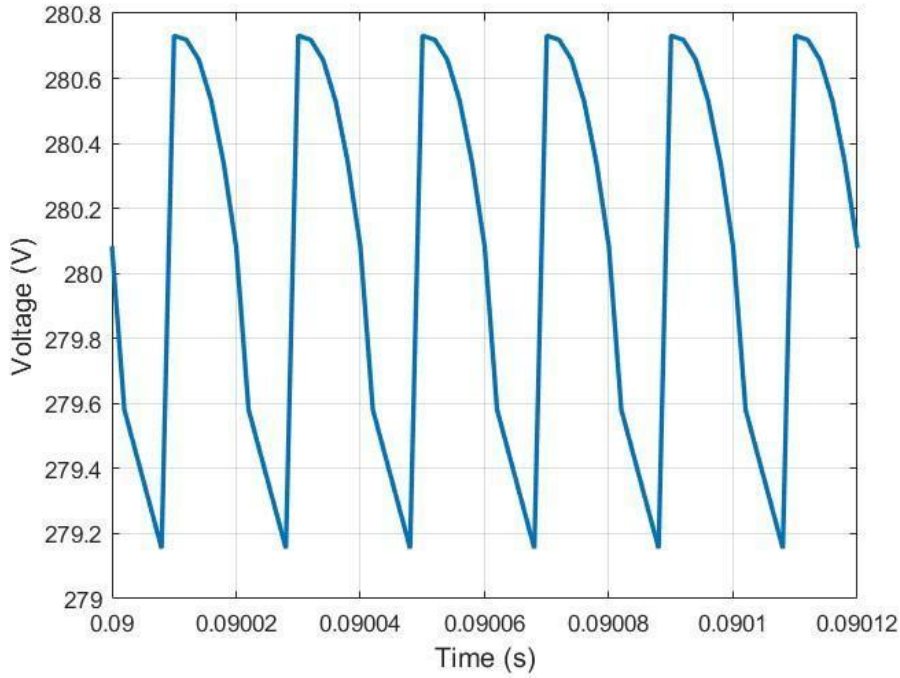


Figure 4.19: PV Closed Loop Output Voltage Ripple

Figure 4.18 shows the output voltage of the PV source with a controller, and Figure 4.18 shows the output voltage ripple of the converter with a ripple of 0.57%

4.3.3 Battery Source Results

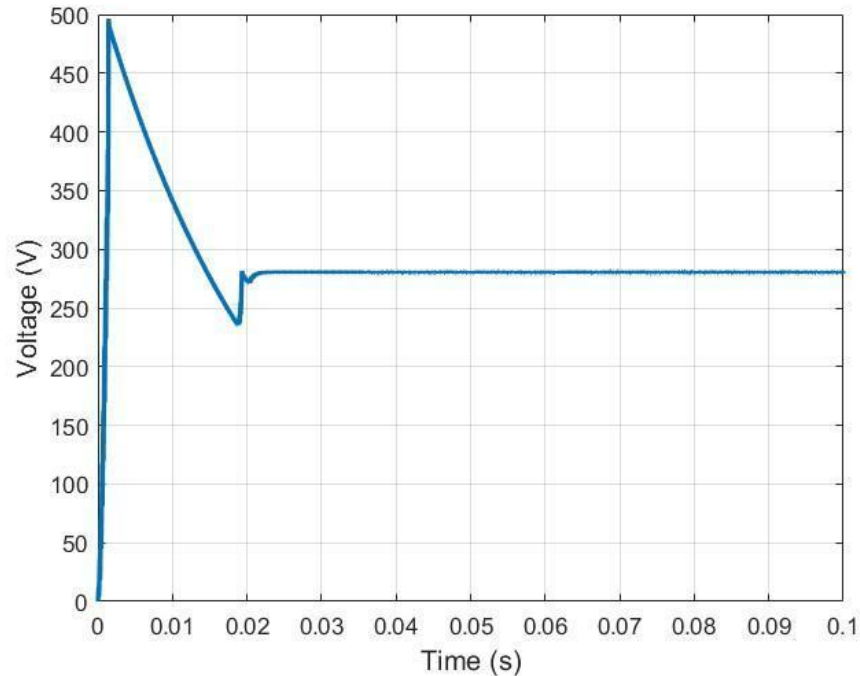


Figure 4.20: Battery Closed Loop Output Voltage

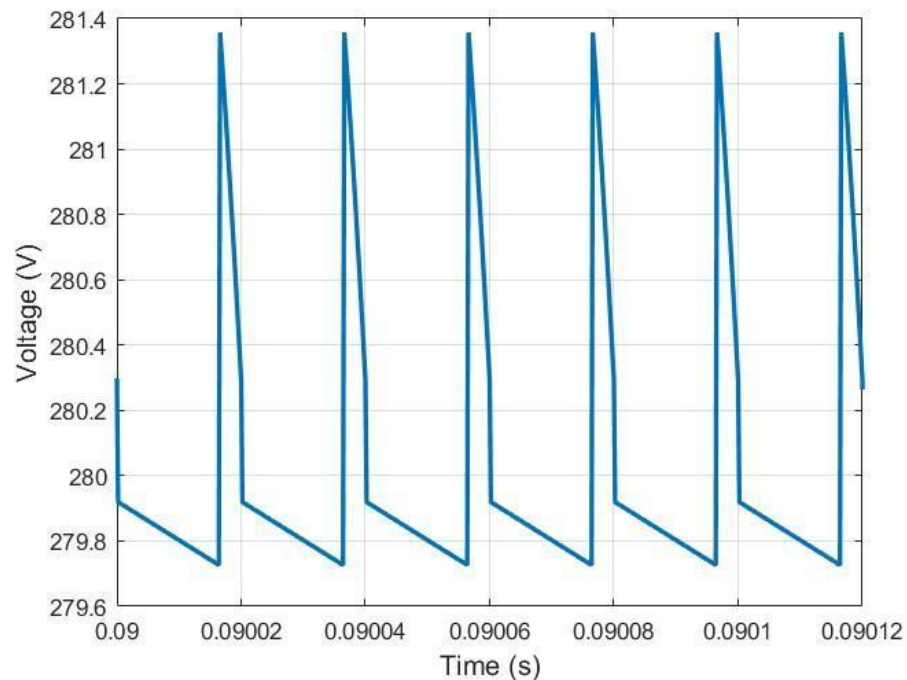


Figure 4.21: Battery Closed Loop Output Voltage Ripple

Figure 4.20 shows the output voltage of the boost converter of the battery source with a voltage ripple of 0.61%, which can be seen in Figure 4.21.

4.4 Output Open Loop Results

4.4.1 High Voltage Buck Converter

With reference to Table 3.5, The high voltage buck converter supplied the needed output voltage with minimal ripple, along with a stable current while the inductor was operating in CCM.

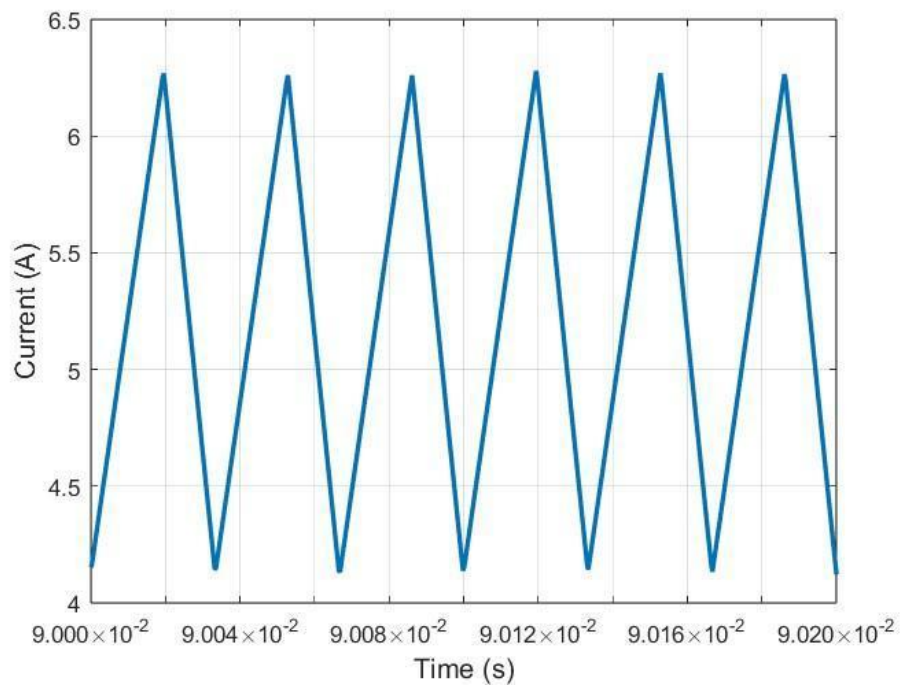


Figure 4.22: High Voltage Open Loop Buck Converter Inductor Ripple Current

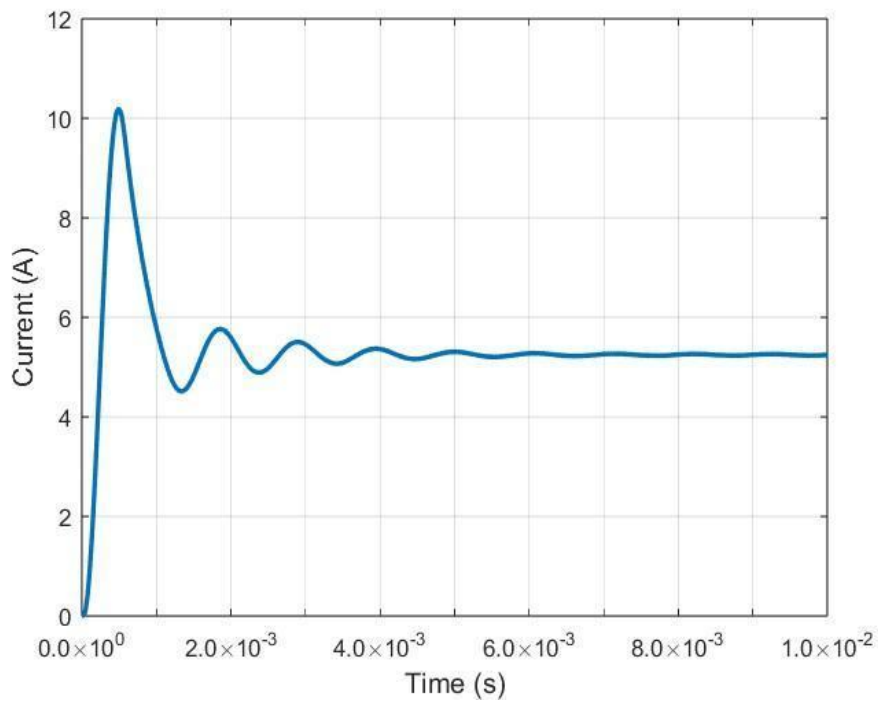


Figure 4.23: High Voltage Open Loop Buck Converter Output Current

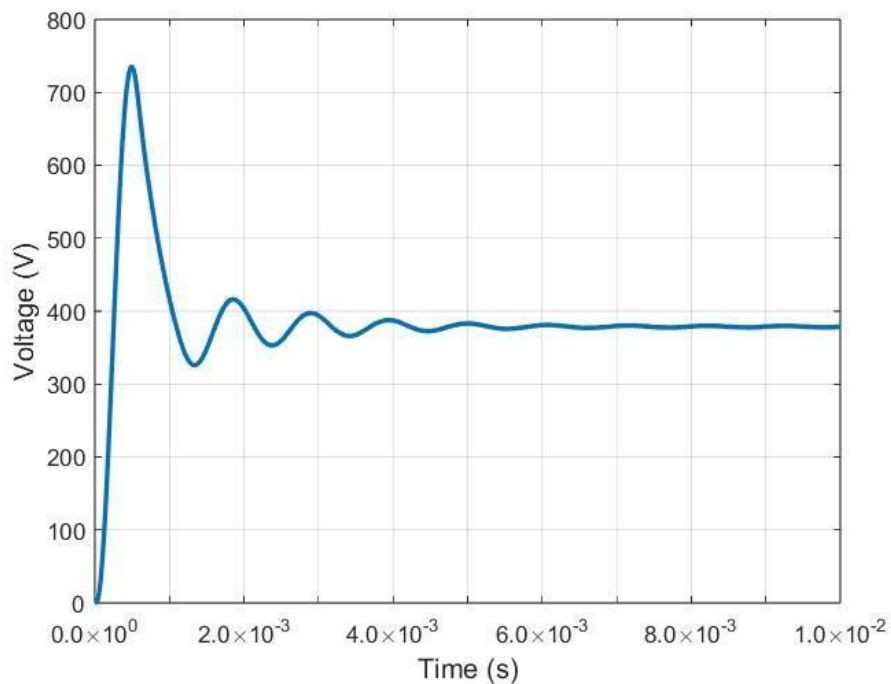


Figure 4.24: High Voltage Open Loop Buck Converter Output Voltage

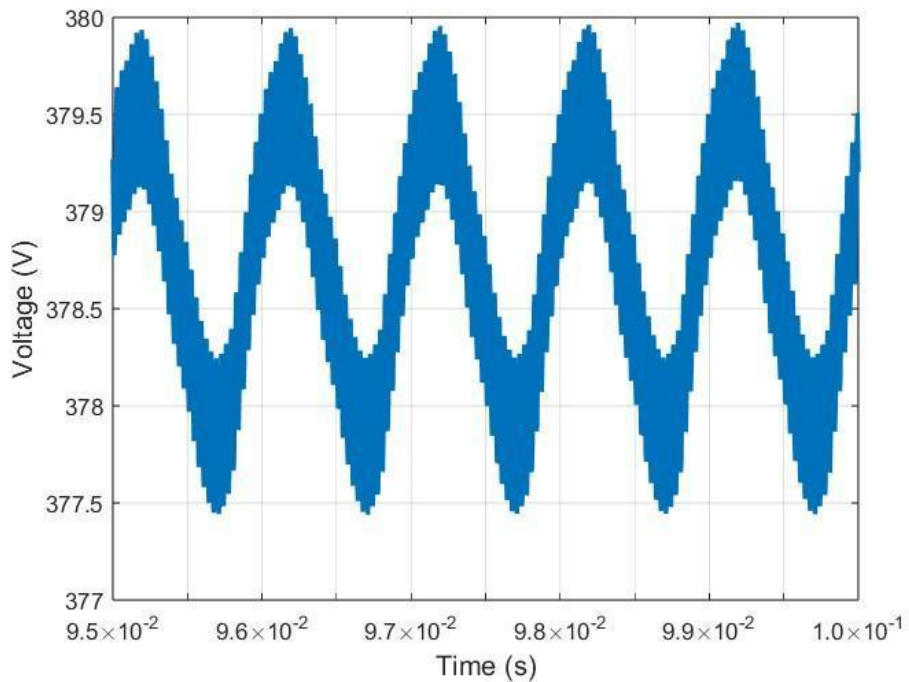


Figure 4.25: High Voltage Open Loop Buck Converter Output Voltage Ripple

As shown in the tables above, the output voltage approximately reached the rated value of 380 V; its maximum value was 379.9 V. The inductor was operating at CCM with a ripple inductor current of 41% and an output voltage ripple of less than 1%, which can be neglected. The graph (ripple voltage) displays that there are two that occurred; one of them is due to the input voltage fluctuations since the input voltage is not an ideal DC voltage, and the other ripple is due to the capacitor sizing; the overall ripple voltage is still minimal and did not negatively impact the results.

4.4.2 Low Voltage Buck Converter

With reference to Table 3.8, the low voltage buck converter supplied the needed output voltage with minimal ripple, along with a stable current while the inductor was operating in CCM.

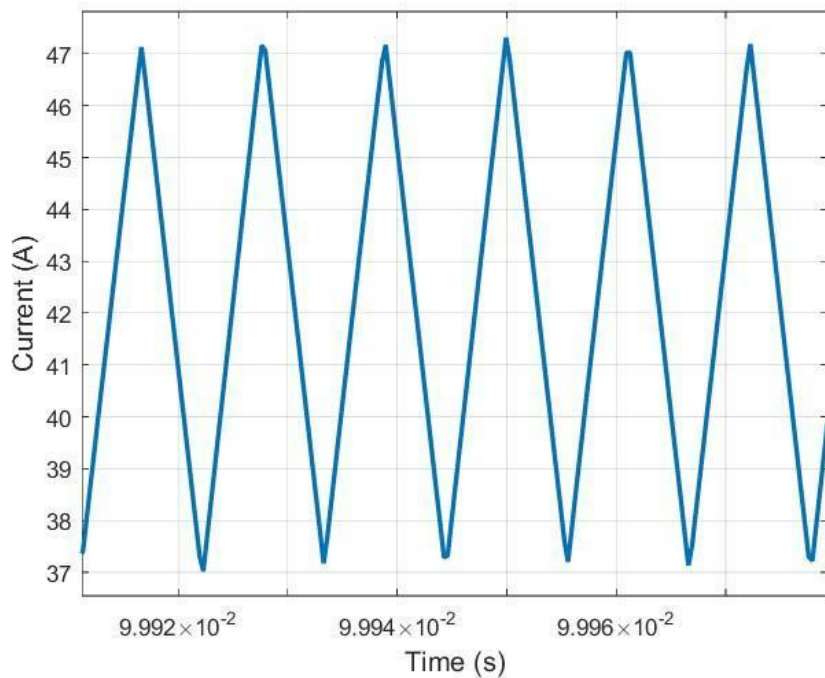


Figure 4.26: Low Voltage Open Loop Buck Converter Inductor Ripple Current

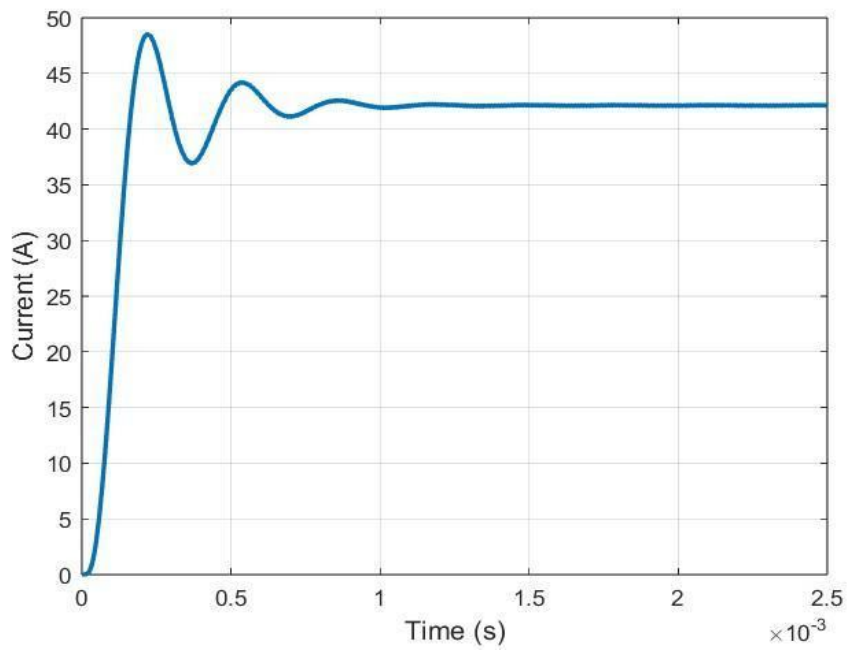


Figure 4.27: Low Voltage Open Loop Buck Converter Output Current

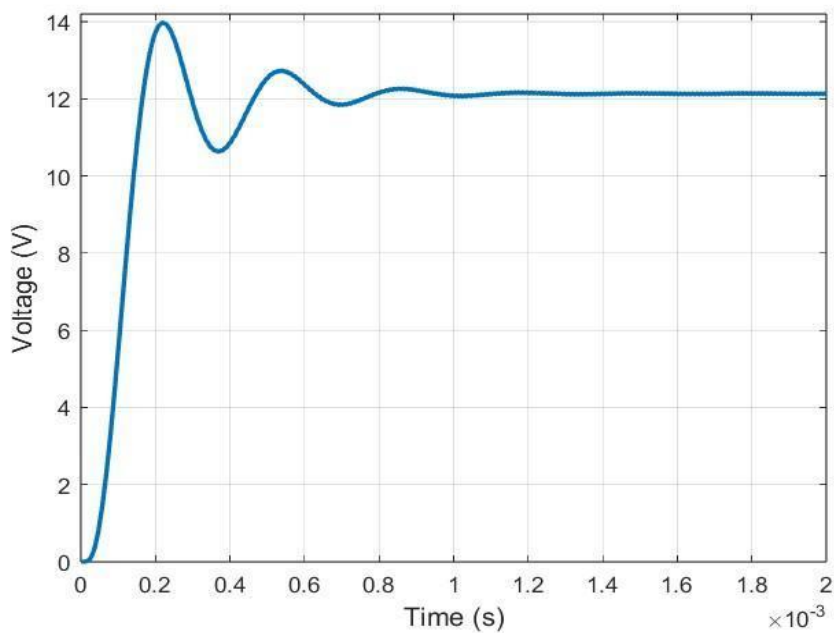


Figure 4.28: Low Voltage Open Loop Buck Converter Output Voltage

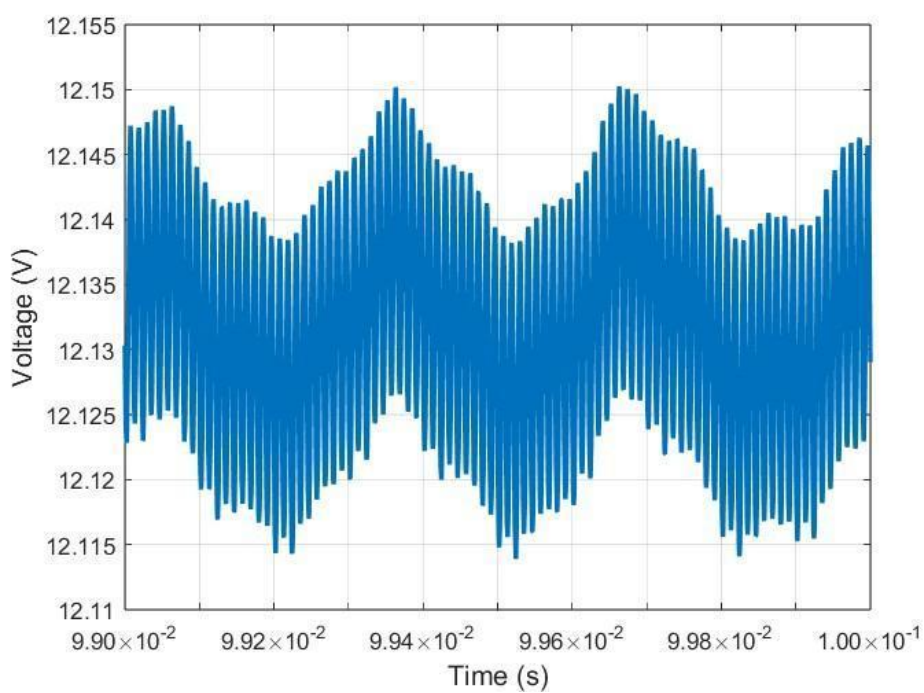


Figure 4.29: Low Voltage Open Loop Buck Converter Output Voltage Ripple

As shown in the figures above, the output voltage approximately reached the rated value of 12V; its average value was 12.30 V. The inductor was operating at CCM with a ripple inductor current of 24% and an output voltage ripple of 3%. The graph (ripple voltage) displays that there are two ripples that occurred; one of them is due to the input voltage fluctuations since the input voltage is not an ideal DC voltage, and the other ripple is due to the capacitor sizing; the overall ripple voltage is slightly higher than desired. The problems of both open-loop converters will be solved in the closed-loop design, especially the transient responses of both output voltages and currents, to ensure peak performance under different circumstances.

4.5 Output Closed Loop Results

4.5.1 High Voltage Buck Converter

With reference to Table 3.10, displaying the modified high voltage buck converter parameters, and with reference to the type-II controller design shown in Table 3.12, the closed-loop high voltage buck converter supplied the needed output voltage with minimal ripple, along with a stable current while the inductor was operating in CCM.

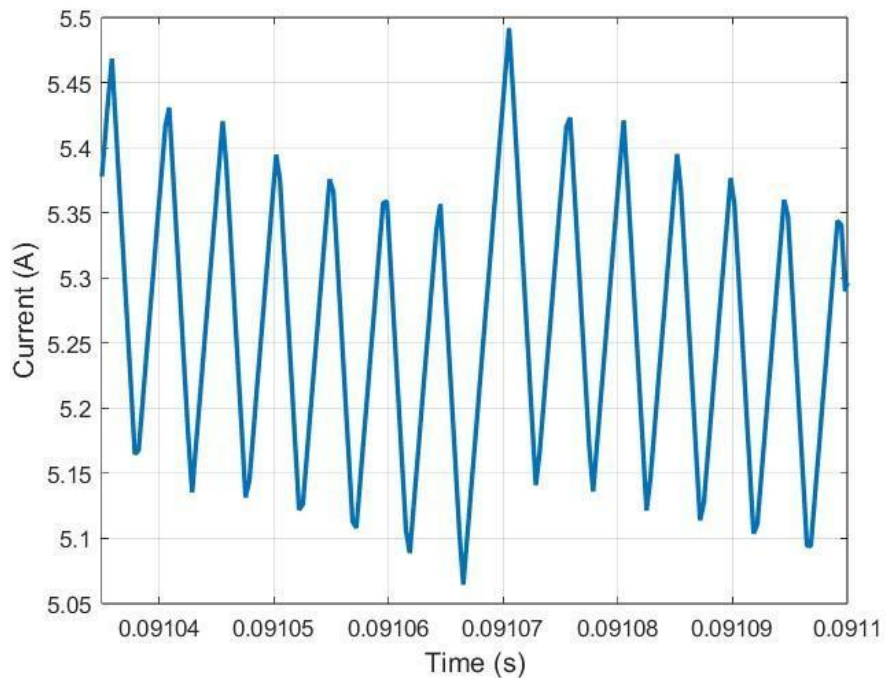


Figure 4.30: High Voltage Closed Loop Buck Converter Inductor Ripple Current

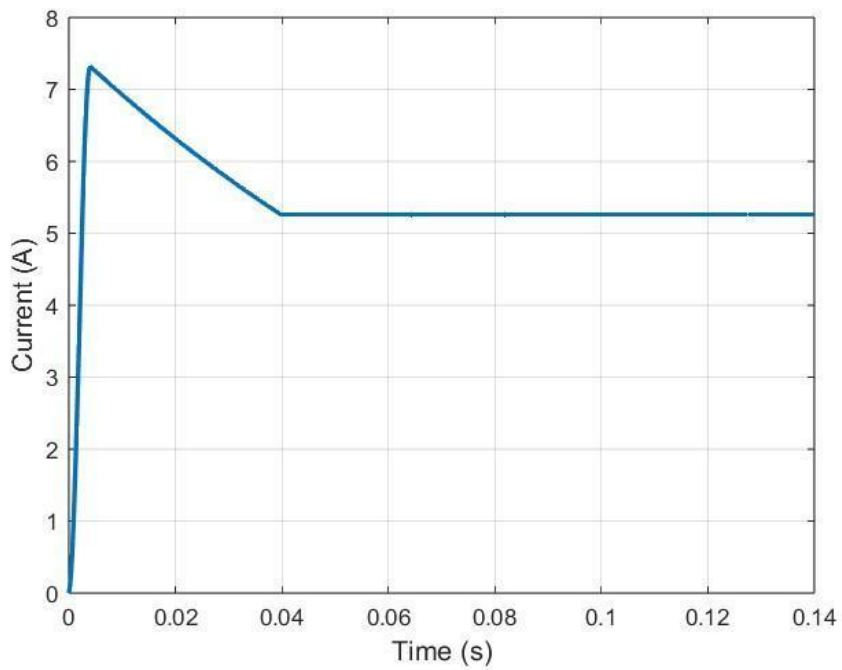


Figure 4.31: High Voltage Closed Loop Buck Converter Output Current

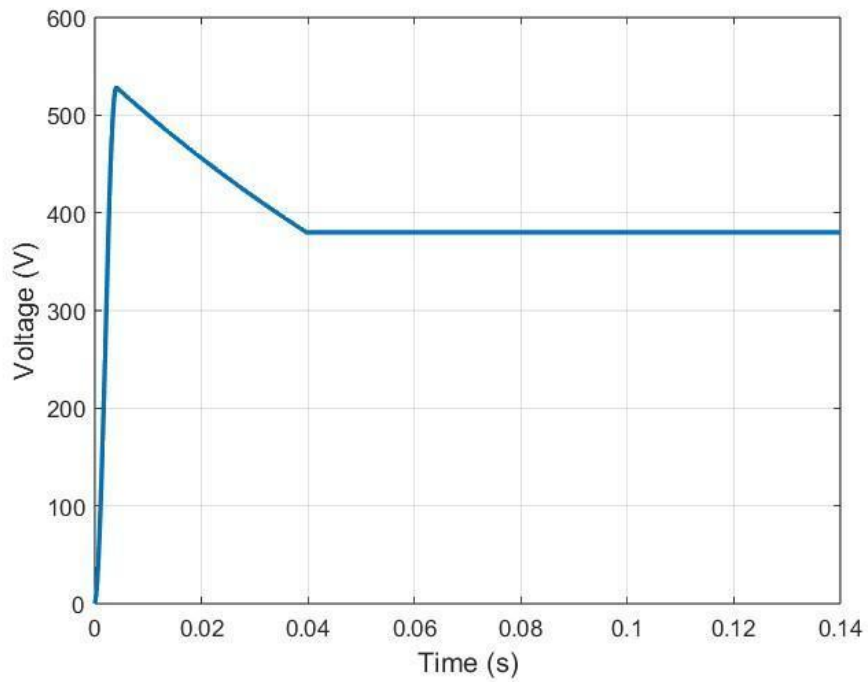


Figure 4.32: High Voltage Closed Loop Buck Converter Output Voltage

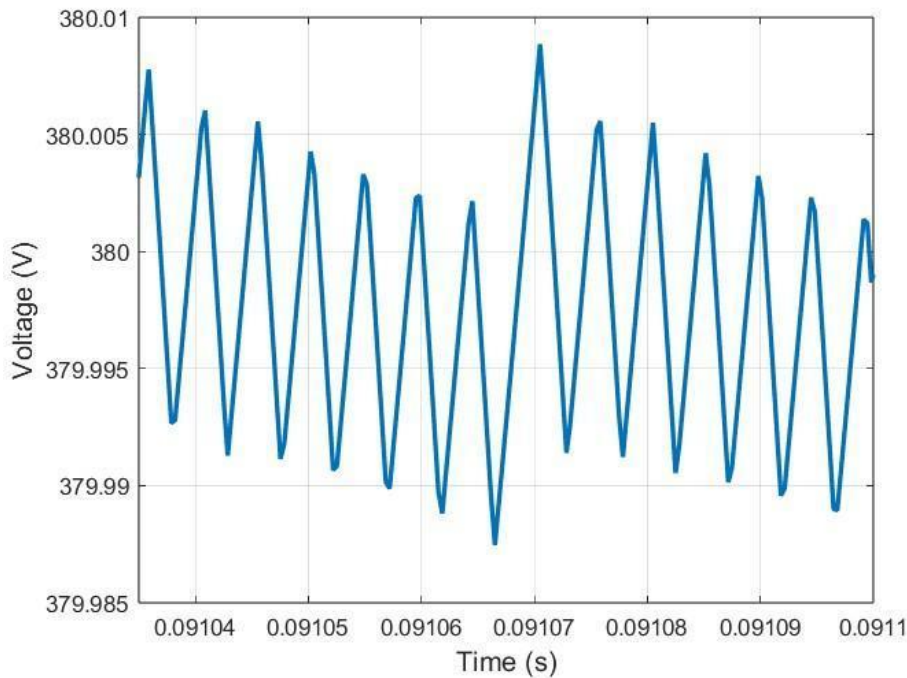


Figure 4.33: High Voltage Closed Loop Buck Converter Output Voltage Ripple

As shown in the graphs above, the closed loop design achieved the desired improvements by decreasing both transient responses of voltage and current outputs, along with decreasing the inductor current ripple to 7.7%, and the voltage ripple can be neglected. The closed loop design outputted an exact average voltage of 380 V. The peak transient current value was 7.2A, which is an accepted value since it is quickly damped to the operating current value of 5.26A.

4.5.2 Low Voltage Buck Converter

With reference to Table 3.11 and with reference to the type-II controller design shown in table Table 3.12. The closed loop low voltage buck converter supplied the needed output voltage with minimal ripple and a stable current while the inductor was operating in CCM.

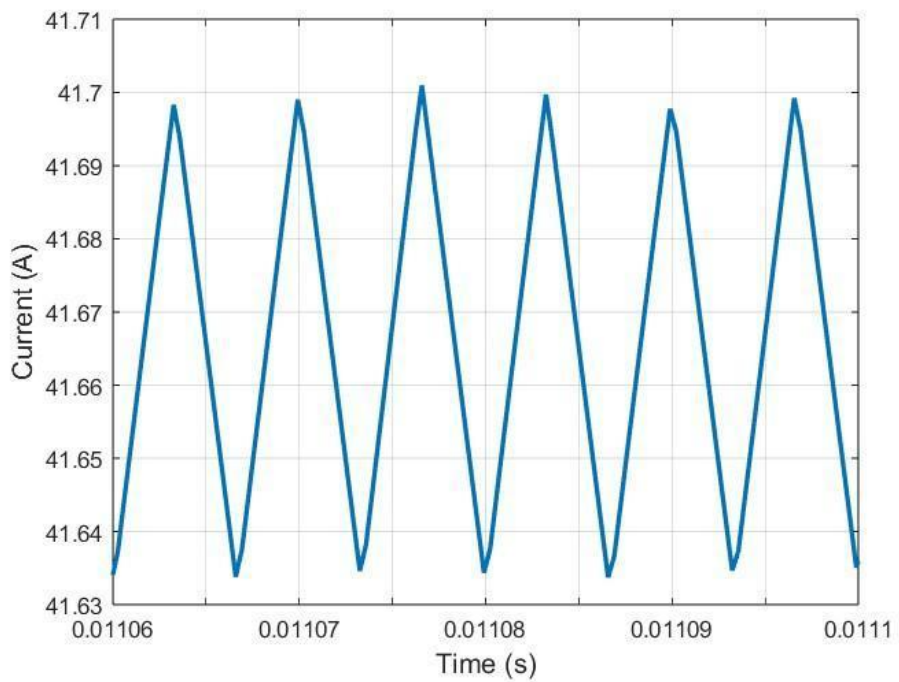


Figure 4.34: Low Voltage Closed Loop Buck Converter Inductor Ripple Current

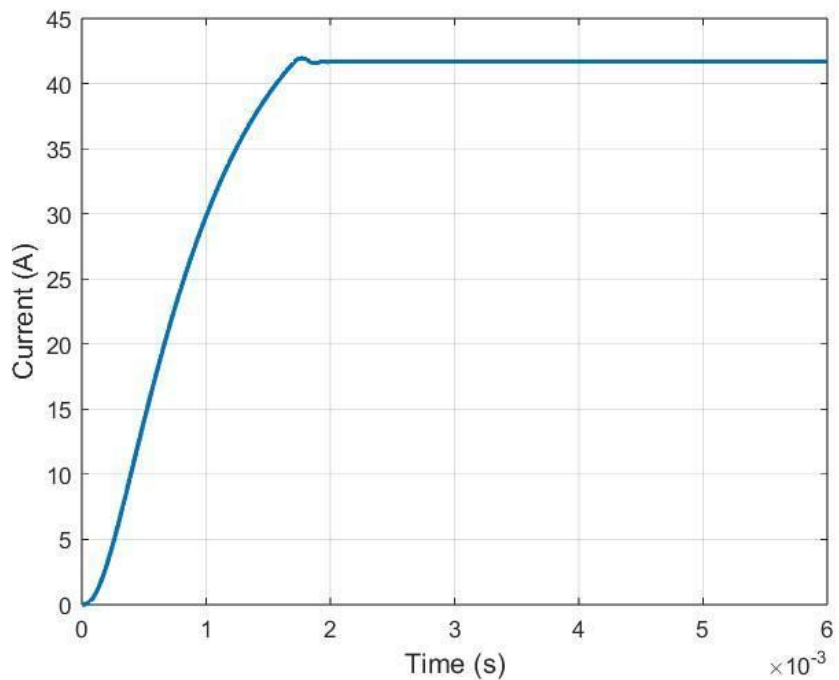


Figure 4.35: Low Voltage Closed Loop Buck Converter Output Current

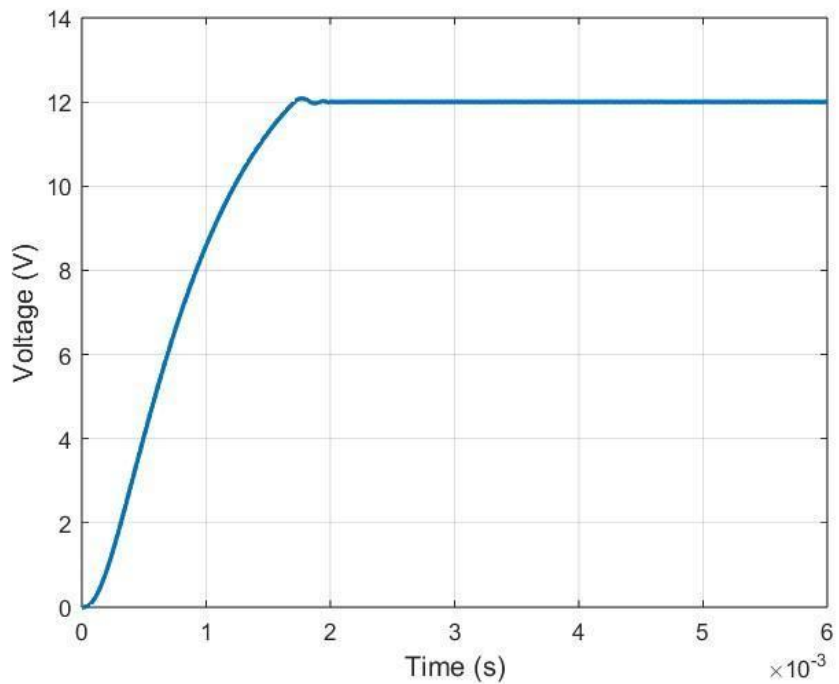


Figure 4.36: Low Voltage Buck Converter Output Voltage After Modification

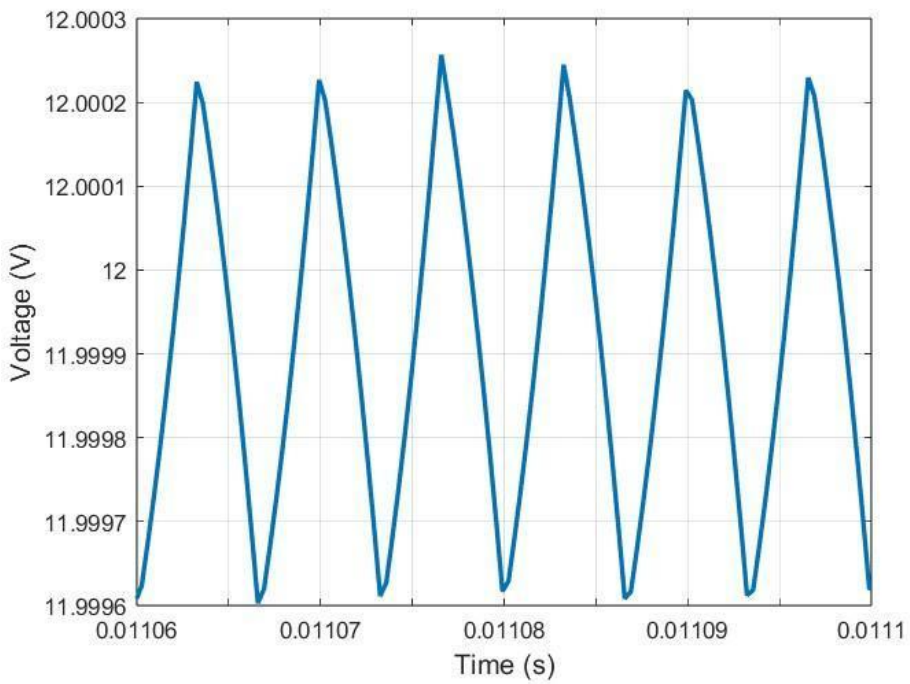


Figure 4.37: Low Voltage Buck Converter Output Voltage Ripple After Modification

As shown in the figures above, the closed loop design achieved the desired improvements by decreasing both transient responses of voltage and current outputs, along with decreasing the inductor current ripple to 0.2%, and the voltage ripple can be neglected. The closed loop design outputted an exact average voltage of 12V.

The closed loop results prove the robustness and high error compensation capabilities of the type-II controller, validating that power supply voltage control by using a type-II controller is the correct choice.

4.6 Full Circuit Results

4.6.1 Testing Multiport Converter (MPC)

The following three cases were carried out to test further system flexibility, robustness, and response to possible scenarios and disturbances.

- Case 1: EV is charging at 2000 W while household consumes no power
- Case 2: EV is disconnected, and the household operates at a rated power of 500 W
- Case 3: PV is shaded, load operating at total rated power (EV = 1500 W, household = 500 W)

These three cases represent the most common scenarios that can occur in the microgrid. In case 1, most EV drivers charge their car overnight while going to sleep so it can be fully charged in the morning. In case 2, when the car does not need further charging, and the household is operating at full capacity, this is a very common scenario bound to happen during day time, especially on holidays. Finally, in case 3, when the PV is shaded, this occurs every night when the sun is down, and occurs for prolonged periods during cloudy conditions, where the PV is also shaded during the day.

The following were the output voltages for each case.

- Case 1

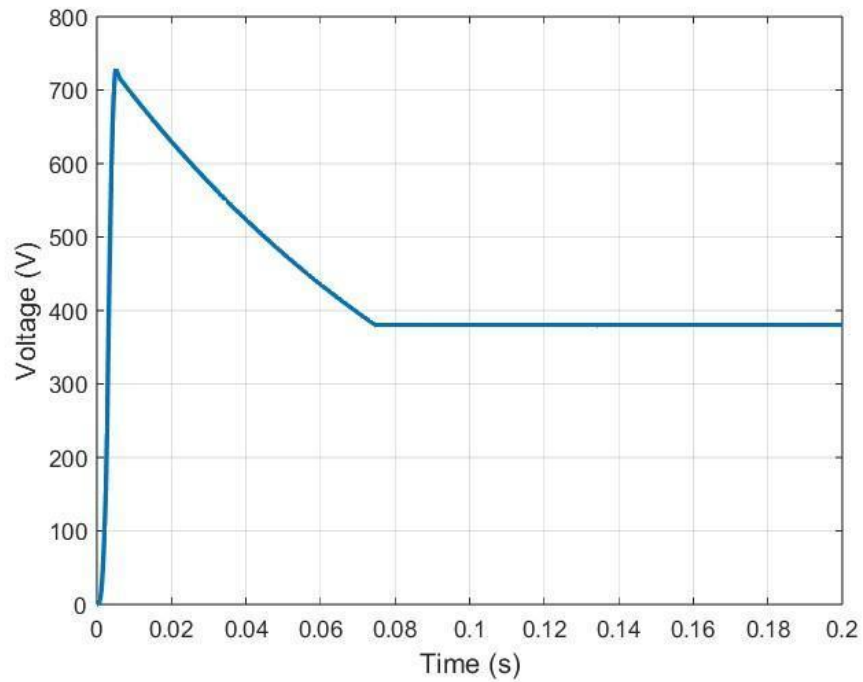


Figure 4.38: EV Voltage in Case 1

- Case 2

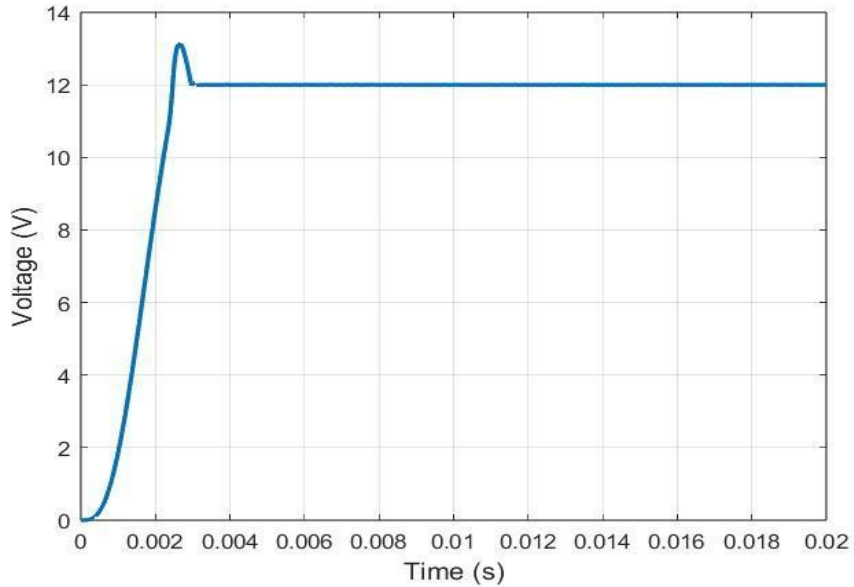


Figure 4.39: Household Voltage in Case 2

- Case 3

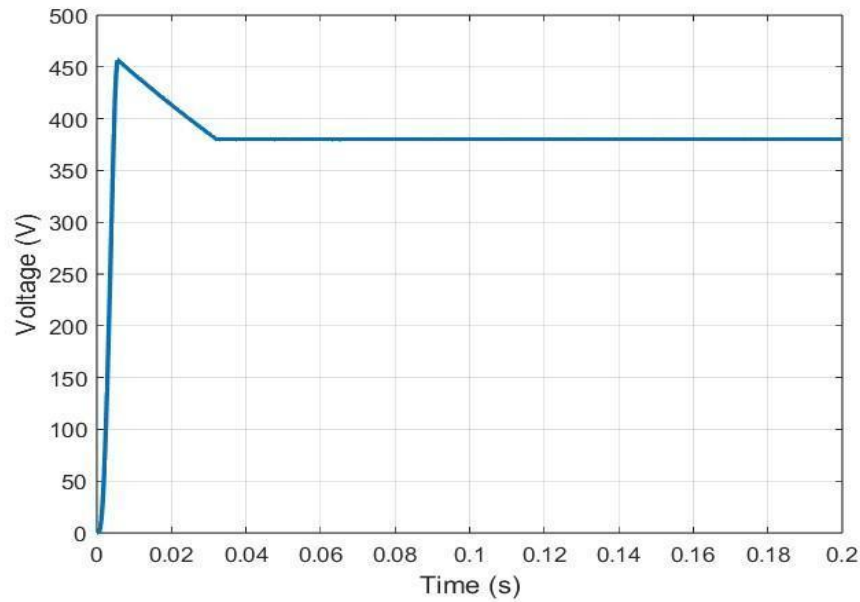


Figure 4.40: EV Voltage in Case 3

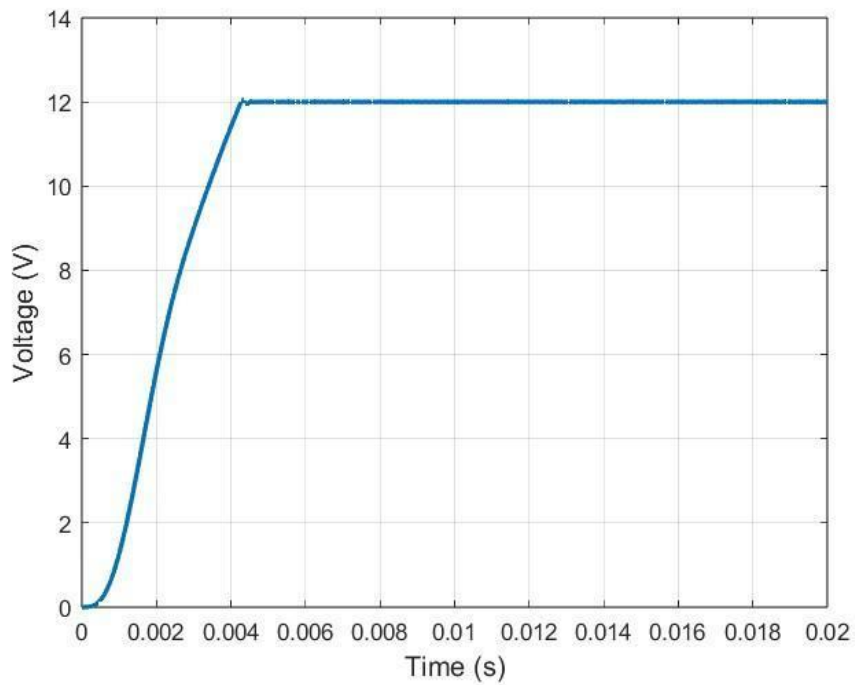


Figure 4.41: Household Voltage in Case 3

The following three cases were chosen based on their high probability of occurring. In the three cases, the mpc delivered the required output voltages for the EV and the household and was unaffected by the load and input changes. A notable change occurred in case 3, when the PV is shaded, the transient response for both load voltages is greatly improved, where the maximum voltage reached by the EV decreased from 725 V to 455 V.

After the closed-loop analysis for all buck and boost converters was conducted, the full bridge, along with the three-phase winding transformer design, was completed. All the parts were put together to complete the closed-loop full circuit. Below are the results at the nominal load where the EV consumes 1500 W and the household consumes 500 W; all steady-state transformer currents and voltages are displayed along with the output voltages and currents.

As displayed in Figure 4.5, the leakage inductances previously used to model the transformers were removed from both buck circuits because now the three-winding transformer is connected, and the leakage inductance effect is accounted for.

4.6.2 Transformer Voltages

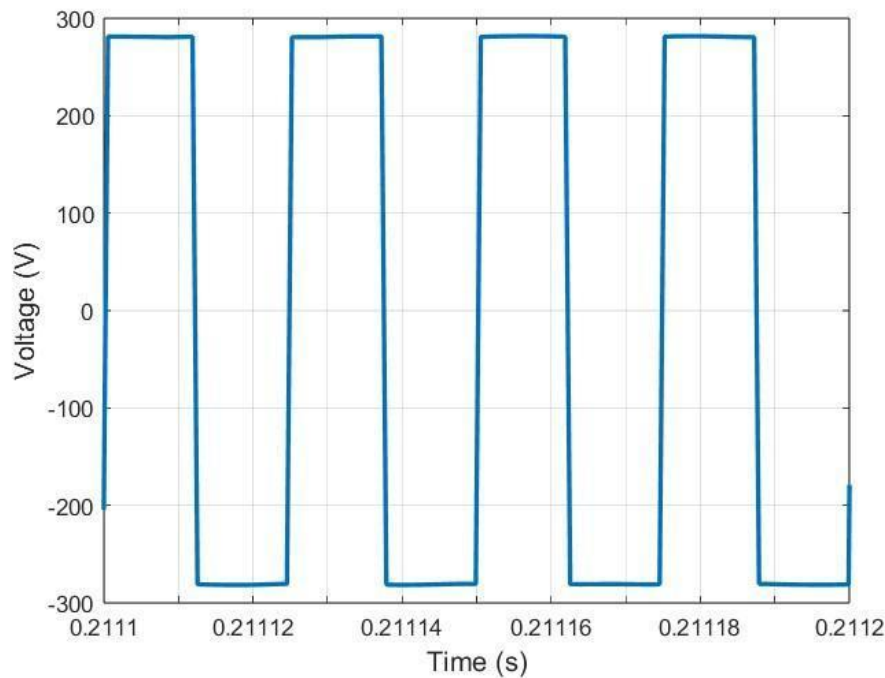


Figure 4.42: Primary Voltage

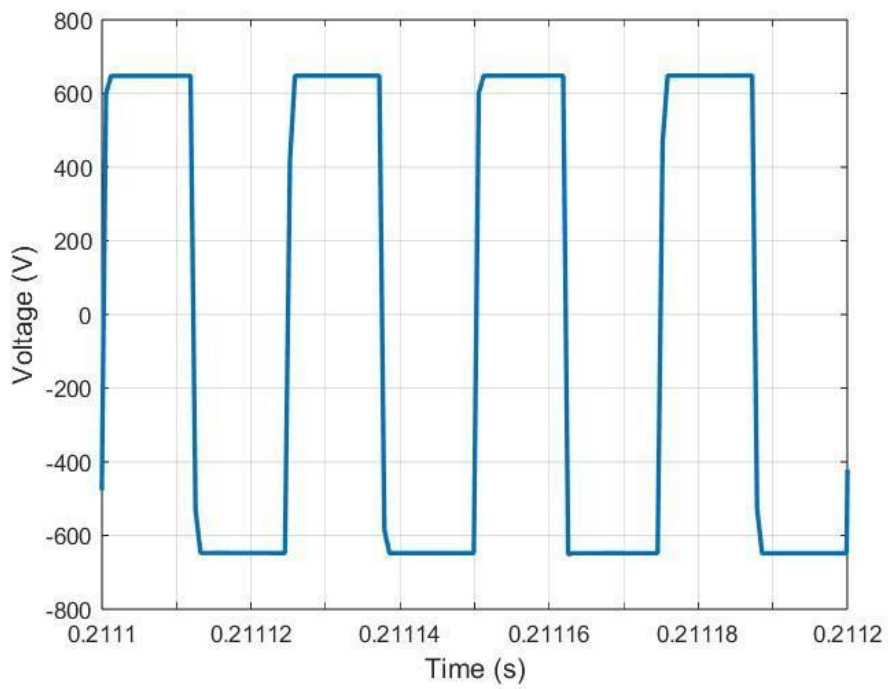


Figure 4.43: Secondary Voltage

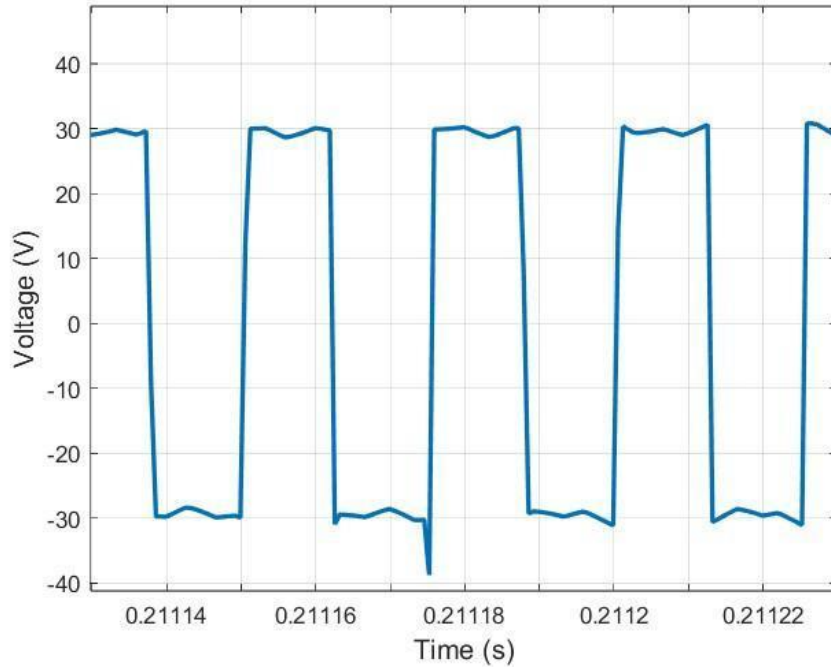


Figure 4.44: Tertiary Voltage

As shown in the figures above, the transformer's primary, secondary, and tertiary voltages were the same values as the calculated, showing the high efficiency and precision of the system, as shown in Figure 4.42, the primary voltage is an ideal square wave voltage with peak amplitude of 280 V, which is the voltage supplied by the DC-link capacitor.

4.6.3 Output Voltages and Currents

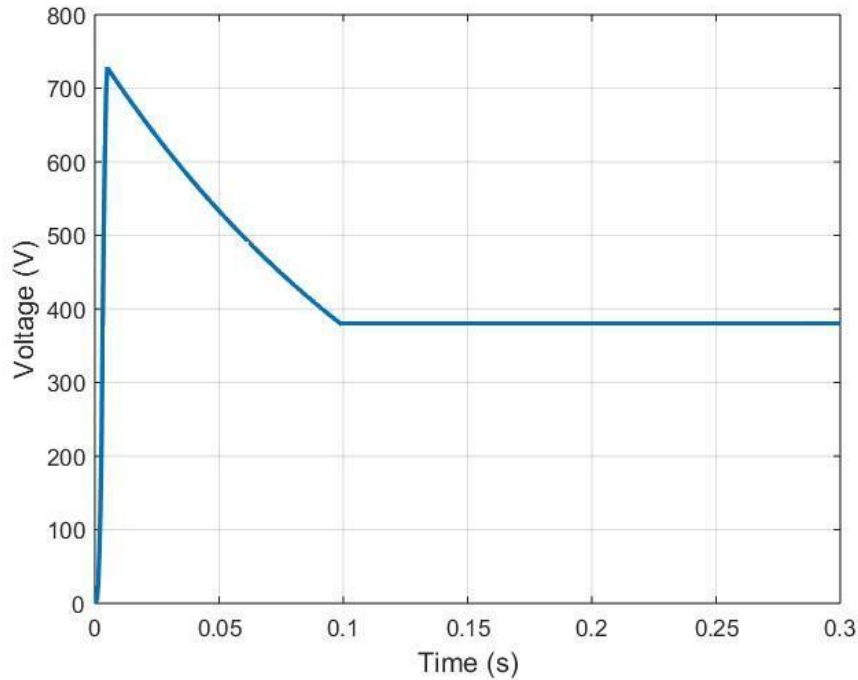


Figure 4.45: High Voltage Buck Converter Voltage Output

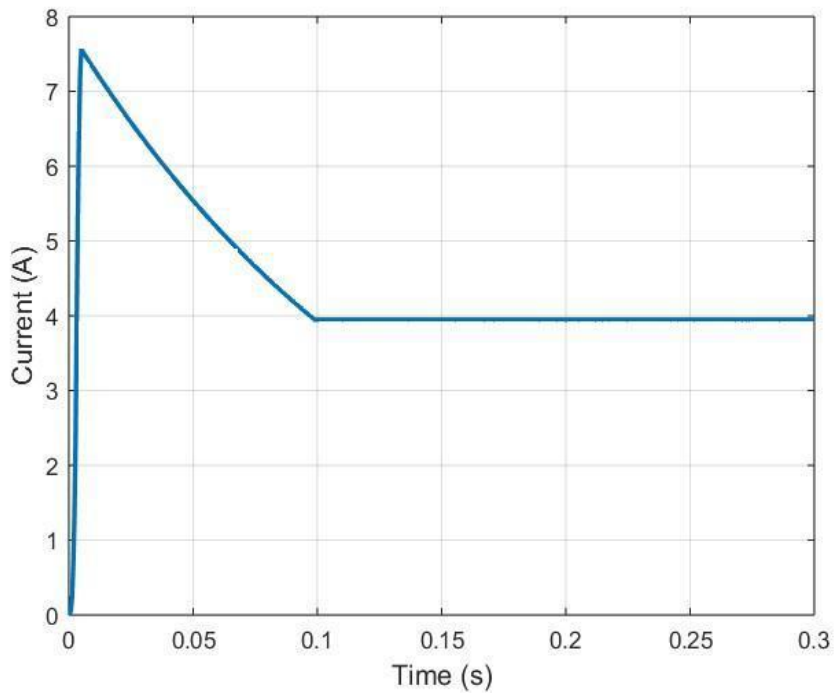


Figure 4.46: High Voltage Buck Converter Current Output

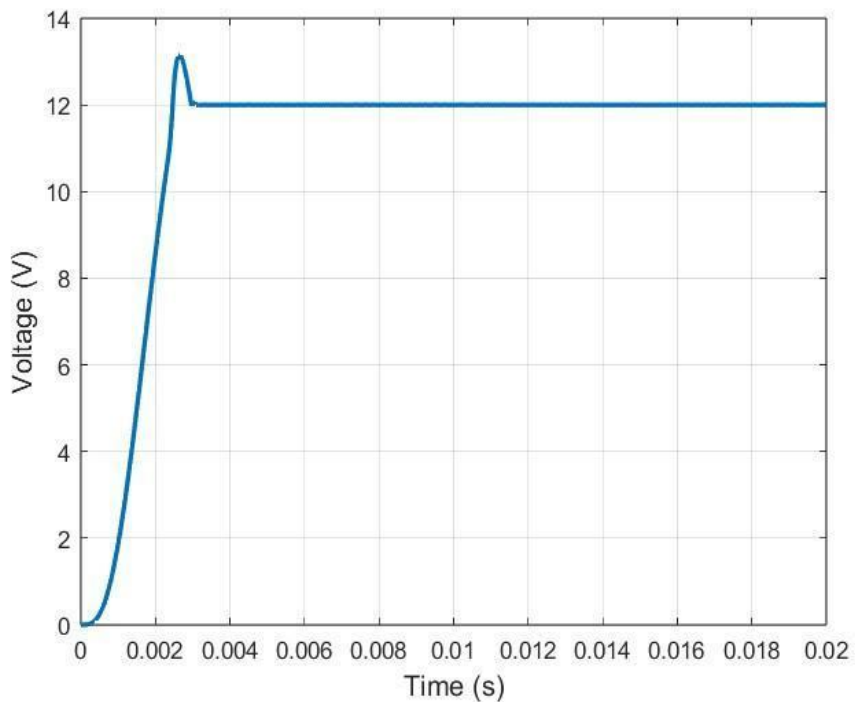


Figure 4.47: Low Voltage Buck Converter Output Voltage

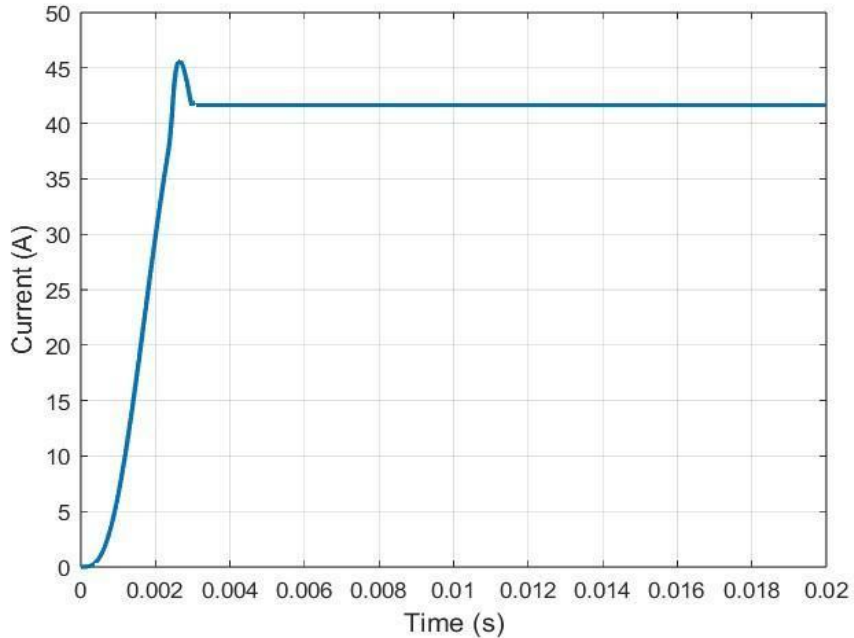


Figure 4.48: Low Voltage Buck Converter Output Current

The final output voltages of the converter met design requirements at nominal load, where the high voltage steady state output was 380 V and the steady state low voltage output was 12 V. The transient responses do not physically damage any of the loads or converter components; this is because they do not reach unreasonable values or dissipate huge amounts of power. For the high-voltage converter, the transient response lasted for 0.1 seconds, which is relatively fast. Meanwhile, the low voltage converter transient response lasted for 0.003 seconds, which is 33 times faster than the high voltage converter; this is due to the low voltage converter having a smaller capacitor and inductor and a higher switching frequency, so it has a faster response time.

With reference to the low voltage converter having a relatively high nominal output current of 41.67A at the steady state output voltage of 12V. These ratings for a household are not used due to the high current consumption, which can lead to high power losses and increasing costs due to the lines carrying this current having a high cross-section area to safely connect the converter to the household appliances. In theory and simulation, the low voltage buck converter fully worked with no problems, although practically lower currents are suggested at the specified voltage level, but the specified voltage levels were successfully met.

The output voltage level requirements are achieved, proving the validation of the design. This is also proven by the output voltages of both input boost converters and all transformer voltages, primary, secondary and tertiary voltages. Where all voltages successfully reached the values that were desired. The low ripple shown in the closed loop results also shows the validation of the converter parameter along with the correct choice and design of the type-II and type-III controllers.

4.6.4 Full Circuit Efficiency Test

In order to meet design requirements, the full circuit efficiency at nominal load should be at least 90%. The EV connected to the high voltage circuit consumed 1500W, while the household consumed 500W, making a total output power of 2000W, which is the nominal load, under the mentioned load conditions. The efficiency of the mpc, was tested under full load conditions at 2000W and also under the following output power ratings: 1500W, 1000W, 500W, 100W. The table below displays the input and output power ratings along with the efficiency of the converter at each dissipation stage.

Table 4.1: Input and Output Power Ratings and Converter Efficiency

Input Power (W)	Output Power (W)	Efficiency(%)
106.000	100	94.00
529.416	500	94.44
1029.390	1000	97.145
1529.676	1500	98.060
2049.856	2000	97.568

Table 4.2: The Parameters of Mosfets and Diodes

Parameter	Value
Number of MOSFETS	8
Number of Diodes	14
R_{ds} (mΩ)	4.8
Diode Resistance (mΩ)	1
Diode Forward Voltage (V)	0.3
Diode Reverse Recovery Time (nS)	35

Efficiency is the percentage ratio of output power to input power. Equation 4.1 below shows that the efficiency (*Eff*) of the full circuit is 97.568%.

$$Eff = \frac{Total P_{out}}{Total P_{in}} \times 100\% \quad (4.1)$$

This result proves the high efficiency of the converter, which is 97.568% at full load; it is completely normal that the input power generated was greater than 2000 W, where it drew 2049.856 W because the converter draws additional power from the input sources to meet the nominal load demands. At nominal load, the power lost was 49.856 W. With reference to Table 4.2, this is mostly

due to the power lost due to the resistance values of the MOSFETs and capacitors, along with the resistance, forward voltage, and reverse recovery time of the diodes present in the converter. Even with the power dissipated on the MOSFETs and diodes and also the power lost due to ESR, the efficiency of the mpc is still high, and the minimum efficiency requirement of 90% is achieved under nominal load.

Table 4.1 shows the efficiency of the converter under different loads was not heavily effected, where the minimum efficiency was 94%, when the output load was only consuming 100W, and the maximum efficiency was 98.06% while the load was consuming 1500W. The results prove the high efficiency of the converter under various load conditions.

4.6.5 Voltage Regulation

The converter's voltage regulation was tested by substituting each of the EV and household loads by $10 \text{ M}\Omega$ to simulate the no-load effect. After conducting the test for both outputs, $V_{OH_{N.L}} = 381.5 \text{ V}$ $V_{OL_{N.L}} = 13.3 \text{ V}$. As shown, the increase in both voltages did not increase by more than 10.83%. These results approximately achieve the required voltage regulation design requirement. The voltage regulation achieved is very close to the required voltage regulation; the difference between the desired and the actual voltage regulation is only 0.83%. The voltage regulation of the system is still high and does need further improvement.

4.6.6 Fault Test

For the fault test, a short circuit fault has been introduced to the household load; since the topology is isolated and both loads have separate controllers, the fault does not affect the functionality of the high-voltage side output.

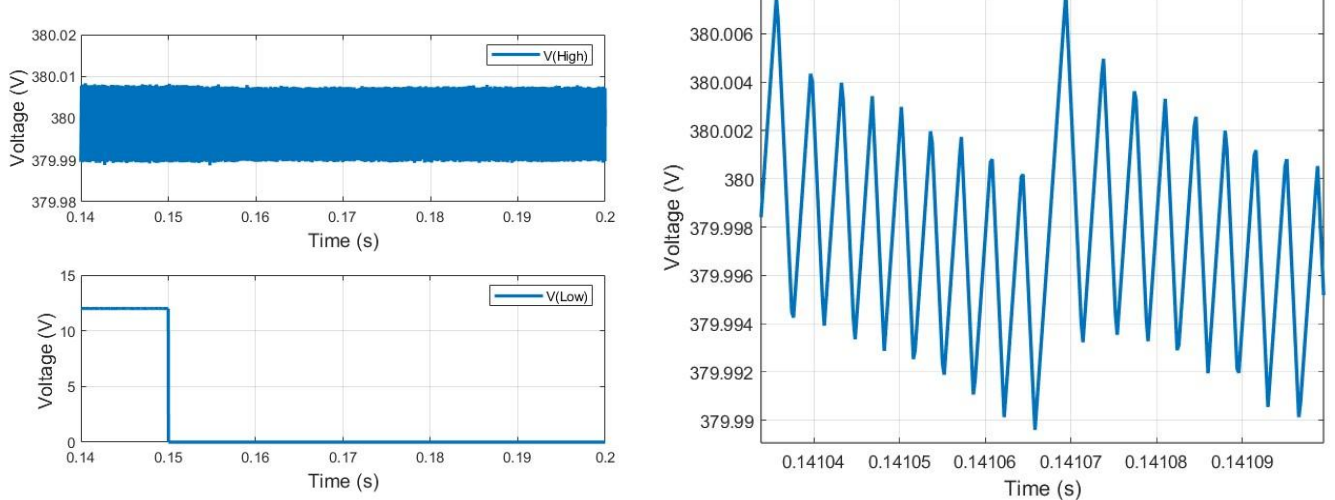


Figure 4.49: Output Voltage and Ripple at High Voltage Output During Short Circuit Fault at Low Voltage Output

As shown in Figure 4.49, the voltage on the high-voltage side (EV-side) was not affected by the short circuit fault on the low-voltage load (household side). The isolation provided by the transformers and each load having its independent and tailored analog controller allowed for the output load to be unaffected by a possible short circuit on the other output terminal. The IEEE 1547 standard mentioned in section 3.3.1 is successfully satisfied.

4.6.7 Validation of The Requirements

Table 4.3: Validation Summary

	Parameter	Required	Achieved	Reference
	PV Input Source	150-250 V	×	sec. 3.6.1.3 sec. 4.3.2
	Battery Input Source	48-52 V	48-52 V	sec. 3.6.1.4 sec. 4.3.3
	Output Voltage	380 V and 12 V	380 V and 12 V	sec. 3.6.2 sec. 4.4
	PV Power Rating	1000 Wp	1000 Wp	sec. 3.6.1.1

Requirements				sec 4.3.1
	MPPT	Implementation	✓	sec. 3.6.1.2 sec 4.3.1
	Battery Capacity	180 Ah	–	Can not be validated through simulation
	System Power Rating	2 kW	2 kW	sec. 3.6.2 sec. 4.6.4
	Simulation Tools	PSIM or MATLAB	PSIM and MATLAB	All simulations and results were conducted using PSIM and MATLAB
	Conversion Efficiency	>90%	97.568%	sec. 4.6.4
	Voltage Regulation	90%-110%	110.83%	sec. 4.6.5
Engineering Standard	Service Continuation During Fault	Continuation of Service	✓	sec 4.6.6
Economic Constraints	Cost	<500 JOD	✓	System was modelled using simulation tools, no cost was needed
Manufacturability and Sustainability Constraints	Voltage and Power Level	Reduced Voltage and Power Level	–	System was modelled using simulation tools, no reduction was needed
Environmental constraints	–	–	–	–

5 Conclusion and Future Work

5.1 Conclusion and Future Work

This investigation tackled the design of a multiport port converter, having two inputs and two outputs, where the inputs are a PV array and a 48 V battery, and the outputs are an EV and a small household, creating an independent DC microgrid. This investigation successfully presented a new and never-before-seen design to successfully interface multiple input sources with multiple output loads at different voltage levels. The converter successfully met the output voltage levels of 380 V for the EV and 12V for the small household while respecting input voltage source restrictions.

The conversion efficiency requirement was met, where the multi-multi converter achieved a 97.568% efficiency at full load. Moreover the converter had a minimum efficiency of 94% at 100W load, and a maximum efficiency of 98.060% at 1500W load. So the mpc work efficiency under various load conditions.

For the 1000 Wp PV array, the MPPT function was successfully used by implementing the perturb and observe algorithm. Two boost converters were used to interface both input sources, and then the output of both boost converters entered a full bridge to inverter the DC voltage. A three-phase winding transformer was used for isolation, protection, and to control the voltage levels entering the output buck converter circuits. The AC voltage supplied by both secondary and tertiary windings was then rectified by using an H-bridge and further smoothed by a filter capacitor to supply both buck converters with a DC voltage with minimal fluctuations. The AC voltage supplying the high-voltage buck converter was 650 V, while the AC voltage supplying the low-voltage buck converter was 30 V. Finally, both buck converters output exactly the required voltage levels at nominal loads of 380 V and 12 V.

Analog voltage-mode control was used for both buck and boost circuits in the system. Both boost converters required a type-III controller with compensations to output the tailored voltage levels needed successfully. Furthermore, both buck converters required a type-II controller with error compensation to flawlessly deliver the required output voltage levels. Both controllers offered proficient, efficient, and robust voltage control; the three tests prove this was carried out on the converters. The robustness of the control system, as a whole, means that the multi-multi converter can handle extreme scenarios, which was proved. The system was tested when the EV was not charging, the household was completely turned off, and the PV was shaded on a cloudy day. The multi-multi-port converter proved that no matter the input or output fluctuations, the system competently supplied the needed voltage for the load or loads connected.

The concept of multiport converters with multiple inputs and outputs at the same time is the future of DC microgrids. This investigation laid the basis for further studies to implement multi-input, multi-output converters on a larger scale and with further enhancements. This investigation opens the door for further studies regarding the addition of a soft starter to dampen the transient response further. Establishing two bidirectional power flow loops. The first loop is between both input sources, where the PV charges the battery when sunny conditions are imminent; this reduces

battery aging, decreases costs, and further increases system efficiency. The other bidirectional power flow loop is from the EV battery to load, where the EV battery can operate as an input source to the household during night time. If implemented properly, this will further decrease costs while prolonging both the battery lives of the 48V battery and the EV battery. Modifications are needed to allow power to flow in both directions, to make a bidirectional full-bridge converter, and to add bidirectional power flow effectively and efficiently. This requires switching control, such as using the dual active bridge DAB. The implementation of a DAB offers bidirectional power flow and better efficiency since soft switching is introduced.

Finally, the tackled project can be enhanced by increasing the converter's power rating to supply a handful of apartments along with multiple EVs sufficiently. This can be efficiently achieved by applying bidirectional power flow with the addition of a dual active bridge, soft starters, and further control techniques to achieve soft switching and to ensure converter reliability and robustness under varying loads.

References

- [1] “(PDF) Operation cost minimization of droop-controlled DC microgrids based on real-time pricing and optimal power flow,” *ResearchGate*, 2015, doi: <https://doi.org/10.1109/IECON.2015.7392709>.
- [2] N. M. Kandari, "DC Microgrids," in *Microgrids*, Academic Press, 2022, pp. 91-139.
- [3] SEngineer corner aa, “Gilbert M. Masters-Renewable and Efficient Electric Power System (2013),” *Academia.edu*, 2023. https://www.academia.edu/44366784/Gilbert_M_Masters_Renewable_and_Efficient_Electric_Power_System_2013_ (accessed Apr. 30, 2024).
- [4] J. Sun, W. Lin, M. Hong, and K. A. Loparo, “Voltage Regulation of DC-Microgrid with PV and Battery: A Passivity Method,” *IFAC-PapersOnLine*, vol. 52, no. 16, pp. 753–758, Jan. 2019, doi: <https://doi.org/10.1016/j.ifacol.2019.12.053>.
- [5] A. H. Sabry, A. H. Shallal, Hayder Salim Hameed, and Pin Jern Ker, “Compatibility of household appliances with DC microgrid for PV systems,” *Helijon*, vol. 6, no. 12, pp. e05699–e05699, Dec. 2020, doi: <https://doi.org/10.1016/j.heliyon.2020.e05699>.
- [6] Pouya, Kolahian., Hadi, Tarzamni., Amir, Nikafrooz., Mohsen, Hamzeh. (2019). Multi-port DC-DC converter for bipolar medium voltage DC micro-grid applications. *Iet Power Electronics*, doi: 10.1049/IET-PEL.2018.6031
- [7] Y.-K. Tran and Drazen Dujic, “A multiport medium voltage isolated DC-DC converter,” *Infoscience (Ecole Polytechnique Fédérale de Lausanne)*, Oct. 2016, doi: <https://doi.org/10.1109/iecon.2016.7793699>.
- [8] S. Biswas, Sairaj Dhople, and N. Mohan, “Zero-ripple analysis methods for three-port bidirectional integrated magnetic Cuk converters,” Oct. 2014, doi: <https://doi.org/10.1109/iecon.2014.7048759>.
- [9] J. Sun, W. Lin, M. Hong, and K. A. Loparo, “Voltage Regulation of DC-Microgrid with PV and Battery: A Passivity Method,” *IFAC-PapersOnLine*, vol. 52, no. 16, pp. 753–758, Jan. 2019, doi: <https://doi.org/10.1016/j.ifacol.2019.12.053>.
- [10] Fahad Saleh Al-Ismail, “DC Microgrid Planning, Operation, and Control: A Comprehensive Review,” *IEEEaccess*, vol.9, pp.36154–36172, Jan. 2021, doi: <https://doi.org/10.1109/access.2021.3062840>.
- [11] Jackson John Justo, F. Mwasilu, J. Lee, and Jin Woo Jung, “AC-microgrids versus DC-microgrids with distributed energy resources: A review,” *Renewable & sustainable energy reviews*, vol. 24, pp. 387–405, Aug. 2013, doi: <https://doi.org/10.1016/j.rser.2013.03.067>.

- [12] C. Ndeke, M. Adonis, and A. Almaktoof, “Energy Management Strategy for DC Micro-Grid System with the Important Penetration of Renewable Energy,” *Applied Sciences*, vol. 14, no. 6, pp. 2659–2659, Mar. 2024, doi: <https://doi.org/10.3390/app14062659>.
- [13] G. Rueter, “How EVs can store energy for homes and power grids,” *dw.com*, Dec. 27, 2024. <https://www.dw.com/en/how-evs-can-store-energy-for-homes-and-power-grids/a-71171661>
- [14] D. W. Hart, *Power electronics*. New York, N.Y.: McGraw Hill, 2011.
- [15] I. X. Zanatta, Marcello Mezaroba, Alessandro Batschauer, Ricardo, and B. Lodi, “A DC-DC ZVS Phase-Shift PWM full-bridge current-mode controlled converter with multiples outputs for photovoltaic applications,” vol. 6, pp. 1–6, Nov. 2015, doi: <https://doi.org/10.1109/cobep.2015.7420180>.
- [16] R. Sankar and N. K. Kala, “Implementation of full-bridge three-port converters with wide input voltage range for renewable energy systems,” pp. 3675–3680, Aug. 2017, doi: <https://doi.org/10.1109/icecds.2017.8390149>.
- [17] Mohsen Asgari Moqaddam and M. Hamzeh, “PWM plus secondary-side phase-shift controlled full-bridge three-port bidirectional converter for application in MVDC distribution networks,” Jan. 2017, doi: <https://doi.org/10.1109/pedstc.2017.7910318>.
- [18] “SP-M10/144H530W-560W (Black Frame),” *Enfsolar.com*, 2023. <https://www.enfsolar.com/pv/panel-datasheet/crystalline/59610>
- [19] “IEEE Standards Association,” *IEEE Standards Association*, Jan. 03, 2025. <https://standards.ieee.org/>
- [20] Ang, S., & Oliva, A. 2010. *Power-Switching Converters* (2nd ed.).

Appendices

Appendix A: PV Datasheet

Specifications

Solar Cell (Type/Sizes)	Mono(182mm)
Solar Cells Number	144Pcs (6*24*2)
Dimensions	2279*1134*35mm
Weight	28.32KG/Pcs
Structure	3.2 Glass+EVA Film+Back
Frame	Anodized aluminum alloy
Junction Box	IP68/3*Bypass Diode
Cable Cross Section Size	4.0mm ² /300mm
Mechanical Load	Front 5400Pa/Back 2400Pa
Packing Number	31Pcs/Pallet
Carton Size	2309*1125*1250mm
40'HQ Container	620 Pcs

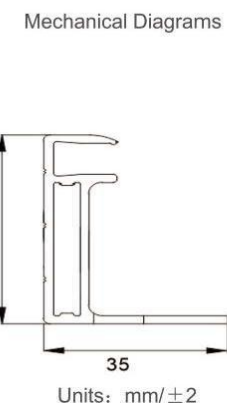
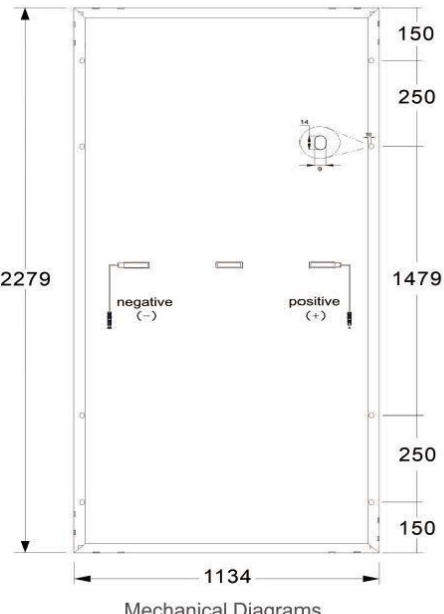
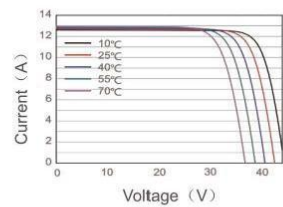
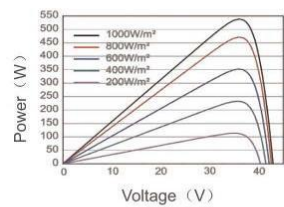
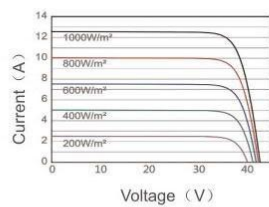
Electrical Parameters at STC

Module Type	PMH525W	PMH530W	PMH535W	PMH540W	PMH545W	PMH550W
Rate Maximum Power (Pmax)	525W	530W	535W	540W	545W	550W
Module Efficiency	20.30%	20.50%	20.70%	20.90%	21.10%	21.30%
Voltage at Pmax (Vmp)	41.10V	41.27V	41.45V	41.62V	41.80V	41.97V
Current at Pmax (Imp)	12.78A	12.85A	12.91A	12.98A	13.05A	13.11A
Open Circuit Voltage (Voc)	48.95V	49.15V	49.35V	49.55V	49.75V	49.95V
Short Circuit Current (Isc)	13.67A	13.74A	13.82A	13.89A	13.97A	14.05A
Power Tolerance	0~+5W					
Temperature Coefficient of Isc	+0.046%/ $^{\circ}$ C					
Temperature Coefficient of Voc	-0.276%/ $^{\circ}$ C					
Temperature Coefficient of Pmax	-0.350%/ $^{\circ}$ C					
STC	Irradiance 1000W/m ²	Cell Temperature 25 $^{\circ}$ C	AM1.5			

Operating Conditions

Operating Temperature	-40~+85 $^{\circ}$ C
Maximum System Voltage	1500VDC
NOCT	45±2 $^{\circ}$ C
Fireproof Performance	Glass C
Maximum Series Fuse	25A
Temperature Coefficient of Voc	-0.276%/K
Temperature Coefficient of Isc	+0.046%/K

Characteristics



Units: mm/±2

Appendix B: CODE

Boost Converter MATLAB code:

```
clear all  
close all  
CLC  
  
s=tf('s');  
  
L=350e-6;  
  
C=150e-6;  
  
R=78.4;  
  
r=120e-3;  
  
rl=0e-3;  
  
D=0.46;  
  
V=150.00;  
  
Q=R*sqrt(C/L);  
  
Le=L/(1-D)^2;  
  
num=(V/(1-D)^2)*(1-s*(Le/(R-rl)))*(1+s*r*C);  
  
den=Le*C*(s^2+(1/(R*C)+r/Le)*s+1/(Le*C));  
  
sys=num/den;  
  
bode(sys);  
  
grid on;  
  
margin(sys);
```

```
fco=2500;  
pm=-177;  
pc=45-pm;  
gm=22;  
G=10^(gm/20);  
K=(tand((pc+90)/4))^2;  
R1=1e3;  
R2=G*R1/sqrt(K);  
C1=sqrt(K)/(2*pi*fco*R2);  
C2=1/(sqrt(K)*2*pi*fco*R2);  
C3=sqrt(K)/(2*pi*fco*R1);  
R3=1/(2*pi*fco*sqrt(K)*C3);
```

High Voltage Adjusted Buck Converter MATLAB code:

```
Vs= 650;
Vo= 380;
P=2000;
R=Vo^2/P;
F=3.00e4;
L=2.5e-3;
C=1.5e-3;
ESR=50e-3;
a=(Vs / (L*C));
b=(C*ESR);
d=(1 / (R*C)+(ESR/L));
e=(1 / (L*C));
num=[1,b];
den=[1,d,e];
s=tf("s");
G=a*(1+ESR*C*s)/(L*C*(s^2+(1/(R*C)+ESR/L)*s+1/(L*C)));
bode(G,{1 10e6})
h = bodeplot(G);
setoptions(h, 'FreqUnits', 'Hz');

fco=3e3;
pm=-125;
pc=45-pm;
gm=107;
G=10^(gm/20);
K=tand((pc)/2);
R1=100
R2=G*R1
C1=K/(2*pi*fco*R2)
C2=1/(K^2*pi*fco*R2)
```